Università del Piemonte Orientale

“Amedeo Avogadro”

Dipartimento di Scienze del Farmaco

Corso di Dottorato di Ricerca in

Chemistry & Biology

Ciclo XXXIII

Synthesis of new contrast agents for biomedical applications

Curriculum: Chemical methodologies for new molecules and nanomaterials

SSD: CHIM/03

Fabio Travagin

Coordinatore: Prof. G. C. Tron

Tutor: Prof. G. B. Giovenzana and Dr. L. Lattuada

UNIVERSITÀ DEL PIEMONTE ORIENTALE
DOTTORATO DI RICERCA
IN CHEMISTRY & BIOLOGY

Via Duomo, 6
13100 – Vercelli (ITALY)

DECLARATION AND AUTHORISATION TO ANTIPLAGIARISM DETECTION

The undersigned ..... Fabio Travagin .....student of the Chemistry & Biology Ph.D course (.....XXXIII..... Cycle)

declares:

- to be aware that the University has adopted a web-based service to detect plagiarism through a software system called "Turnit.in",
- his Ph.D. thesis was submitted to Turnit.in scan and reasonably it resulted an original document, which correctly cites the literature;

acknowledges:

- his Ph.D. thesis can be verified by his Ph.D. tutor and/or Ph.D Coordinator in order to confirm its originality.

Date: ..... 15/11/2020 ..... Signature: ..... Fabio Travagin .....

Table of contents

Chapter 1:

Introduction

Imaging

Imaging comprehends a broad group of diagnostic techniques capable of providing, to an operator or to a physician, visual representations of the internal part of the organism. Imaging has the important aim to support the diagnostic process and the pharmacological and surgical therapy of important illnesses such as tumours, cardiovascular and autoimmune diseases, neurodegenerative and myelodysplastic syndromes, bone fractures and many others.

The most important imaging techniques exploited daily in clinical exams and basic research are radiography (RX), computed tomography (CT), magnetic resonance imaging (MRI), ultrasound sonography (US), positron emission tomography (PET), single photon emission computed tomography (SPECT) and Optical Imaging (OI), which will be explained in detail in the following pages.

Imaging can be classified into two different categories, morphological and anatomical techniques (CT, US, and MRI) and molecular imaging (SPECT, PET and OI).

Morphological and anatomical techniques are characterized by high spatial resolution, but they are not able to give any information about fine changes at the tissue, cell or molecular level. These techniques provide images of the body which allow detecting coarse changes in a tissue such as a tumour. In particular, MRI images present a lower spatial resolution than those obtained with CT, but they show a higher contrast.

Molecular Imaging (MI) techniques, instead, consists in the visualization, characterization and measurement of biological processes at the molecular and cellular level in humans and other living systems. However, SPECT and PET do not possess a great spatial resolution, while OI suffers from limited depth penetration.[1,2]

Combining morphological/anatomical and molecular imaging modalities (for example, PET/CT and PET/ MRI technology), it is possible to obtain improved images of the pathophysiological changes at the early stage of many disease with a high resolution.[3]

Moreover, MRI and US are the only imaging techniques tolerated by pregnant women or children, since they are particularly sensitive to ionizing radiations required by all the other imaging techniques.

The various imaging techniques exploit the energy provided by a source and measure the interaction between this energy and the target organ, obtaining an image. When

the energy coming from the source meets the target organ, part of this energy is reflected backward, part is refracted, and a part is absorbed by the target organ itself. The measurement of these interactions allows, after suitable computed transformations, the generation of an image of the target organ.[1,2,4] (**Table 1.1**)

Modality	Energy form	Advantages	Cost
Computed tomography (CT)	X-Rays	Fast, cross sectional images	High
Ultrasound Sonography (US)	High-frequency sound waves	High sensitivity, portable	Low-medium
Magnetic resonance imaging (MRI)	Radio frequencies	High sensitivity, quantitative	High
Optical imaging (OI)	Visible to infrared light	High sensitivity	Low to medium-high
Single photon emission computed tomography (SPECT)	Gamma rays	High sensitivity, quantitative	Medium-high
Positron emission tomography (PET)	Annihilation photons	High sensitivity, quantitative	High

Table 1.1. The most important imaging techniques currently applied in biomedical research and clinical diagnosis.[1,2]

Contrast agents

As stated above, imaging techniques are very powerful diagnostic tools, but sometimes, for the correct visualization of a certain body district, the natural contrast between different tissues (*i.e.* physiological and pathological ones) is not enough. In fact, a great number of CT, US and MRI exams are acquired taking advantage of contrast agents, while OI, PET and SPECT techniques mandatorily require a contrast

agent. A contrast agent consists in a molecular media used to improve the spatial and temporal resolution of an image.

Moreover, molecular imaging contrast agents are able to visualize, characterize and measure biological processes.[5]

Usually, morphological anatomical techniques require high doses of CA (mg - g) while molecular imaging techniques require very low loadings of probes (ng - μg).[6]

Of course, different imaging techniques require specific and very different contrast agents suitable to enhance the physical phenomenon that the specific imaging modality exploits. In fact, contrast agents are chemical compounds with the highest molecular diversity, but the large part of them are metal complexes, since the great tunability of their inorganic and organic functionalities, the resulting compound shows interesting and important different characteristics. However, all CAs must be biocompatible, present a fast elimination by the organism after the clinical exam and must not provide pharmacologic by-effects whatsoever to the patient.[1,2]

The development of innovative CAs for the early diagnosis of life-threatening illnesses is a very active topic in the literature.

The research in this field is focused on the design of innovative CAs for non-invasive imaging, with high affinity to the target organ, high contrast efficiency, optimal pharmacokinetic profile (*i.e.* good biodistribution, intracellular uptake and ability to pass blood barriers), high imaging resolution and easy preparation.

Chelating agents

A complex is a chemical compound in which a central atom, often a positively charged metal ion, is bound, coordinated, surrounded by ligands, usually neutral or negatively charged.

Ligands, instead, are neutral or charged molecules able to bind (coordinate) a metal ion to form a complex which, usually, possesses very different properties compared to the native metal ion. The ligand, interacting with the metal ion, can in fact increase its solubility, reduce its toxicity, modulate its reactivity etc.

Each ligand in a complex has at least one lone pair which binds the central atom generating a coordinated dative covalent bond.

If the complex is formed between the central atom and more than one binding site on the ligand it is defined as a “chelate”.

The number of donor groups present in the ligand able to coordinate the metal is called denticity (κ), while the number of bonds between the metal and the ligand is called the coordination number (C.N.) of the complex.

Chelates are fairly more stable than ordinary complexes (chelate effect) and if the ligand coordination sites are arranged in a macrocycle, the stability increases even more (macrocycle effect). This is due to the reduced mobility of the chelate imposed by preorganized structural constraint (such as an alkyl chain between two coordinating moieties or a macrocycle). In fact, a monodentate ligand can easily escape a complex having no more than its electrons that keep it anchored to the metal. In a chelating agent or in a macrocycle instead, if one coordinating moiety leaves the metal, all other coordinating groups and the ligand scaffold itself stay still bound to the metal.

Group *d* and *f* metals are excellent Lewis acids, therefore they are able to establish coordinate covalent bonds with molecules or ions that can act as Lewis bases (amines, carboxylic acids, thiols, phosphines etc.).[7] (**Figure 1.1**)

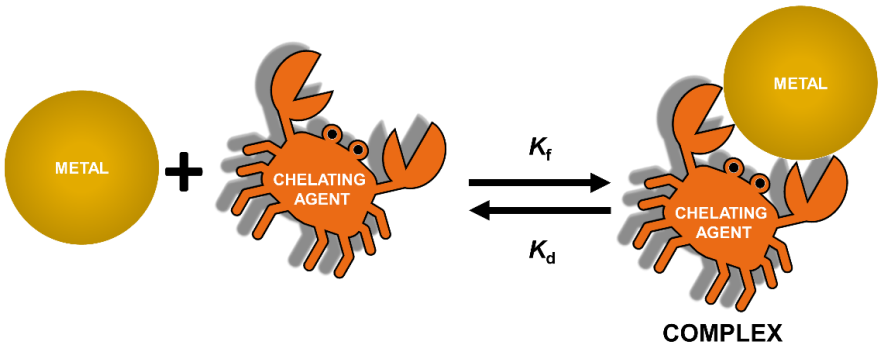

Figure 1.1. Schematic representation of the complexation reaction. The term chelating agent figuratively recalls the claws of a crab (the ligand) grabbing a prey (the metal). K_f and K_d are respectively the formation and dissociation thermodynamic constants of the complexation reaction (vide infra).[7,8]

Ligands that are directly connected with the central ion constitute the sphere of internal coordination, while counterions, compensating the total charge of the system, and solvation molecules constitute the external coordination sphere.

Moreover, in a metal chelate the optimal stability is obtained when the metal and the chelating ligand are arranged in 5-membered units. Usually six membered chelates are less stable, but still possessing, in some case, a reasonable high stability. Rings with less than five members and more than six generally result in unstable complexes.[7] (**Figure 1.2**)

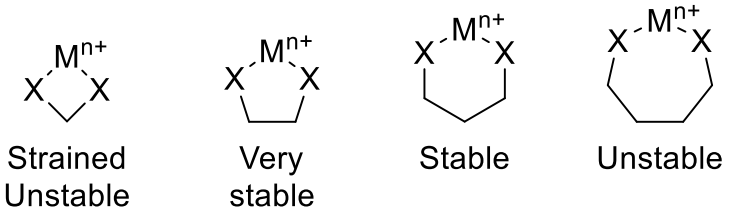

Figure 1.2. Stability of the metal complex as a function of the length of the chain between two donor groups.[7]

Chelating agents are employed today for a large array of applications where an efficient coordination of a metal ion is required.

These applications include pulp and paper manufacturing and food, drug and cosmetic formulation as adjuvants of antioxidant and antibacterial additives. Other uses of chelating agents include water softening, application in the chemical and textile industry, in catalysis, in agriculture as fertilizers, in water and soil remediation and in metal extraction and processing.[9–11] (**Figure 1.3**)

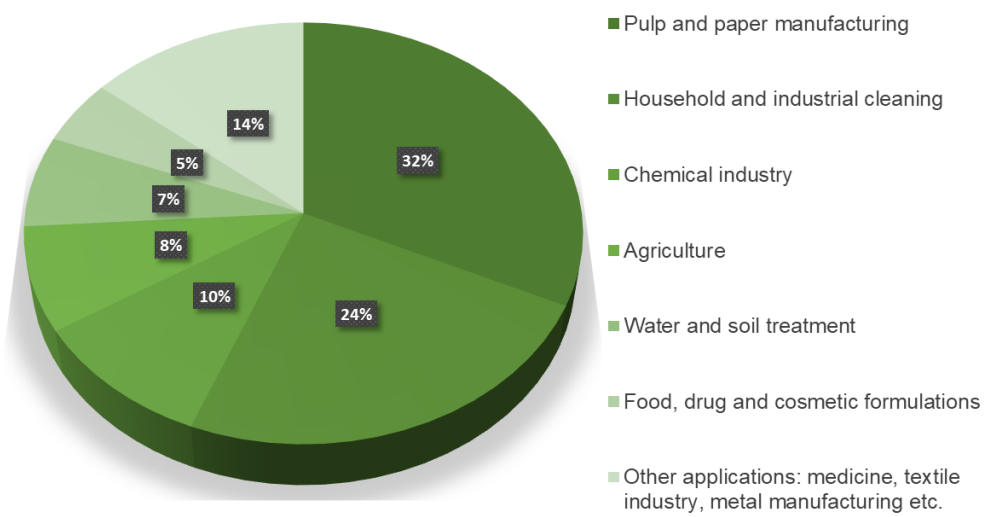

Applications of chelating agents	Global consumption
Pulp and paper manufacturing	32%
Household and industrial cleaning	24%
Chemical industry	10%
Agriculture	8%
Water and soil treatment	7%
Food, drug and cosmetic formulations	5%
Other applications: MEDICINE, textile industry, metal manufacturing etc.	14%

Figure 1.3. Worldwide consumption of chelating agents (weight).[11]

Chelating agents are also extremely important for life in general, in fact endogenous chelating agents are produced by all sorts of living organisms and they are responsible for many physiological processes such as enzymatic activity, oxygen transport, metal accumulation and detoxification etc.[11–15]. Deferoxamine B (**Figure 1.4**), for example, is a natural occurring siderophore produced by *Streptomyces pilosus*, and it exhibits strong affinity and selectivity towards Fe^{3+}. For this reason, deferoxamine B is an important drug for the treatment of iron intoxications and for illnesses characterized by iron chronic overload (*i.e.* hemochromatosis).[16,17]

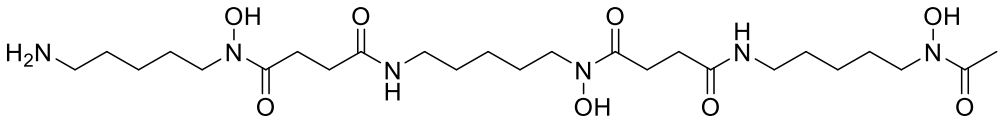

Figure 1.4. Deferoxamine B.

Owing to the importance of chelating agents in all the above cited fields, they have been an important and active research topic for both academia and industry since the beginning of 19th century as documented by the increasing number of dedicated scientific articles and patents published yearly.[10,12] In fact, some properties of chelating agents are still to be improved nowadays, *i.e.* chelation efficiency, toxic reagents (such as formaldehyde and cyanides) and non-renewable starting materials (ethylenediamine and diethylenetriamine) (**Figure 1.5**) and experimental protocols (such as high temperature, long reaction times and management of wastes) required for their synthesis,[18] biodegradability, toxicity (for example NTA is demonstrated to be cytotoxic to cell cultures and mammals)[19] and many others.

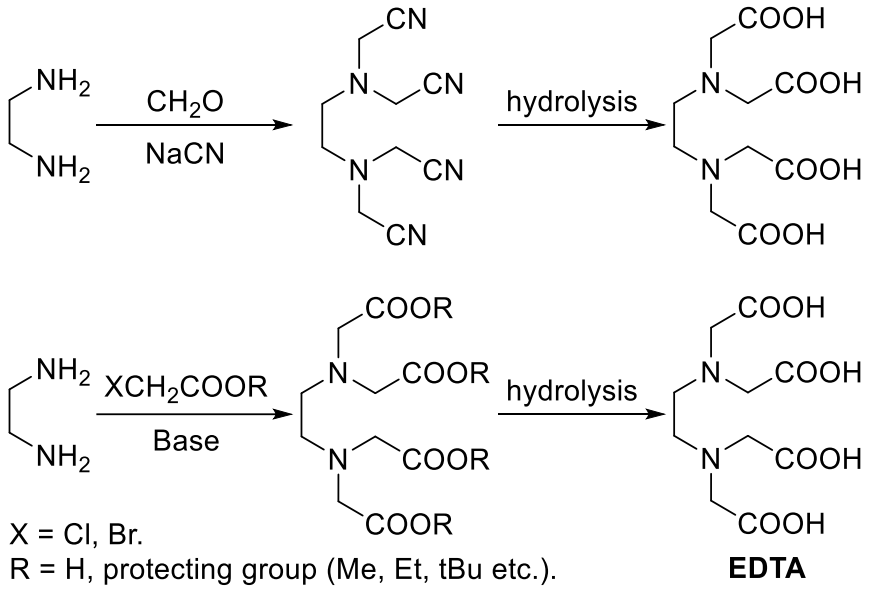

Figure 1.5. EDTA and the most of chelating agents can be prepared by two synthetic strategies, cyanomethylation (first step) and hydrolysis (top) and alkylation (bottom) and hydrolysis (as needed).

NTA (nitrilotriacetic acid, **Figure 1.7**) and EDTA were the first two chelating agents discovered (1936), marketed and exploited for almost all the above cited application and in the year 2000 the production of chelating agents has exceeded the worldwide scale of 200,000 tons/year.[13]

From a chemical point of view chelating agents can be divided into different classes such as polyaminocarboxylic acids, phosphonates and carboxylates. Polyaminocarboxylic acids are the most common chelating agents and they are used for all the above cited application and are able to bind strongly almost all metals. This class is represented, for example, by EDTA, NTA, DTPA (diethylenetriaminepentaacetic acid), IDS (iminodisuccinic acid) and DOTA (1,4,7,10-tetraazacyclododecane-1,4,7,10-tetraacetic acid).

Phosphonates are mainly used for industrial cleaning, water softening and in household products and they bind strongly to almost all metals. The main representatives of this class are DTPMP (diethylenetriaminepentamethylene-phosphonic acid), EDTMP (ethylenediaminetetramethylenephosphonic acid) and NTMP (nitrilotrimethylphosphonic acid).

Carboxylates are much weaker chelating agents, are particularly selective for calcium and zinc and are mainly used as cleaning agents and in food industries for their biodegradability. This class is represented, for example, by gluconates, oxalates and citrates.[9] (**Figure 1.6**)

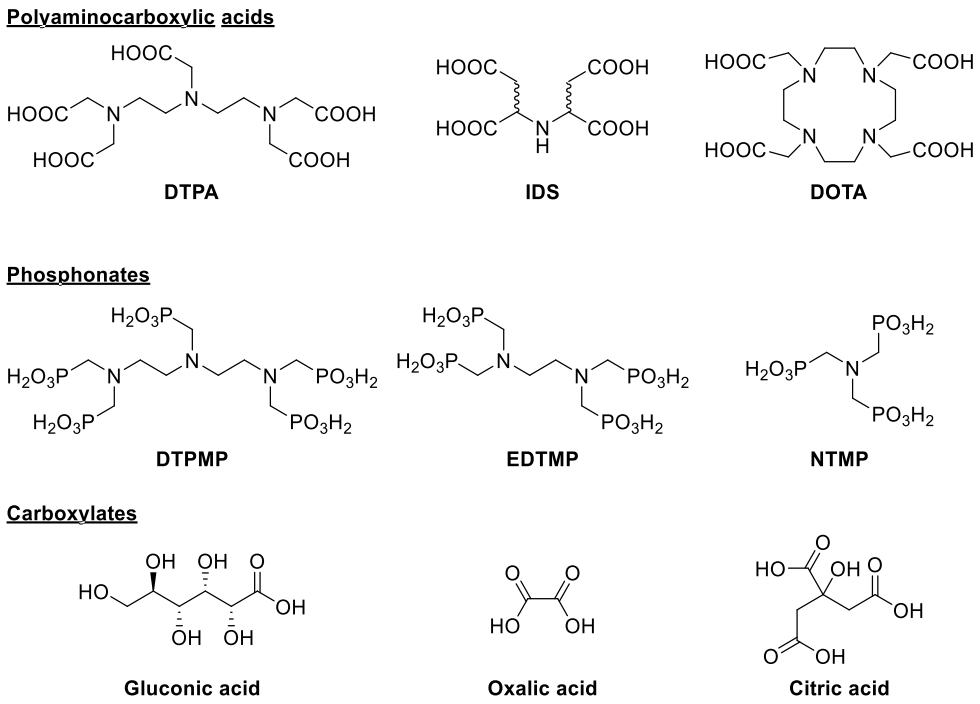

Figure 1.6. Most common chelating agents.

The efficiency of a chelating agent in the coordination of metal ions, can be determined through potentiometric titration, UV and NMR analysis. These tests establish the acid-base behaviour of chelating agents and the affinity towards different metal ions, leading to the determination of the stability constant of the corresponding metal complexes. For this experiment the compounds undergo an initial classical acid-base titration, which is preliminary and fundamental to establish the formation constants of the relative complexes. Since ligands usually possess many amino and carboxylic groups, they often present multiple protonation constants. (**Equation 1.1**)

$$K_i^H = \frac{[H_i L]}{[H_{i-1} L][H^+]}$$

Equation 1.1. The various protonation constants (K) are indicated with a subscript "*i*", representing the sequential order of protonation.

Then the same molecule is titrated in the presence of a fixed concentration of the metal ion to be examined, obtaining the corresponding stability data. High thermodynamic stability and considerable kinetic inertia is required to avoid dissociation of the complex.

Moreover, in solution there may be anions capable of competing with the chelating agent for the formation of stable bonds with the metal ion present in the complex. These anions can subtract the metal from the complex and precipitate it in the form of salt or hydroxide. For example the Fe^{3+} ion at pH values greater than 5.5 precipitates from the complex with EDTA generating $Fe(OH)_3$. Some species capable of altering the balance related to the formation of the complex are, among others, phosphates, carbonates, silicates and citrates.

In fact, the complexation reaction is an equilibrium between the ligand in its completely dissociated form, the metal ion and the complex.

The complexation reaction can be influenced by the pH of the system and by the presence of ions that can compete for the bond with the metal. The completely dissociated form of the chelating agent yields more stable complexes than protonated species and the concentration of the completely dissociated form is higher at high pH values, therefore the chelating agents are more effective as pH increases.[7,20] (**Figure 1.7**)

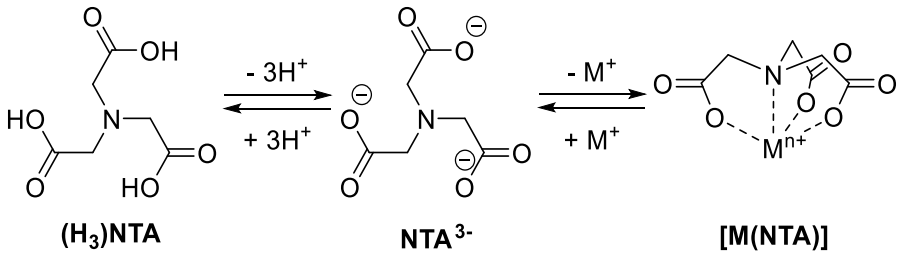

Figure 1.7. Influence of pH in the complexation reaction.

Biomedical applications of chelating agents

Among all previously mentioned applications of chelating agents, their use in medicine (such as in metal poisoning, in pathologic metal excess or deficiency, in autoimmune

syndromes, in cancer treatment, in diagnostic imaging etc.) is the main topic of this thesis.

In the biomedical field, a chelating agent must have the following characteristics to be considered for human application:

• High thermodynamic stability: the metal complex must be stable, *i.e.* it should not dissociate easily to prevent the metal ion leaching and its spreading unbound in the organism causing toxicity. (**Equation 1.2**)

$$M + L \rightleftarrows ML \qquad K_f = [ML] / [M] [L] \qquad K_d = [M] [L] / [ML]$$

Equation 1.2. Complexation reaction and its thermodynamic constants.

• High kinetic inertness: the complexation reaction must take place quickly, but decomplexation reaction must be slow (kinetic inertness) to avoid unwanted release of toxic free metal. For example, if the metal is radioactive, excessive decay must be avoided during complexation.

• Selectivity: the chelating agent must be selective for the metal of biomedical interest and other physiologic metals should not compete for the ligand, causing the leaching of the toxic metal.

• Solubility: the chelating agent must be very soluble in the formulation (usually hydrophilic) of biomedical use (intravenous administration usually) and, of course, in biological fluids (hydrophilic too).

• Toxicity: the metal complex must be stable and must not release the toxic metal in the organism. Free metal ions are able to coordinate oxygen, nitrogen and sulphur atoms physiologically present in cell membranes and biological macromolecules resulting in alterations of the dynamic equilibrium indispensable for life. This can result, for example, in enzyme inhibition, protein conformational changes or alteration of membrane potentials. Moreover, many metal ions, such as Gd^{3+}, can interfere with Ca^{2+} metabolism occupying its natural binding sites. Free chelating agent can also cause toxicity to the organism, since the ligand can sequester life-relevant metal ions

such as Ca^{2+}. Again, the intact complex can induce a wide variety of toxic effects such as a change in osmolarity between intracellular and extracellular compartments. This cause water to flow from inside to outside cells inducing cellular and circulatory damages. Moreover, metal complexes for diagnostic use should not show pharmacologic activity, side effects or other activities apart from the diagnostic feature (*e.g.* the contrast effect).[21]

• Good clearance profile: the metal complex must be quickly and completely eliminated from the body. Complexes with low molecular weight are quite safe due to their efficient excretion from the body. This minimizes the exposure to the chelate and reduces the chance that slow uptake processes could internalize the complex in cells. Instead, complexes bound to macromolecules present a slow excretion, which increase the odds of cellular uptake, leading to the release of potentially toxic by-products, including free metal ions. [7,22–25]

Chelation therapy

Chelation therapy exploits chelating agents to form stable complexes with toxic metals, making them harmless and easily eliminated from the organism. Moreover, recent literature has proposed chelation therapy as an adjuvant treatment also for other pathologies such as hypertension, infections, angina pectoris and metabolic diseases.[26–29]

As an example of a ligand exploited for chelation therapy, we mention TETA (triethylenetetramine, **Figure 1.8**) hydrochloride, which is a copper chelator used in the treatment of Wilson's disease, an autosomal recessive inherited genetic disorder responsible for the accumulation of copper in tissues. The main symptoms of Wilson's disease are hepatolenticular degeneration and neuropsychiatric and liver disorders.

Another example of drug for chelation therapy is EDTA, which is exploited to cure patients with heavy metal intoxication (such as lead poisoning), since it forms easily disposable complexes.[30]

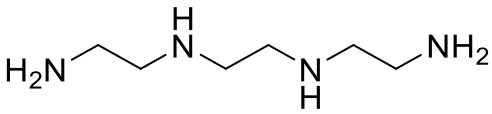

Figure 1.8. TETA, a drug for copper chelation therapy.

Radiography

Radiography (RX) is the first imaging technique discovered and exploited for medical application and it takes advantage of X-rays to acquire images of the body.

X-rays are electromagnetic radiation with wavelengths between 0.01 and 10 nm and are generated by a high-voltage vacuum tube that accelerate electrons from a cathode to a tungsten alloy anode. During this process, accelerated electrons release energy in the form of X-rays (Bremsstrahlung or deceleration radiation), whose energy maximum is dictated by the energy of incident electrons.

In a RX clinical exam, X-rays pass through the human body and the different tissues (*e.g.* bone and muscle or pathologic and healthy) have different and characteristic transparency to X-rays, generating different contrast on an image in grayscale. Tissues that strongly absorb X-ray (*e.g.* bones) appear bright while other that absorb poorly (*e.g.* air) appear dark. (**Figure 1.9**)

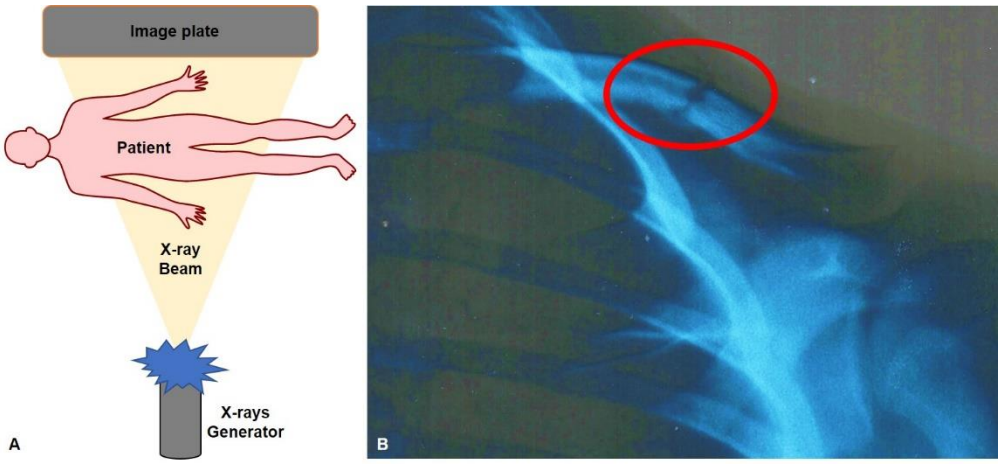

Figure 1.9. A) Scheme of a RX apparatus. B) RX image of a clavicle fracture (circled in red).

However, sometimes, the physiological contrast of human tissues is not sufficient to allow physicians to distinguish between two nearby tissues or to highlight a damage. X-ray contrast agents (or X-ray-opaque substances) represent the best solution to this problem, in fact, when administered they increase the radiologic visibility of some organs.

X-ray contrast agents consist in high density (ρ) materials and/or atoms with high atomic number (Z) for an optimised X-ray absorption. (**Equation 1.3**)

$$\mu = \frac{\rho Z^4}{AE^3}$$

Equation 1.3. μ = X-ray absorption coefficient, A = atomic mass and E = X-ray energy.

Therefore, a good X-ray contrast agent, suitable for clinical application, should present, in its structure, atoms with high Z to obtain a high X-ray absorption efficacy.

Barium sulphate is an example of clinically approved X-ray contrast agent, which, administered orally or with an enema to a patient, allows to acquire useful images of the gastrointestinal tract for anatomical and pathological investigation. In fact, usually, soft tissues are poorly radiopaque and therefore not visible in a routine X-ray exam without a contrast agent.[31]

Computed tomography

Computed tomography (CT) is one of the most widespread clinical diagnostic imaging tools largely used in hospitals.

CT exploits X-rays that, passing through the human body, decrease in intensity according to the density of the crossed tissue. The intensity of the original fan beam is known, and its decrease is measured by a detector located on the opposite side of the X-ray tube and a software converts the attenuation values into an image.

By slowly rotating and moving the fan beam and the detector around and across the whole anatomic region to examine, the CT apparatus acquires cross sections of the body, from which three-dimensional reconstructions on a grey scale can be generated.

CT is a very powerful diagnostic technique for the imaging of various tissue and organ systems in both physiological and pathological condition. (**Figure 1.10**)

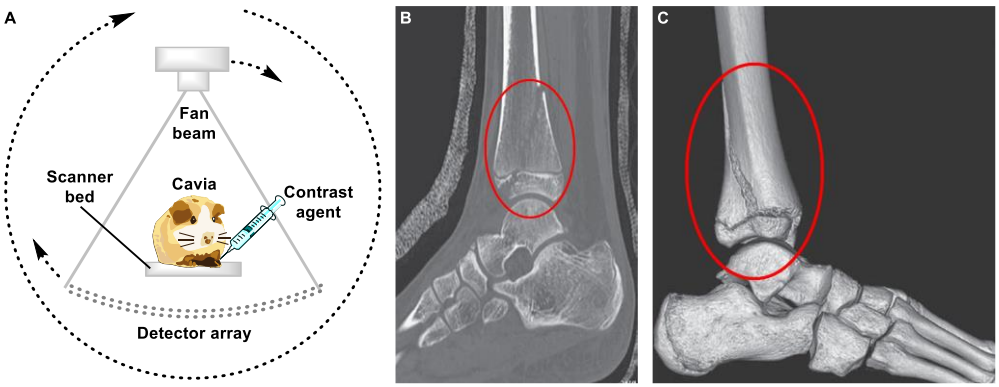

Figure 1.10. A) Schematic representation of a CT apparatus. B) 2D CT scan of a tibial fracture (circled in red). C) 3D reconstruction of the same bone fracture as in B (circled in red).

However, if the contrast between two anatomical regions is not enough for diagnostic purposes, the application of CT contrast agents can enhance the difference between two close tissues.

CT CAs, dealing with X-rays as RX CAs, exploit the same principle explained in the previous section, *i.e.* they present, in their structure, atoms with high atomic number (commonly iodine or bromine) and are frequently used in clinical analysis to obtain suitable images of soft tissues.[2,32,33]

As representative and important examples of CT CAs we can mention iopamidol and iomeprol, both clinically approved intravenous CT CAs.[34] (**Figure 1.11**)

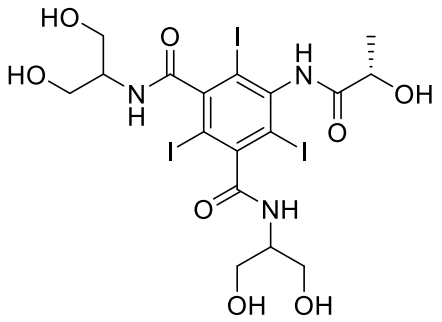

Iopamidol

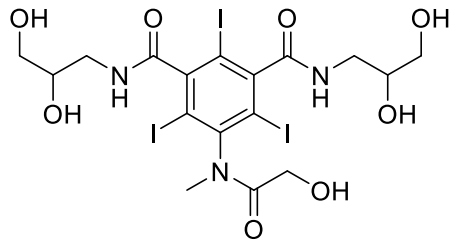

Iomeprol

Figure 1.11. Iopamidol and iomeprol, two CTCAs.

Magnetic resonance imaging

Basics of NMR

Nuclear magnetic resonance (NMR) is a physical phenomenon which arises from the interaction between three main actors, an atomic nucleus, a magnetic field and a radio frequency pulse.

The first actor, the atomic nucleus, can be seen as a rotating sphere, with a certain angular momentum (P) which is responsible for the generation a magnetic momentum (μ).

The ratio between the magnetic momentum and the angular momentum is called gyromagnetic ratio (γ) and is typical of each atom nucleus.

(**Equation 1.4**)

$$\mu = \gamma P$$

Equation 1.4. μ = magnetic momentum, γ = gyromagnetic ratio, P = angular momentum.

Moreover, nuclei with odd mass (A) and odd or even atomic (Z) numbers have a half-integer magnetic quantum number (I) (such as ^{1}H, ^{13}C, ^{19}F, ^{31}P = 1/2 and ^{11}B = 3/2), nuclei with even A and odd Z have an integer I (such as ^{2}H, ^{14}N = 1 and ^{10}B = 3) and nuclei with even A and even Z do not display magnetic properties (I = 0, such as ^{12}C

and ^{16}O). Nuclei with I = 1/2 are magnetic dipoles, while those with I > 1/2 behave as quadrupoles owing to the non-spherical distribution of their nuclear charge. For the sake of simplicity and since their importance in NMR, from now on, if not otherwise specified, it will almost exclusively talk about the former group (*i.e.* those with I = 1/2). These nuclei, being magnetic dipoles, can align themselves to an external static magnetic field (B_0), the second actor, being parallel or antiparallel to it in an almost equal amount.

NMR in general, requires very strong magnetic fields, usually stronger than 1 T. The nuclear spin state parallel to B represents the ground state, with a tiny excess of this alignment (in respect of the antiparallel one) and the NMR phenomenon arises from this slight excess. Moreover, this little excess grows proportionally to B_0 since an increase of the latter rises the energy barrier between the two spin states (parallel and antiparallel).

In an NMR experiment we observe signals arising from this tiny difference which is called macroscopic magnetization (M_0). (**Figure 1.12**)

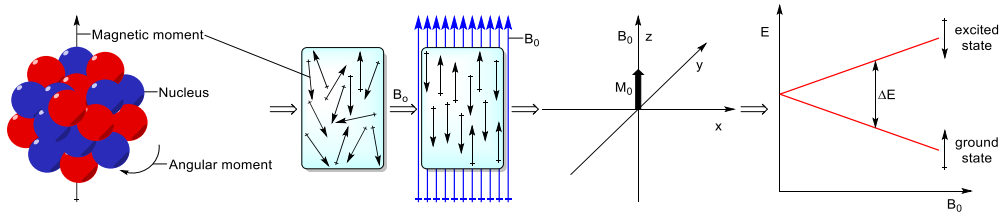

Figure 1.12. Schematic representation of (from left), a NMR-active nucleus, its alignment to a magnetic field, the resulting macroscopic magnetization and the increasing of the energy difference between excited and ground state with the increasing of B_0.

The third actor is the radiofrequency (rf) pulse, whose fluctuating magnetic field (B_1) is perpendicular to B_0, and causes M_0 to align perpendicularly to B_0 (and parallel to B_1). The latter phenomenon is called excitation, and after that the radiofrequency is turned off and M_0 can go back (relax) to its original position (parallel to B_0). Now, M_0 is rotating along its axis (angular momentum) and meanwhile it is relaxing (returning parallel to B_0) and the resulting movement is called precession, something similar to

a flicked rotating spinning top. The frequency of precession (ω_0) is typical of a certain nucleus, in a given magnetic field, in a certain chemical environment and in NMR experiments gives, once measured and elaborated, precious information about molecular structure.[35] (**Equation 1.5**)

$$\omega_0 = \gamma B_0$$

Equation 1.5. ω_0 = precession frequency, γ = gyromagnetic ratio, B_0 = magnetic field.

Since the energy difference between ground state (M_0 parallel to B_0) and excited state (M_0 perpendicular to B_0), unlike other spectroscopic techniques, is very small (in fact just a rf is enough!) relaxation is not spontaneous and must be encouraged.
In fact, two main different relaxation phenomena are altogether responsible for M_0 to return back to its original position, and they are longitudinal relaxation and transversal relaxation.
Longitudinal relaxation time (T_1) is an exponential time constant that indicates the amount of time needed for M_0 to return parallel to B_0 along Z axis (*i.e.* the axis along with B_0 lays). Longitudinal relaxation accounts for enthalpic interactions between the excited nucleus and the environment, for dipolar coupling with other spins or for interaction with paramagnetic particles (*i.e.* with unpaired electrons). Here the energy is lost as heat transferred to other nuclei as vibrational and rotational energy. In fact, moving particles in the environment (especially paramagnetic ones) creates a complex magnetic field and a distribution of frequencies among which an excited nucleus can find its proper resonance frequency thus relaxing quickly.
Transversal relaxation time (T_2), instead concerns the disappearance of the signal in the xy plane (perpendicular to B_0), it is an entropic phenomenon and T_2 is always shorter than T_1 and always an exponential phenomenon. Transversal relaxation is caused by spin-spin interactions between the excited nuclei and other spin systems which dephase the signal (*i.e.* the various magnetic moments lose their precessing phase coherence) or by inhomogeneities in the magnetic field.[23] (**Figure 1.13**)

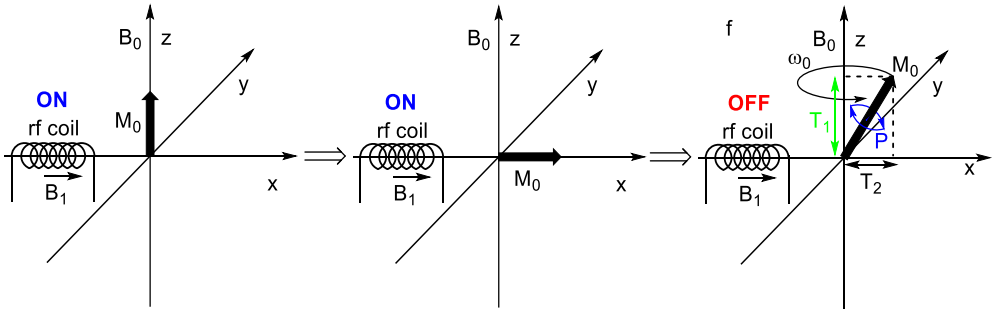

Figure 1.13. Schematic representation of (from left), excitation of M_0, its alignment to B_1 and relaxation with its parameters.

Basics of MRI

When a person is placed in an NMR apparatus we speak about magnetic resonance imaging (MRI) and some important differences from single molecules NMR must be explained.

First of all, in MRI just ^{1}H nuclei are imaged (those of water, triglycerides, membrane phospholipoids and many other biological molecules) since their high concentration in tissues, since ^{1}H has an isotopic abundance close to 100% and since its high γ and μ. However, also ^{13}C, ^{31}P and ^{19}F – based experiments are gaining importance in MRI for similar reasons, which will be explained later.

In MRI a fourth important actor comes on the stage, *i.e.* gradients. Note that gradients are very important also for NMR in general, but for the sake of simplicity here we are just dealing with their implications in MRI. A gradient is a known linear variation of the magnetic field in respect of the position, superimposed to B_0 for few milliseconds. The gradient is voluntarily introduced in the “sample” by the operator and it is used to localize the signal coming from a particular spot in the body. Of course, different types of protons in different tissues (such as tumors and healthy tissues) have different relaxation times, different concentration of water (so different intensities of the signal) and therefore one can spot a difference between them on an image, but one must also now where this particular signal comes from.[23] This is the role of gradients, in a magnetic field gradient nuclei experiencing a higher magnetic field absorb a higher frequency and vice versa, therefore the gradient creates a correlation between

absorption frequency and nucleus position in space. Applying gradients variable from place to place by the operator along the three dimensions (x, y, z) one can understand from which spot that particular signal comes from or choose a “slice” of the body to image. The images picturing the various slices of the body can be used to compute a 3D representation of the target organ.[36] (**Figure 1.14**)

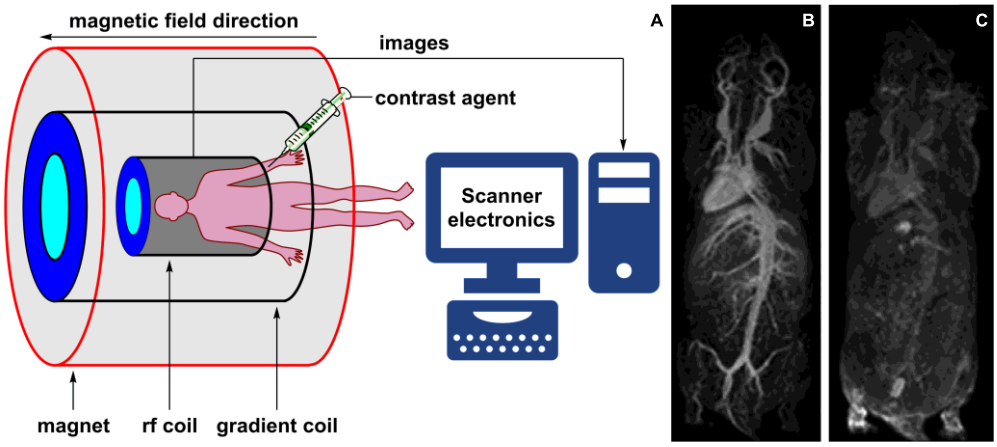

Figure 1.14. A) General scheme of an MRI apparatus. B) and C) MRI images obtained after intravenous injection of Gd-AAZTA-MADEC (a blood pool agent) in a mouse after, 2 min (B) and 30 min (C).

As stated above, in a normal MRI exam the contrast between different tissues is obtained thanks to the different relaxation times of different tissues, therefore an image can be T_1 or T_2 weighted. Another parameter often used in MRI is T_2*, which considers both T_2 and all magnetic field inhomogeneities typical of the sample and is usually much smaller than T_2.[23] Weighting images with these parameters is useful to image different tissues, for example T_1-weghted images gives high signal for fat, T_2-weghted images present high signals for water-rich spots (such as tumors, edemas, inflamed tissues etc.)[37] and T_2*-weighted images are useful to image iron rich tissues such as hemorrhages.[38]

Obviously, there are many other weighting techniques (such as proton density) and many other methods in a MRI pulse sequence (such as spin echo) we are not deeply exploring here. However, often all of these techniques are inefficient to highlight the

difference between two close tissues and therefore images must be acquired administering to the patient a suitable MRI contrast agent.[23]

MRI contrast agents

Every year, in hospitals all around the World tens of millions of contrast-enhanced MRI exam are performed. In fact, 50% of the total MRI clinical exams take advantage of MRICAs. They usually consist in injections administered to the patient some minutes/hours before the exam, however recently, innovative oral MRI CAs have been investigated. MRI contrast agents might be classified in many categories based on their structure or on their contrast effect.

Moreover, MRI CAs can also be classified according to their biodistribution in three categories, extracellular, intracellular or organ specific MRI CAs.

The most common MRI CAs belong to the "extracellular" group and are typically exploited for the detection of tumor masses, for example in the brain. MRI CAs are usually administered parenterally, then they distribute in a non-specific way in the plasma and in the interstitial space and finally are eliminated from the organism by renal excretion after a period of 17 hours circa.[22]

T_1-contrast agents, paramagnetic ions

T_1-contrast agents, as stated above, are paramagnetic particles that have the ability to interact with excited nuclei (here ^1H of water in the body) and make them relax much quickly enhancing the signal (positive contrast agents). Among paramagnetic materials, Gd^{3+} represents a gold standard in clinic thanks to its seven unpaired *f* electrons, in fact. every year almost fifty tons of gadolinium are administered to patients. However, also Mn^{2+} (five *d* unpaired electrons), Fe^{2+} (four *d* unpaired electrons) and Fe^{3+} (three *d* unpaired electrons) have been successfully exploited as MRI contrast agents (CA).

Since free metal ions are very toxic for the human organism, paramagnetic ions must be imprisoned in chelating agents to serve as MRI CAs.

All T_1-MRICAs share a common structure pictured in **Figure 1.15**, with a chelating agent hugging a metal which coordinates one or more water molecules.[22]

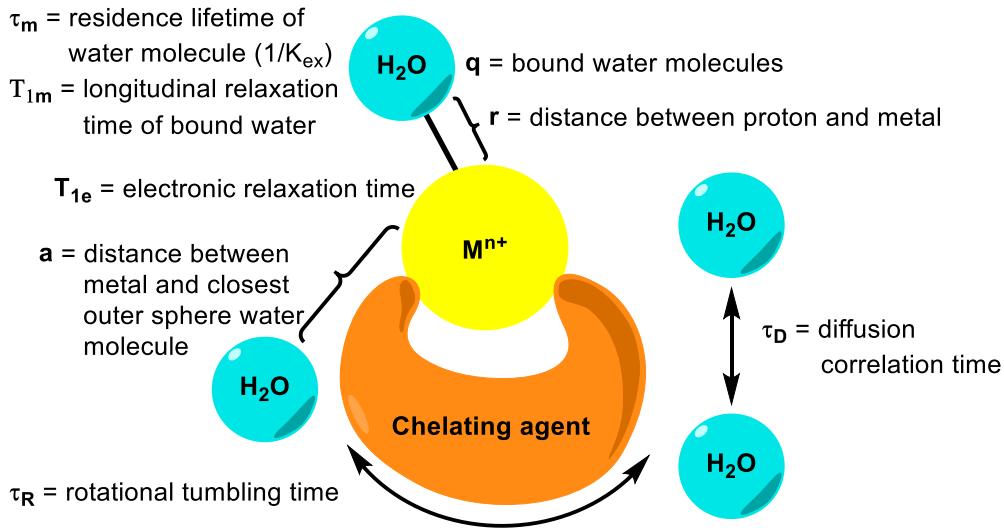

Figure 1.15. General structure and features of a MRICA.

The relaxivity of a MRICA is a parameter which depends on the parameters pictured in **Figure 1.15** and on MRICA concentration in the organism, the higher the relaxivity, the better is the MRICA. (**Equation 1.6**)

$$1/T_1 = 1/T_{1\,0} + r_1[CA]$$

Equation 1.6. T_1 = relaxation time in the presence of a CA, $T_{1\,0}$ = relaxation time of pure water, r_1 relaxivity of the CA, [CA] = concentration of the CA.

In fact, the paramagnetic ion must significantly increase the rate of relaxation of water protons in a target organ or in the whole body, generating a contrast effect in a non-toxic dose. Moreover, the CA must be stable in the body (*i.e.* must not release the metal) and must be completely eliminated immediately after the exam, without pharmacologic effects.

Water molecules directly bound to the metal, the coordinated water molecules (inner sphere), relax really fast, however also other water molecules really close to the ligand (and maybe bound to it for example by means of an hydrogen bond) relax faster than in the absence of a CA (second hydration sphere). In fact, **q** (numbers of water molecules bound to the metal) can be formally fractional. Of course, the higher **q** is,

the more water molecules the metal binds (directly or indirectly), the higher the relaxivity is. But one must pay attention, since a metal generally has a “fixed” coordination number (C.N.), the more water molecules it coordinates, the less room is left for the chelating agent, the more unstable the complex is, the more toxic free metal is released in the organism. For example, Gd^{3+} has a C.N. = 9, and in a typical gadolinium based MRICA **q** = 1 – 2 to obtain the right balance between acceptable stability and efficient relaxivity. Therefore, the typical chelating agent for gadolinium-based MRICAs has a denticity (κ) = 7 – 8. However, q can be increased also acting on the second hydration sphere, introducing in the ligand non coordinating electronegative functional groups prone to form hydrogen bonds with water (*i.e.* hydroxyl groups, phosphate, phosphonates etc.).

Instead, τ_m is the residence time of inner sphere water and it is = $1/K_{eq}$, *i.e.* the exchange constant of coordinated water. The higher τ_m is, the better is the relaxivity, since a water molecule binds to the metal, quickly relaxes and it is immediately replaced by another water molecule ready to relax.

The proton-metal distance in the inner sphere (r) and in the outer sphere have a great impact on relaxation, in fact relaxivity is inversely proportional to proton-metal distance with a factor of 10^6. Therefore, in an ideal MRICA **a** and **r** should be minimized.

Rotational correlation time (τ_R) indicates the rotational mobility of the paramagnetic complex and grows as a function of molecular weight of the latter. Relaxivity and complex stability increase as the rotational correlation time is increased. In particular, the paramagnetic complex catalyses the relaxation of water nuclei when the rotational speed of the CA matches the precession frequency of the nucleus (resonance condition). Since proton, for example, has a precession frequency of few hundreds Hz (*i.e.* 300 Hz at 7 T) and small molecules in water at room temperature rotate much faster, their rotation must be slowed down.

T_{1e} is the electronic relaxation time, it depends on the structure of the chelating agent and on the magnetic properties of the metal and increasing this parameter relaxivity grows.

T_D is the diffusion correlation time, *i.e.* the rate of diffusion of solvent molecules in which the CA is dissolved. As stated above the paramagnetic ion must move to increase the relaxivity and solvent (normally water) molecules must reach the

paramagnetic center, relax and leave the room for another solvent molecule as quick as possible, therefore, high τ_R values increase relaxivity.[23]

Other important parameters for T_1-MRICAs are thermodynamic and kinetic stability of metal complexes. As stated above, free metal ions (especially gadolinium) are really toxic for the organism, it accumulates for example in the brain, kidney, bone etc. after repeated administrations and causes severe side effect especially in compromised patients (*e.g.* with renal failure).[24,25] To avoid these problems, the metal complex must show high thermodynamic and kinetic stability, being stable over time also in the presence of physiologic competing metal ions (*i.e.* Ca^{2+}, Mg^{2+} etc.), chelating molecules (*i.e.* aminoacids, phosphates etc.) or acidic pH.

The following table reports the values of the parameters reported above for some MRI-relevant Gd^{3+} complexes (**Table 1.2**), whose structure and properties will be discussed in the following pages.

Ligand	κ	$LogK_{GdL}$	LD_{50}	k_{obs}	τ_m	τ_R	q	r	r_1	r_2
EDTA	6	17.7	0.3	140000	-	-	3	-	-	-
DTPA	8	22.46	5.6	1.2	130	58	1	3.13	3.8	4.4
DOTA	8	25.3	11	0.021	108	77	1	3.13	4.2	4.75
AAZTA	7	20.24	-	-	-	74	2	-	7.1	
HP-DO3A	8	23.8	12	0.064	-	-	1	-	4.4	5.5
DO3A	7	21.1	7 - 9	2.37	77	66	2	3.15	4.8	-
BOPTA	8	22.59	-	-	-	88	1	2.96	6.7	8.9
NOTA	6	13.7	-	-	-	-	3	-	-	-
PCTA	7	-	-	-	34	70	2	3.1	6.9	-
DOTP	8	28.8	-	-	-	73	3	-	3.5	-

Table 1.2. Complexometric and relaxometric properties of some MRI-relevant Gd^{3+}-complexes. $LogK_{GdL}$ = complex stability constant; LD_{50} in mouse, intravenous, [mmol/kg]; k_{obs} = acid dissociation rate [10^3 s^{-1}]; τ_m = [ns]; τ_R = [ps]; r = distance metal-proton [Å]; r_1 and r_2 = longitudinal and transversal relaxivity (respectively) [mM^{-1} s^{-1}].[39,40]

Drug regulatory agencies around the world (*i.e.* E.M.A., F.D.A. etc.) have approved for human use (since 1989) ten MRICAs, and some of them are still commercially available. (**Figure 1.14**)

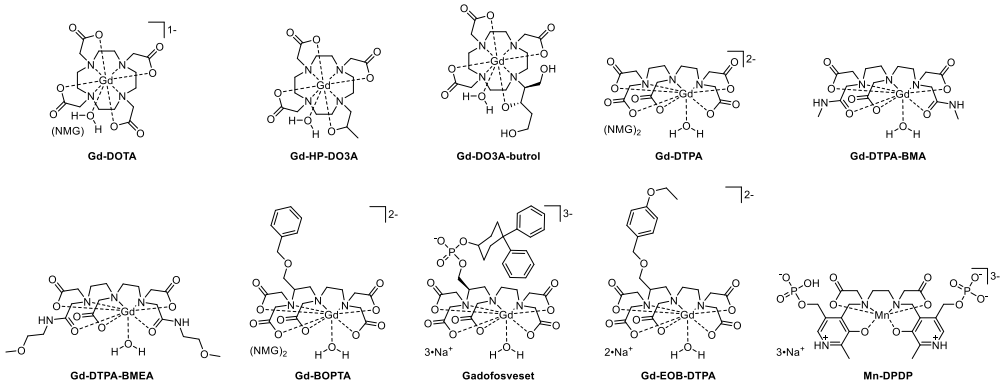

Figure 1.14. Clinically approved MRICAs.

These MRI CAs might be all exploited for general purposes which require the distribution of the CA in all the organs (*i.e.* detection of tumours, brain lesions etc.), however some of them present peculiar characteristics. For example, Gd-BOPTA and Gd-EOB-DTPA, thanks to their benzylic lipophilic chain, are accumulated preferentially in the liver and their contrast effect is optimal in this anatomical region.[22,41–44] On the other hand, gadofosveset works as a blood pool agent, thanks to its lipophilic chain particularly selective for binding human albumin (HSA). In fact, being the CA conjugated to HSA (a large protein), it cannot exit from blood vessels and for this reason it is specific for blood imaging (angiography). This might be particularly useful since angiography, usually, is performed exploiting x-rays, radioactive tracers and invasive injection techniques. Moreover, the supramolecular adduct between a T_1-MRICA and a macromolecule (*i.e.* HSA) shows an increased relaxivity since bigger is the molecule, slower it moves and therefore higher is τ_R.[22,45,46] Mn-DPDP is an example of Mn-based MRICA, which are interesting CAs with some differences compared to Gd-based MRICAs. First of all, Mn^{2+} has just five unpaired *d* electrons while Gd^{3+} has seven *f* unpaired electrons, making the latter a more suitable and efficient paramagnetic CA. Moreover, Mn^{2+} has a C.N. = 6 – 7 and therefore an

ideal ligand should have a κ not higher than six, being hexadentate ligands particularly interesting, since they have a coordination site for one water molecule on the metal. (**Figure 1.15**)

Mn^{2+} ions also tend to form stable complexes with ligands with **κ** = 4 and **q** = 2, such as porphyrins (*i.e.* TPPS).[22]

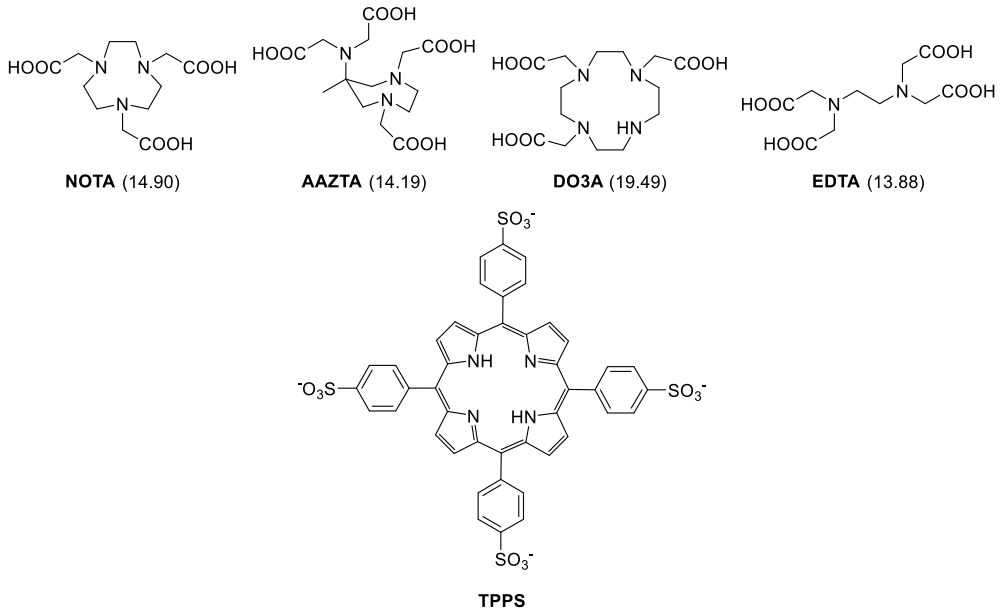

NOTA (14.90) **AAZTA** (14.19) **DO3A** (19.49) **EDTA** (13.88)

TPPS

Figure 1.15. Selected chelating agents forming stable complexes with Mn^{2+} with the stability constant for the Mn-complex in brackets. As one can see, Mn-complexes are rather more unstable than Gd-complexes.

Moreover, manganese has the great advantage of being much less toxic than gadolinium (being an essential element in human metabolism). However, due to since the general instability of Mn-complexes and their limited efficacy as MRICAs, at the moment the market and the scene are dominated by Gd-based MRICAs.[22,47]

It is important to point out, looking at **Figures 1.14** and **1.15**, that MRI-relevant chelating agents can be divided in linear (*i.e.* BOPTA, DTPA, DPDP etc.) and macrocyclic (*e.g.* DOTA, HP-DO3A, DO3A etc.), depending of their chelating structure. Linear chelating agents have almost been abandoned since they form metal

complexes too weak (and for instance too toxic) for human application. Macrocyclic ligands (*i.e.* those bearing a 12-membered or a greater cycle in their structure) are nowadays the best choice for the preparation of MRI CAs, since they represent the best compromise between contrast effect and complex stability.

For example, P03277 (**Figure 1.16**) is a macrobicyclic heptadentate MRICAs approved for clinical trials in 2015 (which are still ongoing). Its Gd-complex is very stable thanks to the macrocyclic structure and it shows high relaxivity thanks to its q = 2 and the presence of hydroxyl groups which increase the effect on relaxation of the second hydration sphere.[48]

However, macrocyclic ligands and complexes thereof are usually plagued by difficult and expensive syntheses and purifications, therefore their preparation suffers of drawbacks such as low yields and high costs.[49–51]

Mesocyclic ligand (*e.g.* AAZTA), otherwise, present a clever solution to these problems, forming stable chelates with MRI-relevant metals and being easily prepared by inexpensive and simple procedures. Mesocyclic ligands consist in chelating agents bearing one or more ring with less than 11 members. AAZTA (**Figure 1.15**), the first example of this class, is a heptadentate ligand (therefore with q = 2) and shows an optimal relaxivity (7.1 mM^{-1} s^{-1} at 20 MHz and 298 K) for application in MRI.[52]

As stated above, also Fe^{2+} and Fe^{3+}, chelated by a proper ligand, might be useful as MRICAs. Fe^{2+}-DTTACN (**Figure 1.16**) offers an example of this technique, consisting in a mesocyclic chelating agent based on TACN (1,4,7-triazacyclononane) and have been successfully exploited as MRICA in vivo (mouse).[22,53]

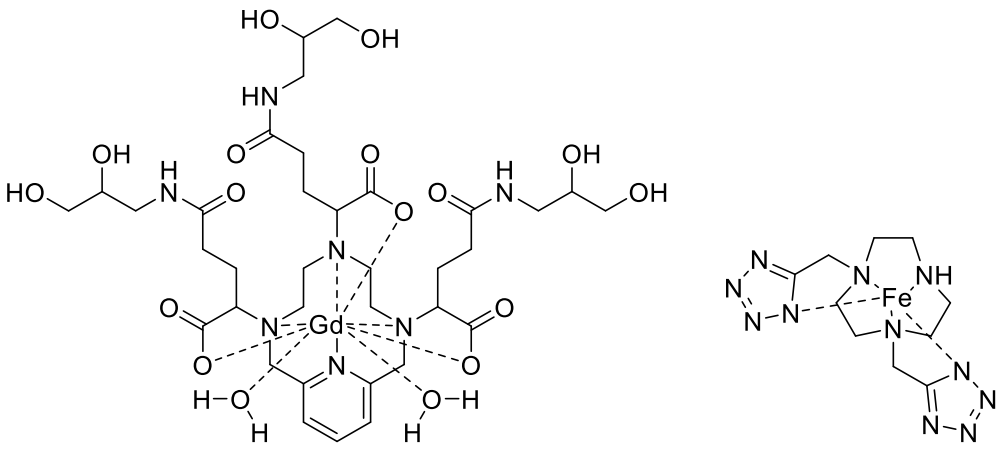

P03277 **Fe-DTTACT**

Figure 1.16. P03277 and Fe-DTTCT, two recently developed MRICAs.

However, being mesocyclic and macrocyclic ligands the main theme of this PhD thesis, they will be treated in more detail in the following pages.

T_2-contrast agents

As stated above, T_2-MRICAs are substances able to show a contrast effect in T_2-weighted images acting as negative CAs (*i.e.* reducing the signal coming from the "highlighted" zone). The effect on the relaxation of water protons, obtained with T_2-MRICAs, can be measured in a very similar way to T_1-MRICAs, *i.e.* following **Equation 1.7**.

$$1/T_2 = 1/T_{2\,0} + r_2[CA]$$

Equation 1.7. T_2 = relaxation time in the presence of a CA, $T_{2\,0}$ = relaxation time of pure water, r_2 relaxivity of the CA, [CA] = concentration of the CA.

Also in this case, higher is the relaxivity of the T_2-MRICAs and more efficient is as a CA. As seen in the previous section, paramagnetic ions might work as T_2-CAs but with limited efficacy, but also the contrary is true. However, some compounds show a very high r_2/r_1 ratio and can be exploited as selective T_2-CAs. They consist in colloidal

materials in which the solid part is constituted by nanoparticles (1 μm – 50 nm) with a superparamagnetic iron oxide core (the active part of the CA) and a biocompatible coating which reduces the overall toxicity of the CA (such as dextran, citrate, oleate etc.). The coating has also the role of avoiding particles aggregation and reducing immunogenicity of the T_2-MRICA.

Moreover, since they exhibit a strong magnetic effect, they generate great magnetic inhomogeneities and for this reason they can be exploited also as CAs in T_2*-weighted images.

An example of T_2-MRICA is ferumoxytol, which have been approved in 2009 for clinical trials as blood pool contrast agent. Ferumoxytol consist in a colloidal solution (isotonic and pH neutral) of nanoparticles with a carbohydrate coated superparamagnetic iron oxide, which is administered as an injection. This CA, being gadolinium-free, might represent an alternative to Gd-based MRICAs in patients with chronic kidney disease, working both as T_1 and T_2 -MRI CA.

However, since this results are very promising, concerning about their pharmacokinetic (*i.e.* elimination of the drug from the body) and their safety are still ongoing issues, making nowadays Gd-based MRICAs the best choice for contrast-enhanced MRI.[22,54]

^{19}F-contrast agents

The CAs so far analysed, act on water protons (physiological) since the MRI apparatus records images on the “channel” of ^{1}H. But as stated above, also other nuclei are suitable to record MRI images and in this section the ^{19}F-based MRI CAs are analysed. Of course, the body only contains trace amounts of fluorine, therefore the background noise is almost zero and the contrast effect is maximised. Nonetheless, a CA is always needed to obtain an image and there are many different solutions. In fact, in principle any non-toxic fluorinated (^{19}F, which has a natural abundance of 100%) compound can be used as ^{19}F-MRICAs, and here some examples are reported without claiming to be complete. (**Figure 1.17**)[22,55,56]

An interesting improvement of ^{19}F-MRICAs is obtained with fluorinated paramagnetic complexes, very similar to those exploited as T_1-MRICAs. In fact, the close proximity

of the paramagnetic centre to fluorine atoms significantly shortens longitudinal and transversal relaxation rates of fluorine atoms with a mechanism similar to the one explained above for water. (**Figure 1.17**)[22,57]

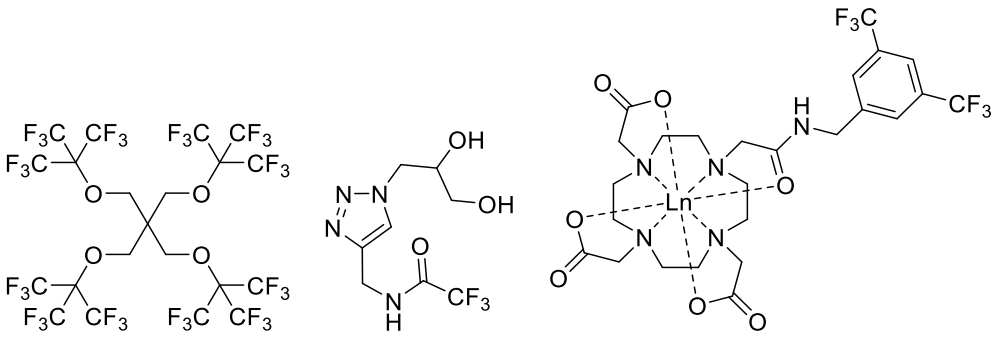

Figure 1.17. Examples of ^{19}F-MRICAs.

Chemical Exchange Saturation Transfer MRICAs

The CEST (Chemical Exchange Saturation Transfer) phenomenon is acquiring a continuous and increasing interest in the field of MRI. It exploits the exchangeable protons of a suitable CA to decrease the intensity of the signal of bulk-water, generating a negative contrast effect. During a CEST experiment, a radiofrequency pulse, at the frequency of the exchangeable proton, saturates the latter and meanwhile the acquisition is running on the usual frequency of water. Since the saturated proton exchanges with the water protons, the saturation is transmitted too and spreads all over the bulk, reducing the intensity of the water NMR signal. The fastest the exchange and the farther are the exchangeable proton and the water signals, the higher is the contrast effect. (**Figure 1.18**)

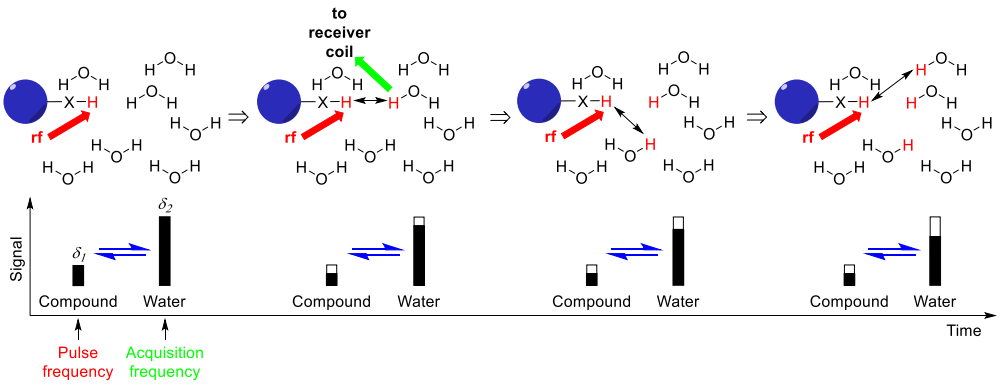

Figure 1.18. Schematic representation of CEST principles. δ_1 and δ_2 are respectively the chemical shift of the exchangeable proton of the CA and of water.

All compounds with exchangeable protons are potential CEST MRI CAs, in particular those bearing an amide, a hydroxy, an amino group or similar. Therefore, metabolites physiologically present in cells (*i.e.* proteins, amino acids, lactic acid) could do the trick as well, but unfortunately, they are naturally too diluted and CEST MRI CAs are usually effective only in high concentration.[58] However, glucose for example, administered intravenously, has been successfully exploited as a CEST MRI CA thanks to its exchangeable OH protons. Cancer cells tend to accumulate nutrients, and glucose as well, faster than healthy ones and therefore its use as CEST MRI CA has led to a significant contrast effect in the imaging of tumours (such as glioblastoma) in both mice and human. Obviously, glucose has been already approved for intravenous administration in human and it is perfectly biocompatible, biodegradable and tolerated.[59,60] (**Figure 1.19**)

“Drug repositioning” is an important issue in CEST MRI, since it is a novel and very versatile technique requiring only an exchangeable proton and a well-established safety profile in human even in high doses. For example, iopamidol, a CT CA approved for human use, meets all these requirements and presents also two different amide protons thanks to which it is sensible to tiny pH variation of tissues. A different pH value can in fact dramatically affect (reduce or increase) the proton exchange rate and the CEST effect. Pathologic tissues, such as tumours or ischemic lesions, are usually characterised by an acidic extracellular pH mainly due to hypoxia and necrosis

and for this reason, iopamidol has been used as a contrast agent in murine tumor model (*i.e.* breast cancer) with promising results.[61,62] (**Figure 1.9**)

Complexes of paramagnetic ions offer a great improvement in the CEST technique (paraCEST), in fact the water protons directly bound to the metal centre or exchangeable protons in the second sphere, possess a greater distance, in terms of chemical shift, from the bulk water signal then any diaCEST CA. DOTAM complexes of lanthanides (Nd^{3+}, Eu^{3+}, Tb^{3+}, Tm^{3+}, Dy^{3+} and Yb^{3+}) and of transition metals (Fe^{2+}, Co^{2+}, Cu^{2+}, and Ni^{2+}) show a strong CEST effect and have been also exploited as a pH sensible probes.[63] (**Figure 1.19**)

Finally, CEST CAs, suitably functionalised with redox responsive moieties, may serve as oxygen or NADH concentration sensors. For example, the Eu^{3+} complex of DO2A-$(gly)_2$ with two *N*-methylquinolinium residues, as redox responsive moieties, have shown interesting CEST properties, increasing the contrast effect as the NADH concentration increase as consequence of a variation in the coordination sphere of the paramagnetic ion.[22,64] (**Figure 1.19**)

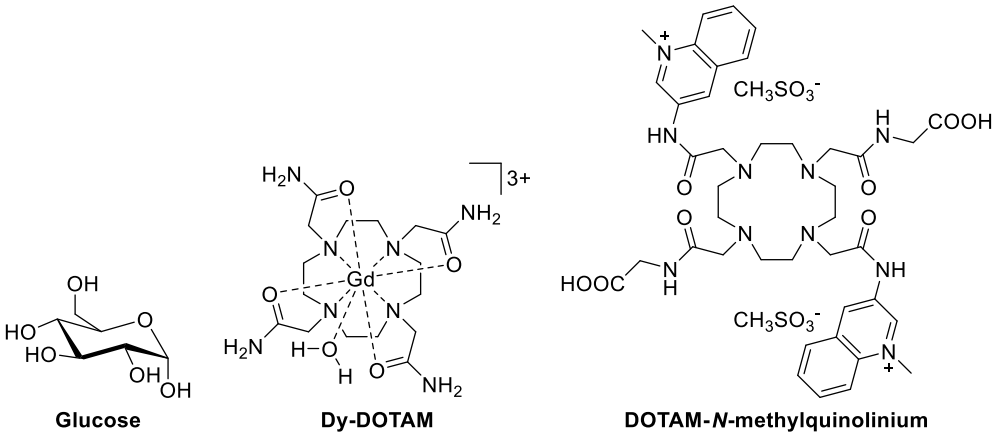

Figure 1.19. Selected examples of CEST MRICAs.

Hyperpolarised MRICAs

As explained above, MRI suffer from the limitation that the signal (deriving from relaxing nuclei) arises from a small excess of nuclei aligned parallel (ground state) to B_0. This is an equilibrium condition, but if one could break this equilibrium preparing a

compound with a great excess of spins in the ground state or in the excited state, the signal, deriving from the relaxation of all of them, would be significantly higher. This phenomenon, called hyperpolarization, can be obtained in four different ways, *i.e.* optical pumping, dynamic nuclear polarization, parahydrogen-induced polarization and signal amplification by reversible exchange.

In optical pumping light is used to raise nuclear spins from a lower energy level to a higher one, obtaining in this way the population (of spin) inversion (making them equally aligned) typical of hyperpolarised systems.[22,65] (**Figure 1.20**)

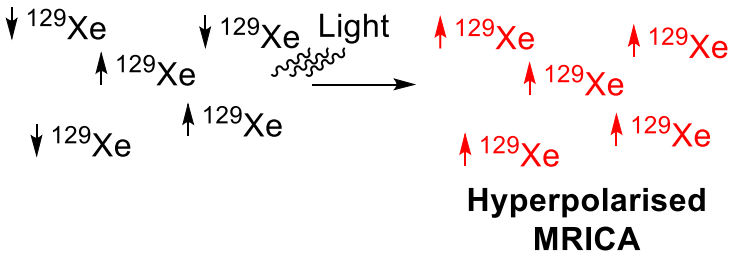

Figure 1.20. Example of optical pumping.

In dynamic nuclear polarization, hyperpolarization is obtained by means of a stable radical (*e.g.* trityl) cooled to 1 – 5 K in a strong magnetic field (3 – 5 T). In these conditions radical electron spins are all aligned to the external magnetic field and this hyperpolarisation can be transferred to a ^{13}C atom using a microwave radiation close to the magnetic resonance frequency of the radical electron spin.[66–68] (**Figure 1.21**)

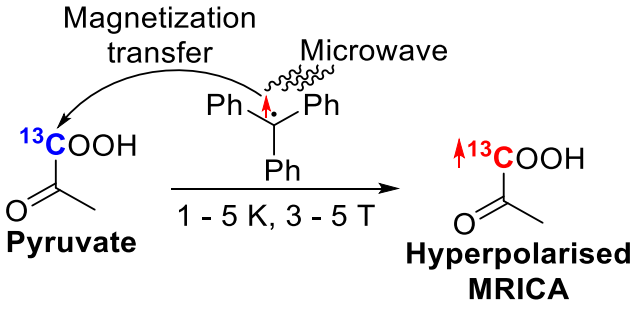

Figure 1.21. Example of dynamic nuclear polarization.

Parahydrogen-induced polarization, instead, exploits parahydrogen (H_2 molecules with the two atoms nuclear spin aligned antiparallel to each other, therefore hyperpolarised) to hydrogenate an unsaturated substrate. These hydrogenation reactions must be really fast and normally exploit homogenous catalysis and usually rhodium or iridium-based complexes as catalysts. Then, the magnetisation (*i.e.* the hyperpolarization coming from parahydrogen) is transferred to a nearby ^{13}C atom through *J*-coupling, being $J_{H\text{-}H}$ and $J_{H\text{-}C}$ values close. The selective magnetisation transfer from ^{1}H to ^{13}C can be obtained by eliminating quickly all external magnetic fields acting on the ^{13}C-marked parahydrogenated substrate and then restoring slowly all external magnetic fields (diabatic-adiabatic magnetic field cycling). This magnetization transfer can be obtained also with specific radiofrequency pulses or by a combination of these and diabatic-adiabatic magnetic field cycling.[69–71] (**Figure 1.22**)

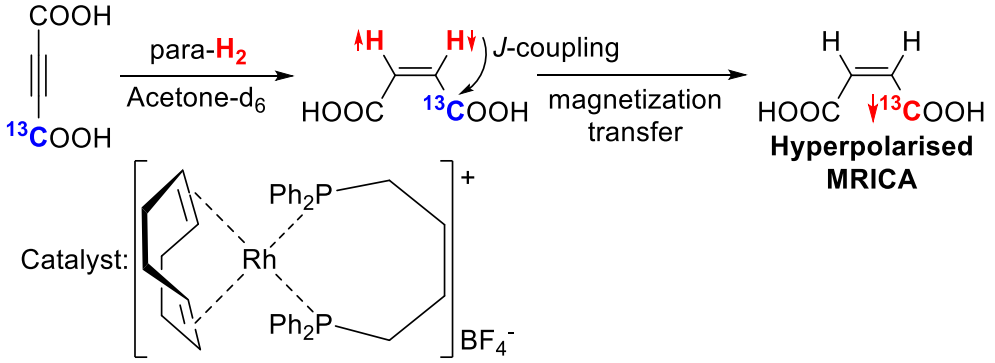

Figure 1.22. Example of parahydrogen-induced polarization.

Signal amplification by reversible exchange involve the coordination of a substrate (usually a pyridine) to an organometallic catalyst. Also here, parahydrogen coordinates the catalyst as well, transferring its hyperpolarization to the substrate in a catalytical manner.[72,73] (**Figure 1.23**)

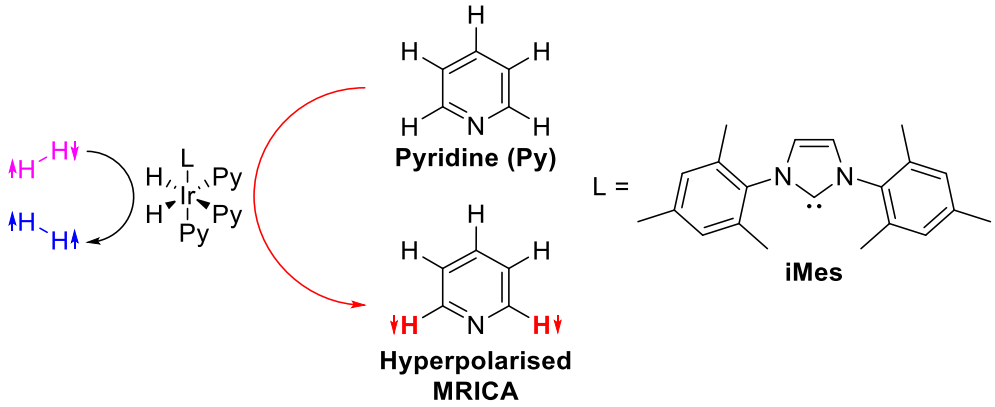

Figure 1.23. Example of signal amplification by reversible exchange

After hyperpolarization, the contrast agent might be purified, dissolved in an appropriate solvent, brought nearby physiological temperature and injected to the patient very quickly, to limit the relaxation of the hyperpolarized molecule. Images can be recorded with normal a MRI apparatus tuned on the resonance frequency of the hyperpolarised nucleus (*i.e.* in examples above, ^{13}C and ^{129}Xe).

Dynamic nuclear polarization has been used to prepare hyperpolarised pyruvate ^{13}C-labeled in position 1. Since tumours present continuous growth and constant nutrients supply, hyperpolarised pyruvate (and eventually its metabolites still hyperpolarised) accumulates preferentially in the tumour increasing the contrast in this region. Being pyruvate an important and central physiologic metabolite, it is safe to use in human. (**Figure 1.21**)

In principle, every NMR-active nucleus with a long T_1 (to ease workup of the contrast agent) can be exploited as hyperpolarised MRI CA, and this is the case of ^{13}C and ^{129}Xe.

In fact, ^{129}Xe, hyperpolarised by optical pumping, is clinically approved as MRI CA for lung imaging and it is administered to the patient by inhalation.[22,65] (**Figure 1.20**)

Ultrasound Sonography

Ultrasound Sonography (US) is a very common and non-invasive imaging technique that provides real-time anatomical images in cross sections of soft tissues. US exploits ultrasounds, *i.e.* soundwaves with frequencies higher than 20 kHz, but clinical diagnostic US scanners use frequencies between 1 MHz and 20 MHz.

During an US exam, ultrasound pulses are sent through the patient's body which partially absorbs and partially reflect ultrasound waves (different tissues absorb and reflect differently) creating echo effects. The latter, once analysed and processed, allows to reconstruct a 2D grayscale image with intensity as a function of echo return. (**Figure 1.24**)

Resolution of US images improves increasing the ultrasound frequency, while depth penetration decreases, therefore the choice of the right frequency allows the operator to find a good balance between resolution and depth penetration. This phenomenon is caused by the fact that soundwaves with a short wavelength interact better with the living matter and therefore they are less reflected.

US presents several advantages among other imaging techniques, such as low cost, safety (no ionising radiation are required), and ease of use and implementation.[74,75]

In some US exams, US CAs are exploited to improve US imaging. US CAs are prepared with materials characterized by different acoustic properties if compared to human tissues. The most common US CAs are intravenously injections of small air or gas bubbles (microbubbles) that improve the doppler signal from blood vessels and the sensitivity of US technique in general. These microbubbles are typically coated with lipids or biopolymers to enhance reflection and signal-to-noise ratio of blood.[76] The external coating might present vector molecule (such as proteins) which can target the US CA to a specific cellular type or tissue (such as inflamed tissues).[77,78] US CAs are successfully clinically applied, for example, to study angiogenesis and to image microcirculation.[76] As an innovative example of general non-targeted US CA we mention sulphur hexafluoride microbubbles, with a phospholipidic coating, which have been approved as US CA for clinical use in 2014.[79]

Figure 1.24. A) Schematic illustration of an US apparatus. B) 2D US image of a human foetus. C) 3D US image of a human foetus.[2,80]

Optical Imaging

Optical Imaging comprehends numerous non-invasive imaging modalities applied in the diagnostic and biomedical field to detect pathological changes, employing different wavelengths of light (UV, visible and near-IR), absorbed, emitted or scattered by molecules, cells and tissues.[81] (**Figure 1.25**)

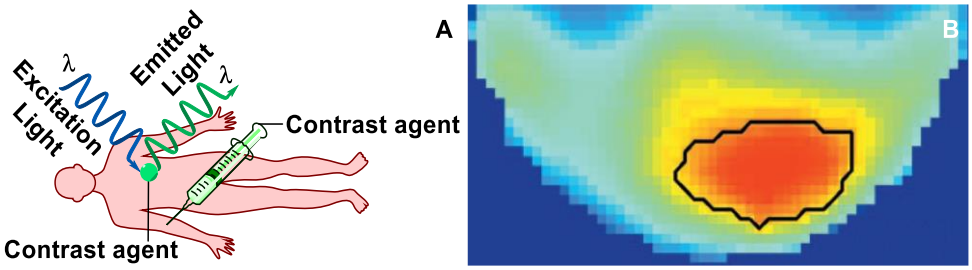

Figure 1.25. A) Scheme of an OI apparatus. B) OI image based on haemoglobin concentration of breast cancer (the mass is circled in black).[82,83]

Optical imaging is really an innovative technique that exploits light to excite a contrast agent, administered to the patient, and then the CA releases back the photons absorbed (usually with less energy, *i.e.* fluorescence) which are captured by the optical imaging apparatus, analysed and transformed in an image.

OI CAs can be endogenous (*i.e.* oxygenated or deoxygenated haemoglobin and cytochromes) or exogenous molecules (*i.e.* fluorescent dyes and lanthanide complexes).[2]

Chelating agents for lanthanides (*i.e.* DOTA-like, DO3A-like, AAZTA-like derivatives) bearing one or more side arms on their backbone with a fluorochrome can be applied as OI CAs or as OI/MRI CAs if the lanthanide is gadolinium.[84] Lanthanides-based OI CAs offers long luminescent lifetime thanks to the antenna (*i.e.* the above cited fluorochrome) that capture the light energy, promotes its electrons to the triplet excited state, which transfers its energy to the metal centre. Moreover, lanthanides (particularly Eu and Tb) present suitable and large fluorescence emission in the visible region generated from electronic transition in the non-bonding 4*f* electron shell. Here, chelating agent must present a C.N. > 8 to avoid the leaching of toxic metal and the coordination of water molecules that could quench the fluorescence. (**Figure 1.26**)

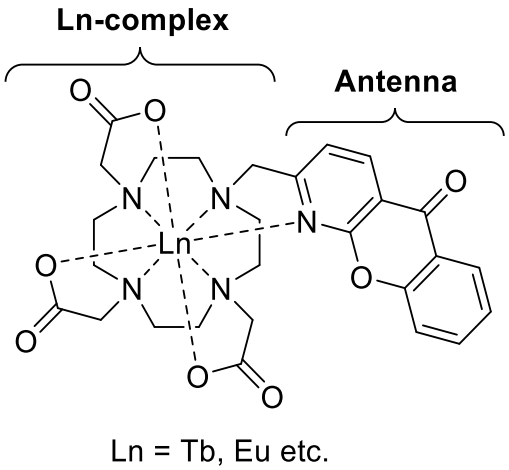

Figure 1.26. Lanthanide-based OICA.[85]

OI can be combined also with all the other imaging technique to obtain more detailed images of a target organ.[2]

Moreover, many fluorescent dyes are reported in the literature and some of them are currently applied in fluorescent imaging applications, such as indocyanine green (ICG) (**Figure 1.27**), which is approved for *in vivo* use. Indocyanine green and other cyanine

derivatives have been synthesized and studied as OI CAs for the visualization of cancer cells.[86]

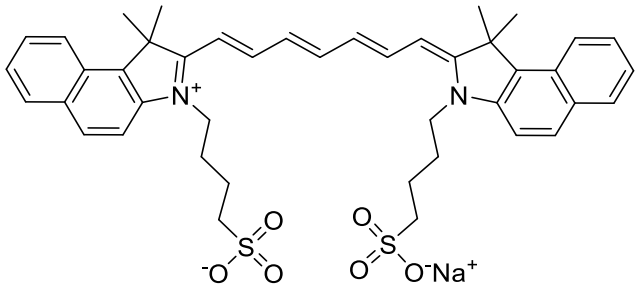

Figure 1.27. Indocyanine green.

OI can image the body at different levels, being useful to acquire images of organs and tissues, but also to track cellular and molecular changes in the body. The main disadvantage of OI is the scarce depth penetration of light, ranging from < 1 mm for UV to few inches for IR.[87]

Positron emission tomography

Positron emission tomography (PET) is an innovative technique, which exploits positron-emitting radionuclides with short half-life to obtain images. In fact, PET CAs are necessary to obtain PET scans since, luckily, our organism does not emit positrons spontaneously. PET radiolabeled contrast agents are administered intravenously at low concentrations and emit positrons that annihilate with neighboring electrons generating two opposite collinear γ-rays. Positron-emitting nuclei present an excess of protons, which makes them unstable. That instability is rectified by transforming a proton into a neutron, a positron and a neutrino. (**Figure 1.28**)[1,2]

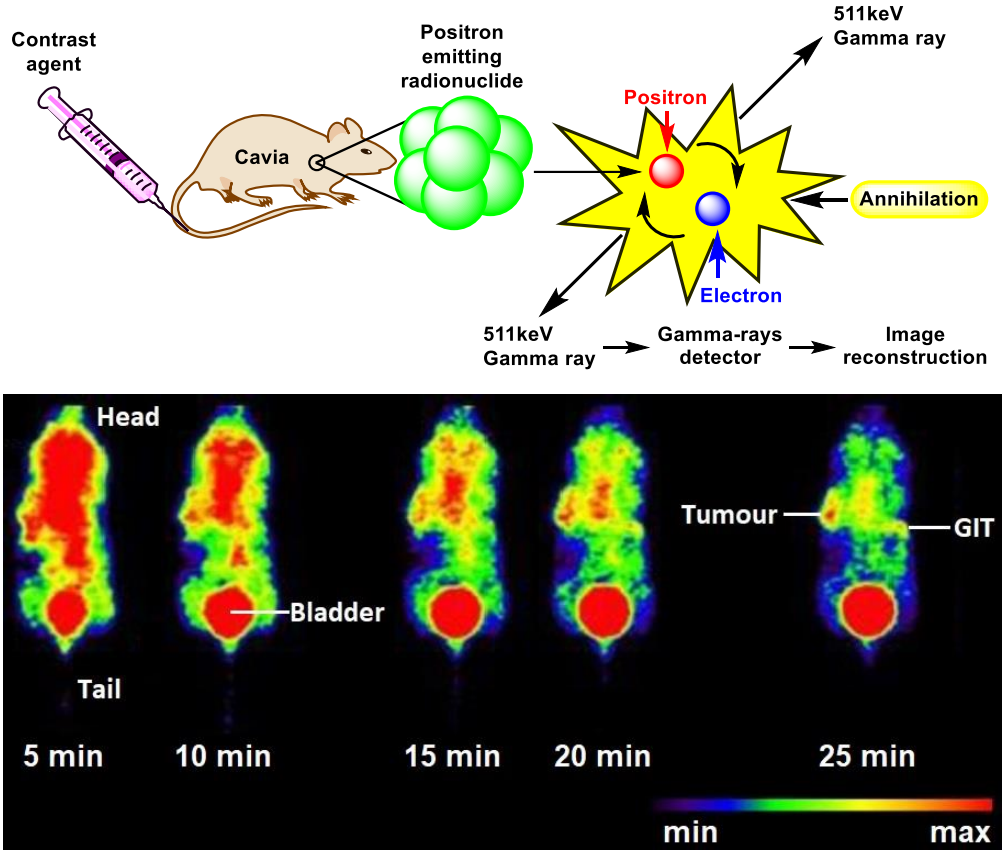

Figure 1.28. Schematic representation of a PET apparatus (top) and PET scans (bottom) acquired on a mouse xenografted with a A431-CCK2 positive tumour after administration of a PET CA at different times. Here the CA consist in the gallium complex of an AAZTA-like BFCA (bifunctional chelating agent) linked to a vector molecule, *i.e.* a minigastrin analogue (*vide infra*).[88]

Several detectors, placed around the patient, collect the pair of rays emitted by the radionuclide and reconstruct the emission point projecting a 2D or 3D image of patient's body.[1,2]

PET imaging finds many diagnostic applications including the detection of tumors and the diagnosis of neurological and psychiatric disorders, such as Alzheimer's and Parkinson's disease.[89]

“Non-metal” PETCAs

The first PET-relevant radio nuclides exploited in research and clinic were "non-metal" isotopes such as ^{11}C, ^{13}N, ^{15}O, ^{18}F, generated by a cyclotron, *i.e.* a particle accelerator that speeds up protons thanks to a magnetic field.[90,91]

These radioisotopes are usually introduced in natural-like molecules and these probes and/or their decaying products are naturally occurring biomolecules, therefore PET CAs do not alter the physico-chemical and biochemical properties of tissues (except for ionizing radiations, obviously).[92]

PET CAs work as functional tracers, allowing *in vivo* diagnostic studies or the localization of pathological tissues following their accumulation. in fact, metabolized radiopharmaceuticals are accumulated in the “hotspot” (*e.g.* a tumor) and emit positrons or γ rays which are registered by tomographs.

These radionuclides present covalent bonds to the rest of the contrast agent, therefore, for their synthesis, they require common reactions and purification procedures. The latter must be quick enough to avoid excessive nuclear decaying (which leads to inefficacy) and accurate enough to fulfill (as any other drugs) the strict rules of good manufacturing practices.

Actually, ^{18}F is the clinical gold standard since its availability, ease of introduction in organic molecules and its half-life of 110 min, a good compromise between a proper (not excessive) radiation exposure for the patient, and a sufficient amount of time for operators to react and workup the contrast agent. One of the most widely used PET contrast agent is [^{18}F]-fluorodeoxyglucose, also known as ^{18}F-FDG. (**Figure 1.29**) It is used to monitor glucose metabolism and is very important for the clinical diagnosis of tumors, considering that cancer cells are quite hungry for sugars.

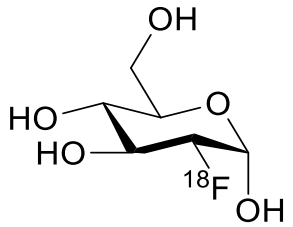

Fludeoxyglucose (^{18}F)

Figure 1.29. Structure of 2-[^{18}F]-fluoro-deoxy-D-glucose.

Also ^{11}C (another positron emitter isotope) has found valuable diagnostic applications (*vide infra*), but it is not clinically relevant as ^{18}F since its shorter half-life of 20.3 min.[1,2,93]

"Metal" PETCAs

Recently, metal radioisotopes have found many applications in PET imaging, considering that ^{11}C and ^{18}F-labelled contrast agents display, after all, a very short half-life and difficult preparation and purification procedures.

In fact, ^{61}Cu, ^{62}Cu, ^{64}Cu, ^{64}Ga, ^{67}Ga, ^{68}Ga, ^{44}Sc, ^{86}Y, ^{89}Zr and many other isotopes of metal ions are used to prepare PET CAs to study biochemical processes. They possess a longer half-life and they may also be easily bound to a vector molecule through complexation (*vide infra*).[2,94,95]

Two gallium isotopes are currently available for clinical applications, ^{67}Ga ($t_{1/2}$ = 78.3 h by electron capture) has a sporadic role in scintigraphy while ^{68}Ga ($t_{1/2}$ = 67.7 min, β^+ emission) has found, in last decade, vast clinical applications. This is mainly due to the broad diffusion of benchtop ^{68}Ge/^{68}Ga generators providing $^{68}Ga^{3+}$ in acidic aqueous solution[96] and to the high clinical value of ^{68}Ga-based (PET) radiopharmaceuticals[97]. Moreover, ^{68}Ga has a high positron yield (89%, 1.9 MeV)[98] and its half-life matches the pharmacokinetics of low molecular weight radiopharmaceuticals.

^{68}Ge/^{68}Ga generator, necessary for the synthesis of these innovative PET CAs exploits the nuclear reactions depicted in **Figure 1.30**.

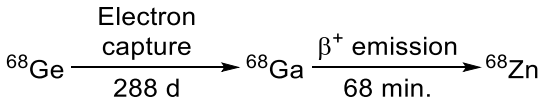

Figure 1.30. Reaction happening in benchtop $^{68}Ge/^{68}Ga$ generators.

Unlike “non-metal” PET CAs, the introduction of a radioactive metal ion (such as $^{68}Ga^{3+}$) in a diagnostic carrier (say a chelating agent) consists in a simple one-step reaction (a complexation reaction).[99,100] The ideal chelator must show a high selectivity and affinity for the metal ion, a rapid complexation kinetics to avoid an excessive decay of the radionuclide and high kinetic inertness to avoid dissociation of the complex in the organism before excretion.

1,4,7,10-tetraazacyclododecane-1,4,7,10-tetraacetic acid (DOTA) is, to date, the gold standard for the preparation of metal PET CAs, many DOTA-like chelating agents are commercially available, but usually their Ga^{3+}-complexes are formed slowly.[101] Many other chelating agents have been exploited to prepare PET CAs, such as NOTA, HBED and AAZTA[98,102–105] (**Figure 1.31**)

In particular, AAZTA[52] and its derivatives (such as DATA and DATA-like chelating agents) (**Figure 1.31**) possess promising properties for the preparation of innovative PET CAs. In fact, they quickly (in less than 15 minutes) and quantitatively form, at room temperature, thermodynamically stable complexes with gallium[106] scandium and other PET-relevant metals.[107]

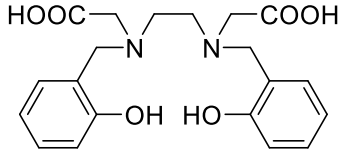

HBED

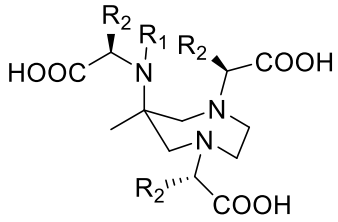

DATA = R_1 = CH_3, R_2 = H.
DATA-like = R_1 = CH_3 or Ph, R_2 = H or CH_3

Figure 1.31. HBED, DATA and DATA-like chelating agents.

Single-photon emission computed tomography

SPECT imaging exploits, as CAs, radioactive isotopes properly trapped in a chelating agent to limit their toxicity. After administration to the patient, the radiopharmaceutical (and metabolites thereof) is accumulated in the points of interest, emits γ rays which are registered by γ cameras, rendering an image to the operator. (**Figure 1.32**)

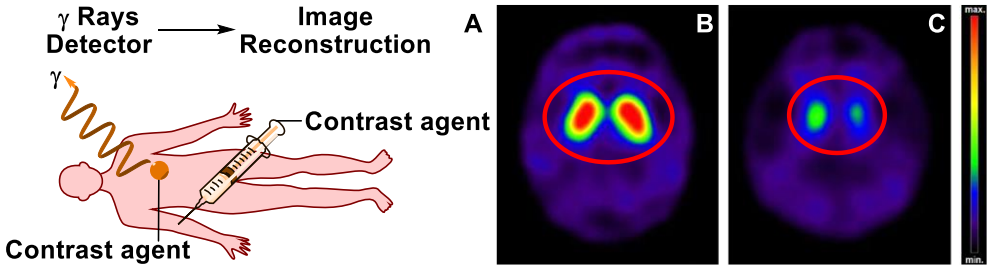

Figure 1.32. A) Schematic representation of a SPECT apparatus. B) SPECT image of the brain of a control patient after administration of a SPECT CA (ioflupane, *vide infra*) selective for the dopamine system. C) SPECT image of the brain of a patient affected by Parkinson's disease treated with the same CA as in B.[108]

To obtain good quality images, the energy emitted by the radionuclides must be between 100 and 250 keV. During a SPECT clinical exam multiple 2D projections from multiple angles are acquired and sent to a computer dedicated to the reconstruction of images. If a 360° rotation is performed, it is possible to obtain an optimal 3D reconstruction. However, SPECT imaging has a lower sensitivity and resolution than PET.

Obviously, SPECT imaging mandatory requires a CA to acquire images and, as stated for PET CAs, also SPECT CAs can be divided into two categories, "Non-metal" and "Metal" SPECT CAs.

As an example of non-metal based SPECT CAs, we mention ioflupane (^{123}I), a clinically approved cocaine/dopamine analogue, which targets the dopaminergic system in the brain and is particularly useful for Parkinson's disease diagnosis. Here

the radionuclide is ^{123}I, which decays by electron capture emitting a γ ray. (**Figure 1.33**)

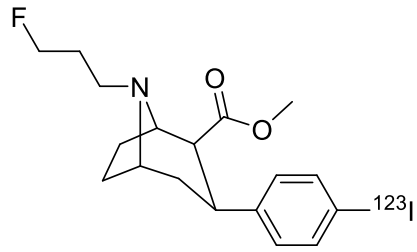

Ioflupane (^{123}I)

Figure 1.33. Ioflupane (^{123}I) is a clinically approved cocaine/dopamine analogue and a SPECT CA selective for the dopaminergic system used for Parkinson's disease diagnosis.[108]

"Metal" SPECT CAs, instead, represent an innovative class of CAs and present the same advantages explained for analogues PET CAs, *i.e.* easy one-pot synthesis, tunability and many others.

Many metal isotopes emit useful γ rays that can be used in clinical SPECT imaging, such as ^{99m}Tc, ^{67}Cu, ^{67}Ga, ^{90}Y, ^{111}In and ^{201}Tl, and in particular their corresponding ions, carefully complexed by chelating agents, can form many different γ emission complexes useful as SPECT CAs.[109]

The most important element used for SPECT imaging is ^{99m}Tc which emits γ rays (decaying to ^{99}Tc) with the energy of 140 keV, optimal for the detection with γ cameras. Although ^{99m}Tc short half-life (about 6 hours) might represent a limitation for its clinical application (in fact long complexation procedure could dramatically affect the efficacy of the radiotracer), the existence of a dedicated generator makes it easily available for diagnostic purposes. ^{99m}Tc-based radiopharmaceuticals are exploited to image many major diseases, *i.e.* to detect bone metastases or hidden fractures, using as CA a ^{99m}Tc-diphosphonate (such as technetium (^{99m}Tc) medronate) which is accumulated in the bones.

Other important clinically approved ^{99m}Tc-based radiopharmaceuticals are technetium (^{99m}Tc) exametazime and technetium (^{99m}Tc) bicisate (used in the imaging of cerebral

blood flow for example in patients with stroke) and technetium (^{99m}Tc) sestamibi (exploited for the imaging of myocardial perfusion and cancer).[110] (**Figure 1.34**)

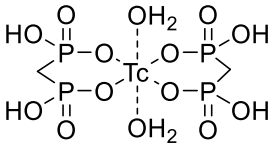

Technetium (^{99m}Tc) medronate

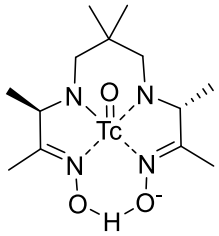

Technetium (^{99m}Tc) exametazime

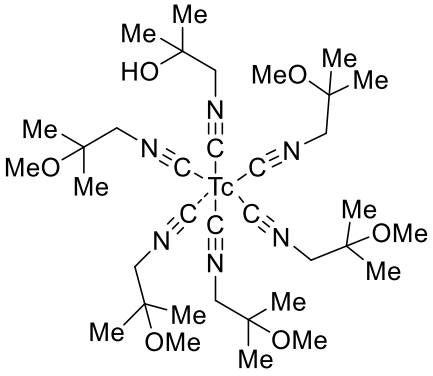

Technetium (^{99m}Tc) sestamibi

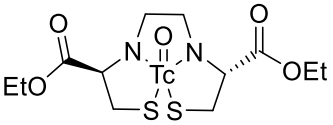

Technetium (^{99m}Tc) bicisate

Figure 1.34. Technetium-based clinically approved radiopharmaceuticals.

Another SPECT-relevant metal-based radionuclide is ^{67}Cu. The divalent ion Cu^{2+} shows a rich coordination chemistry exploited in a wide variety of complexes with nitrogen-based ligands, including cyclen (1,4,7,10-tetraazacyclododecane) derivatives. This ion has coordination numbers ranging from 4 to 6 and therefore Cu^{2+}-complexes can assume different geometries ranging from square, square pyramidal, trigonal bipyramidal to octahedral shapes. Several $^{67}Cu^{2+}$-complexes have been designed and synthesized to detect tumors with SPECT imaging.[111]

Also $^{67}Ga^{3+}$ can be exploited for the preparation of chelates used as SPECT CAs, thanks to the availability of this nuclide through a dedicated generator, preparing

complexes with hexadentate ligands that can satisfy the requirements of this hard trivalent ion.[112]

AAZTA, DOTA and DO3A derivatives are currently finding vast applications as SPECT CAs thanks to their ability to form stable complexes with most SPECT relevant metal ions in a reasonable amount of time, compatible with the usually short half-lives of these isotopes.

Bioconjugation

Targeted CAs are gaining great research and clinical importance in the last few years since their impressing diagnostic and therapeutic value. They present many differences if compared to classical, general, and simple CAs, such as their complex structure and their really high selectivity. In fact, classical CAs are very useful for general purpose, for example body scans, molecular imaging of a vast organ such as the brain and so on. If the structure of the CA is analogous to a physiological substance, classic CAs can become selective for a particular anatomic region (*i.e.* the bone). But targeted-CAs bring selectivity to the next level, through a very general technique called bioconjugation, they ensure a high contrast effect in patients with a particular (usually pathological) molecular pattern. The latter usually correlate with an important pathology (such as cancer) which is highlighted with a selectivity and a contrast effect infinitely higher than classical CAs.

A general structure of a targeted CA is represented in **Figure 1.35**, a metal (*e.g.* radionuclide, paramagnetic etc.) is chelated by a bifunctional chelating agent (BFCA, a chelating agent with a reactive functional group) bound, by means of a reactive linker to a vector. When administered to a patient, the targeted-CA searches for its target in the body, strongly binds it and, by means of classical imaging apparatus, it is possible to obtain images of the spots of the body containing that particular target strongly highlighted.

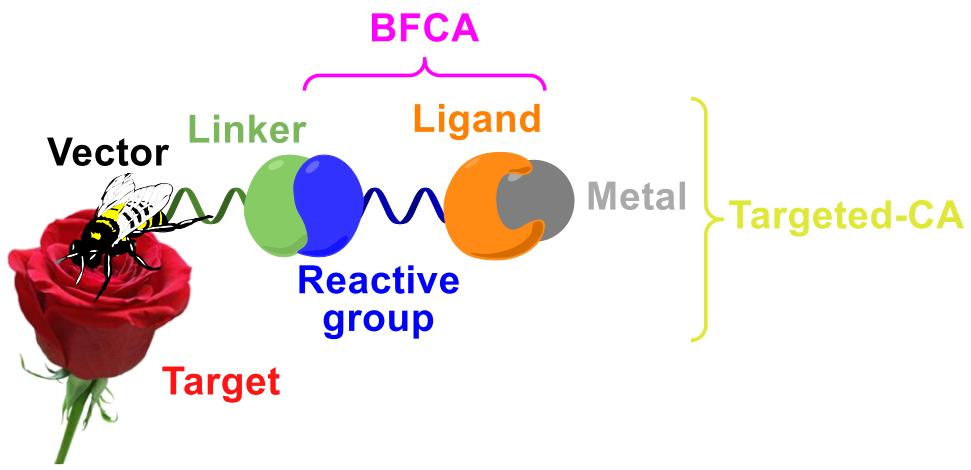

Figure 1.35. Scheme of a targeted CA bound to its specific physiopathological target.

In the literature there are plenty of examples of targeted-CAs, and some of them have become clinically approved in the last few years.[1,51,113]

Since a comprehensive review of the subject could not be done here, the discussion will be limited to the most relevant examples of targeted-CAs. It will show how their structures match with **Figure 1.35**, hoping that it could serve as a general example able to represent also other targeted-CAs reported in the literature.

The attention will be focused on two recently approved targeted-CAs, *i.e.* DOTATATE (approved by FDA in 2018) and DOTATOC (approved by FDA in 2019).

They are administered to the patient as complexes of radionuclei including ^{68}Ga, ^{177}Lu, ^{64}Cu and ^{90}Y and are approved in the diagnosis and therapy of various malignancies such as neuroblastoma and brain, gastrointestinal, breast, lung, and lymphatics cancer. In fact, as thoroughly explained previously, DOTATATE and DOTATOC complexes with the above mentioned radionuclei can be exploited as targeted-PET CAs but also as drugs for targeted-radiotherapy. The latter is a great and recent breakthrough in cancer treatment: drugs for targeted-radiotherapy consist in radiometal chelates bound to a vector selective for a cancer-associated molecular signal (*i.e.* overexpressed hormones receptors). In a similar way to targeted-CAs, when administered to the patient, drugs for targeted-radiotherapy seek for their molecular tumour-associated target, strongly bind them delivering selectively just

there, where needed, a high dose of radiation provided by radionuclei.[114] DOTATATE and DOTATOC share a common structure, they consist in a radiometal ion (among those mentioned above) chelated by a DOTA-like BFCA. DOTA forms stable chelates with most transition metals, ensuring that the metal, by means of the chelating agents, stays strongly bound to the vector, securing the targeted delivery of the radiotherapy dose. This DOTA-like BFCA chelates the metal with the four "cyclen" amine groups, with three acetic acid residues and with the carbonyl group of the amide. The vector molecule instead consists in a somatostatin analogue (octreotate for DOTATATE and octreotide for DOTATOC) selective for somatostatin receptors overexpressed by the malignancies listed above. The linker between the BFCA and the vector molecule is represented by an amide group. The latter is obtained by the condensation reaction between an unprotected carboxylic acid (the reactive group) on the BFCA and an unprotected amine group on the vector which is obtained by classical supported Fmoc peptides synthesis. The condensation reaction between the vector and the BFCA is promoted by a classical stoichiometric condensing agent such as HATU.[115–118] (**Figure 1.36**)

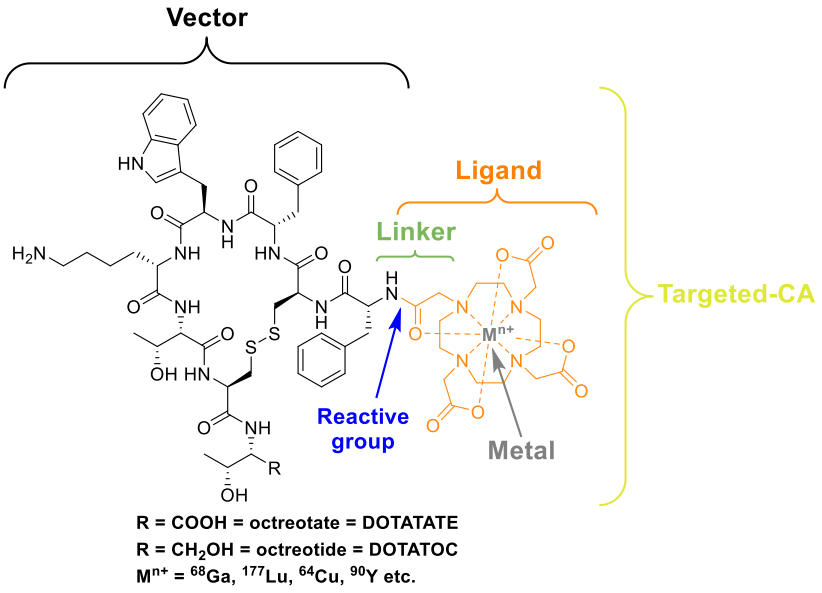

Figure 1.36. DOTATATE and DOTATOC, recently approved targeted PETCAs and drugs for targeted radiotherapy.

However, the synthesis of BFCA and their conjugation to vectors of biomedical interest is treated in more detail in **Chapter 4**.

As stated above, here just two examples of targeted-CAs are presented, in particular two PET targeted CAs which are also approved for targeted radiotherapy. However, bioconjugation can be exploited to prepare targeted CAs also for MRI, SPECT and for multimodal imaging (*i.e.* PET/CT).[119]

Moreover, other types of chelating agents can be exploited to prepare BFCAs (*i.e.* AAZTA and DTPA-like ligands) and many other vectors are suitable for the preparation of targeted-CAs and drugs for targeted radiotherapy (*i.e.* oligonucleotides, small molecules, metal sensors and many other).[1,51,113]

Theranostics

Theranostics consist in an innovative approach to the diagnosis and therapy of many illnesses since it exploits the same (or almost the same) molecular tool to image and simultaneously (or immediately after) treat the pathology.

The target of a theranostics agent is a pathology or a pathology-associated antigen, for example a protein overexpressed by a tumour.

The “take aim” of theranostics consist in a targeted-CA selective for the pathology-associated antigen, for example a targeted PET CA.

The magic bullet here is, instead, a targeted drug for the pathology, for example a radiometal complex labelled with a vector molecule selective for the pathology-associated antigen.

The tight succession of diagnosis and therapy and the targeted nature of theranostic agents have shown many clinical benefits, such as early diagnosis, higher efficacy and fewer side effects if compared to classical non targeted therapies.

An example of a theranostic agent has been reported in the previous section, *i.e.* ^{68}Ga/^{177}Lu-DOTATATE. In fact, the same vector-bound chelating agent (DOTATATE) can serve as both PET CA, in the form of ^{68}Ga-complex, and as drug for targeted radiotherapy, in the form of ^{177}Lu-complex. This theranostic agent is very valuable for neuroendocrine tumours and DOTATATE and DOTATOC metal complexes are nowadays the only two clinically approved theranostic agents, but many preclinical

and clinical studies are currently in progress. Here, the target is the somatostatin receptor (the pathology-associated antigen overexpressed by the tumour) and the magic bullet is the radiometal complex linked to a somatostatin analogue (octreotide or octreotate, the vector).[120]

Another example of theranostic pair consist in ^{68}Ga/^{177}Lu PSMA-617, a theranostic agent currently in phase II clinical trials for the treatment of prostate cancer.[119,121,122] It consists in a ^{68}Ga or ^{177}Lu-complex of a DOTA-like BFCA linked through an amide bond to a PMSA (Prostate-specific membrane antigen) inhibitor named PMSA-617.[123] PMSA is a transmembrane protein with enzymatic activity (*i.e.* glutamate-preferring carboxypeptidase) overexpressed in prostate cancer and is the target of the theranostic agent ^{68}Ga/^{177}Lu PSMA-617.[124] (**Figure 1.37**)

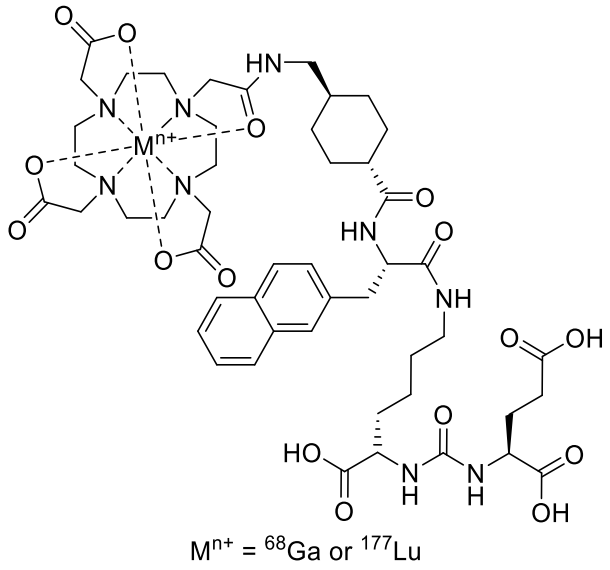

Figure 1.37. Structure of theranostic agent ^{68}Ga/^{177}Lu PSMA-617.[123]

As explained above, also here the ^{68}Ga-complex acts as PET CA and the ^{177}Lu-complex is the therapeutic agent, while PSMA-617 is the vector molecule.[123]

References

(1) Weissleder, R. *Molecular Imaging: Principles and Practice*; PMPH-USA, 2010.

(2) James, M. L.; Gambhir, S. S. A Molecular Imaging Primer: Modalities, Imaging Agents, and Applications. *Physiological Reviews* **2012**, *92* (2), 897–965. https://doi.org/10.1152/physrev.00049.2010.

(3) Cheng, Z.; Yan, X.; Sun, X.; Shen, B.; Gambhir, S. S. Tumor Molecular Imaging with Nanoparticles. *Engineering* **2016**, *2* (1), 132–140. https://doi.org/10.1016/J.ENG.2016.01.027.

(4) Harisinghani, M. G.; Barentsz, J.; Hahn, P. F.; Deserno, W. M.; Tabatabaei, S.; van de Kaa, C. H.; de la Rosette, J.; Weissleder, R. Noninvasive Detection of Clinically Occult Lymph-Node Metastases in Prostate Cancer. *N. Engl. J. Med.* **2003**, *348* (25), 2491–2499. https://doi.org/10.1056/NEJMoa022749.

(5) Gourtsoyiannis, N.; McCall, I.; Reiser, M.; Silberman, B.; Bischof Delaloye, A.; Carrió, I.; Cuocolo, A.; Knapp, W. White Paper of the European Society of Radiology (ESR) and the European Association of Nuclear Medicine (EANM) on Multimodality Imaging. *Eur Radiol* **2007**, *17* (8), 1926–1930. https://doi.org/10.1007/s00330-007-0698-7.

(6) L. Pimlott, S.; Sutherland, A. Molecular Tracers for the PET and SPECT Imaging of Disease. *Chemical Society Reviews* **2011**, *40* (1), 149–162. https://doi.org/10.1039/B922628C.

(7) Atkins, P. *Shriver & Atkins' Inorganic Chemistry*, 5th ed. edition.; Oxford University Press: Oxford ; New York, 2010.

(8) Chelates and Chelation. In *Van Nostrand's Scientific Encyclopedia*; American Cancer Society, 2005. https://doi.org/10.1002/0471743984.vse1659.

(9) Dixon, N. J. Greener Chelating Agents. In *Handbook of Green Chemistry*; Anastas, P. T., Ed.; Wiley-VCH Verlag GmbH & Co. KGaA: Weinheim, Germany, 2012.

(10) Chauhan, G.; Pant, K. K.; Nigam, K. D. P. Chelation Technology: A Promising Green Approach for Resource Management and Waste Minimization. *Environ. Sci.: Processes Impacts* **2015**, *17* (1), 12–40. https://doi.org/10.1039/C4EM00559G.

(11) Koodynska, D. Chelating Agents of a New Generation as an Alternative to Conventional Chelators for Heavy Metal Ions Removal from Different Waste Waters. In *Expanding Issues in Desalination*; Ning, R. Y., Ed.; InTech, 2011.

(12) Nowack, B. Chelating Agents and the Environment. *Environmental Pollution* **2008**, *153* (1), 1–2. https://doi.org/10.1016/j.envpol.2007.12.016.

(13) Nowack, B.; VanBriesen, J. M. Chelating Agents in the Environment. In *Biogeochemistry of Chelating Agents*; Nowack, B., VanBriesen, J. M., Eds.; American Chemical Society: Washington, DC, 2005; Vol. 910, pp 1–18. https://doi.org/10.1021/bk-2005-0910.ch001.

(14) Pinto, I. S. S.; Neto, I. F. F.; Soares, H. M. V. M. Biodegradable Chelating Agents for Industrial, Domestic, and Agricultural Applications--a Review. *Environ Sci Pollut Res Int* **2014**, *21* (20), 11893–11906. https://doi.org/10.1007/s11356-014-2592-6.

(15) Kontoghiorghes, G. J. Advances on Chelation and Chelator Metal Complexes in Medicine. *IJMS* **2020**, *21* (7), 2499. https://doi.org/10.3390/ijms21072499.

(16) Günter, K.; Toupet, C.; Schupp, T. Characterization of an Iron-Regulated Promoter Involved in Desferrioxamine B Synthesis in Streptomyces Pilosus: Repressor-Binding Site and Homology to the Diphtheria Toxin Gene Promoter. *Journal of Bacteriology* **1993**, *175* (11), 3295–3302. https://doi.org/10.1128/jb.175.11.3295-3302.1993.

(17) Franchini, M. Hereditary Iron Overload: Update on Pathophysiology, Diagnosis, and Treatment. *American Journal of Hematology* **2006**, *81* (3), 202–209. https://doi.org/10.1002/ajh.20493.

(18) Madhavi, D. L.; Deshpande, S. S.; Salunkhe, D. K. *Food Antioxidants: Technological: Toxicological and Health Perspectives*; CRC Press, 1995.

(19) Final Report on the Safety Assessment of EDTA, Calcium Disodium EDTA, Diammonium EDTA, Dipotassium EDTA, Disodium EDTA, TEA-EDTA, Tetrasodium EDTA, Tripotassium EDTA, Trisodium EDTA, HEDTA, and Trisodium HEDTA: *International Journal of Toxicology* **2016**. https://doi.org/10.1080/10915810290096522.

(20) Connors, K. A. *Binding Constants: The Measurement of Molecular Complex Stability*, 1 edition.; Wiley-Interscience: New York, 1987.

(21) Oksendal, A. N.; Hals, P.-A. Biodistribution and Toxicity of MR Imaging Contrast Media. *Journal of Magnetic Resonance Imaging* **1993**, *3* (1), 157–165. https://doi.org/10.1002/jmri.1880030128.

(22) Wahsner, J.; Gale, E. M.; Rodríguez-Rodríguez, A.; Caravan, P. Chemistry of MRI Contrast Agents: Current Challenges and New Frontiers. *Chem. Rev.* **2019**, *119* (2), 957–1057. https://doi.org/10.1021/acs.chemrev.8b00363.

(23) *The Chemistry of Contrast Agents in Medical Magnetic Resonance Imaging*; Merbach, A., Helm, L., Tóth, É., Eds.; John Wiley & Sons, Ltd: Chichester, UK, 2013. https://doi.org/10.1002/9781118503652.

(24) Kanda, T.; Ishii, K.; Kawaguchi, H.; Kitajima, K.; Takenaka, D. High Signal Intensity in the Dentate Nucleus and Globus Pallidus on Unenhanced T1-Weighted MR Images: Relationship with Increasing Cumulative Dose of a Gadolinium-Based Contrast Material. *Radiology* **2014**, *270* (3), 834–841. https://doi.org/10.1148/radiol.13131669.

(25) Guo, B. J.; Yang, Z. L.; Zhang, L. J. Gadolinium Deposition in Brain: Current Scientific Evidence and Future Perspectives. *Front Mol Neurosci* **2018**, *11*. https://doi.org/10.3389/fnmol.2018.00335.

(26) Peguero, J. G.; Arenas, I.; Lamas, G. A. Chelation Therapy and Cardiovascular Disease: Connecting Scientific Silos to Benefit Cardiac Patients. *Trends in Cardiovascular Medicine* **2014**, *24* (6), 232–240. https://doi.org/10.1016/j.tcm.2014.06.002.

(27) Bulman, R. A. The Chemistry of Chelating Agents in Medical Sciences. In *Coordination Compounds: Synthesis and Medical Application*; Structure and Bonding; Springer: Berlin, Heidelberg, 1987; pp 91–141. https://doi.org/10.1007/3-540-17881-3_3.

(28) Singh, S.; Hider, R. C. Therapeutic Iron-Chelating Agents. In *New Comprehensive Biochemistry*; Elsevier, 1994; Vol. 28, pp 189–216. https://doi.org/10.1016/S0167-7306(08)60443-3.

(29) Huang, M.; Gu, X.; Gao, X. Nanotherapeutic Strategies for the Treatment of Neurodegenerative Diseases. In *Brain Targeted Drug Delivery System*; Elsevier, 2019; pp 321–356. https://doi.org/10.1016/B978-0-12-814001-7.00013-5.

(30) Flora, S. J. S.; Pachauri, V. Chelation in Metal Intoxication. *International Journal of Environmental Research and Public Health* **2010**, *7* (7), 2745–2788. https://doi.org/10.3390/ijerph7072745.

(31) Yu, S.-B.; Watson, A. D. Metal-Based X-Ray Contrast Media. *Chem. Rev.* **1999**, *99* (9), 2353–2378. https://doi.org/10.1021/cr980441p.

(32) Smith-Bindman, R.; Lipson, J.; Marcus, R.; Kim, K.-P.; Mahesh, M.; Gould, R.; González, A. B. de; Miglioretti, D. L. Radiation Dose Associated With Common Computed Tomography Examinations and the Associated Lifetime Attributable Risk of Cancer. *Arch Intern Med* **2009**, *169* (22), 2078–2086. https://doi.org/10.1001/archinternmed.2009.427.

(33) Seeram, E. *Computed Tomography - E-Book: Physical Principles, Clinical Applications, and Quality Control*; Elsevier Health Sciences, 2015.

(34) Lusic, H.; Grinstaff, M. W. X-Ray-Computed Tomography Contrast Agents. *Chem. Rev.* **2013**, *113* (3), 1641–1666. https://doi.org/10.1021/cr200358s.

(35) Gunther, H. *NMR Spectroscopy: Basic Principles, Concepts, and Applications in Chemistry*, Revised, Updated edizione.; Vch Pub: Weinheim, 2013.

(36) Brown, W. H.; Iverson, B. L.; Anslyn, E.; Foote, C. S. *Organic Chemistry*, 8th edition.; Cengage Learning: Boston, MA, 2017.

(37) Kuperman, V. *Magnetic Resonance Imaging: Physical Principles and Applications*; Academic Press: San Diego, 1999.

(38) Chavhan, G. B.; Babyn, P. S.; Thomas, B.; Shroff, M. M.; Haacke, E. M. Principles, Techniques, and Applications of T2*-Based MR Imaging and Its Special Applications. *RadioGraphics* **2009**, *29* (5), 1433–1449. https://doi.org/10.1148/rg.295095034.

(39) Caravan, P.; Ellison, J. J.; McMurry, T. J.; Lauffer, R. B. Gadolinium(III) Chelates as MRI Contrast Agents: Structure, Dynamics, and Applications. *Chem. Rev.* **1999**, *99* (9), 2293–2352. https://doi.org/10.1021/cr980440x.

(40) Rohrer, M.; Bauer, H.; Mintorovitch, J.; Requardt, M.; Weinmann, H.-J. Comparison of Magnetic Properties of MRI Contrast Media Solutions at Different Magnetic Field Strengths. *Invest Radiol* **2005**, *40* (11), 715–724. https://doi.org/10.1097/01.rli.0000184756.66360.d3.

(41) Seale, M. K.; Catalano, O. A.; Saini, S.; Hahn, P. F.; Sahani, D. V. Hepatobiliary-Specific MR Contrast Agents: Role in Imaging the Liver and Biliary Tree. *RadioGraphics* **2009**, *29* (6), 1725–1748. https://doi.org/10.1148/rg.296095515.

(42) Junqiang, L.; Yinzhong, W.; Li, Z.; Shunlin, G.; Xiaohui, W.; Yanan, Z.; Kehu, Y. Gadoxetic Acid Disodium (Gd-EOB-DTPA)-Enhanced Magnetic Resonance Imaging for the Detection of Hepatocellular Carcinoma: A Meta-Analysis. *Journal of Magnetic Resonance Imaging* **2014**, *39* (5), 1079–1087. https://doi.org/10.1002/jmri.24354.

(43) Kim, Y.-Y.; Park, M.-S.; Aljoqiman, K. S.; Choi, J.-Y.; Kim, M.-J. Gadoxetic Acid-Enhanced Magnetic Resonance Imaging: Hepatocellular Carcinoma and Mimickers. *Clin Mol Hepatol* **2019**, *25* (3), 223–233. https://doi.org/10.3350/cmh.2018.0107.

(44) An, S. K.; Lee, J. M.; Suh, K.-S.; Lee, N. J.; Kim, S. H.; Kim, Y. J.; Han, J. K.; Choi, B. I. Gadobenate Dimeglumine-Enhanced Liver MRI as the Sole Preoperative Imaging Technique: A Prospective Study of Living Liver Donors. *American Journal of Roentgenology* **2006**, *187* (5), 1223–1233. https://doi.org/10.2214/AJR.05.0584.

(45) Erb-Eigner, K.; Taupitz, M.; Asbach, P. Equilibrium-Phase MR Angiography: Comparison of Unspecific Extracellular and Protein-Binding Gadolinium-Based Contrast Media with Respect to Image Quality. *Contrast Media & Molecular Imaging* **2016**, *11* (1), 71–76. https://doi.org/10.1002/cmmi.1660.

(46) Richardson, O. C.; Bane, O.; Scott, M. L. J.; Tanner, S. F.; Waterton, J. C.; Sourbron, S. P.; Carroll, T. J.; Buckley, D. L. Gadofosveset-Based Biomarker of Tissue Albumin Concentration: Technical Validation in Vitro and Feasibility in Vivo. *Magnetic Resonance in Medicine* **2015**, *73* (1), 244–253. https://doi.org/10.1002/mrm.25128.

(47) Gale, E. M.; Wey, H.-Y.; Ramsay, I.; Yen, Y.-F.; Sosnovik, D. E.; Caravan, P. A Manganese-Based Alternative to Gadolinium: Contrast-Enhanced MR Angiography, Excretion, Pharmacokinetics, and Metabolism. *Radiology* **2018**, *286* (3), 865–872. https://doi.org/10.1148/radiol.2017170977.

(48) Fries, P.; Müller, A.; Seidel, R.; Robert, P.; Denda, G.; Menger, M. D.; Schneider, G.; Buecker, A. P03277—A New Approach to Achieve High-Contrast

Enhancement: Initial Results of an Experimental Extracellular Gadolinium-Based Magnetic Resonance Contrast Agent. *Investigative Radiology* **2015**, *50* (12), 835–842. https://doi.org/10.1097/RLI.0000000000000192.

(49) Skwierawska, A. M. Selective Monoprotection of 1,4,7,10-Tetraazacyclododecane via Direct Reaction with 4-Nitrophenyl Active Esters. *Tetrahedron Letters* **2008**, *49* (44), 6308–6310. https://doi.org/10.1016/j.tetlet.2008.08.059.

(50) Travagin, F.; Lattuada, L.; Giovenzana, G. B. First Synthesis of Orthogonally 1,7-Diprotected Cyclens. *Org. Chem. Front.* **2019**, *6* (9), 1387–1390. https://doi.org/10.1039/C9QO00184K.

(51) Lattuada, L.; Barge, A.; Cravotto, G.; Giovenzana, G. B.; Tei, L. The Synthesis and Application of Polyamino Polycarboxylic Bifunctional Chelating Agents. *Chem. Soc. Rev.* **2011**, *40* (5), 3019–3049. https://doi.org/10.1039/C0CS00199F.

(52) Aime, S.; Calabi, L.; Cavallotti, C.; Gianolio, E.; Giovenzana, G. B.; Losi, P.; Maiocchi, A.; Palmisano, G.; Sisti, M. [Gd-AAZTA]$^{-}$: A New Structural Entry for an Improved Generation of MRI Contrast Agents. *Inorganic Chemistry* **2004**, *43* (24), 7588–7590. https://doi.org/10.1021/ic0489692.

(53) Touti, F.; Singh, A. K.; Maurin, P.; Canaple, L.; Beuf, O.; Samarut, J.; Hasserodt, J. An Electroneutral Macrocyclic Iron(II) Complex That Enhances MRI Contrast in Vivo. *J. Med. Chem.* **2011**, *54* (12), 4274–4278. https://doi.org/10.1021/jm2002298.

(54) Stoumpos, S.; Hennessy, M.; Vesey, A. T.; Radjenovic, A.; Kasthuri, R.; Kingsmore, D. B.; Mark, P. B.; Roditi, G. Ferumoxytol Magnetic Resonance Angiography: A Dose-Finding Study in Patients with Chronic Kidney Disease. *Eur Radiol* **2019**, *29* (7), 3543–3552. https://doi.org/10.1007/s00330-019-06137-4.

(55) Ahrens, E. T.; Helfer, B. M.; O'Hanlon, C. F.; Schirda, C. Clinical Cell Therapy Imaging Using a Perfluorocarbon Tracer and Fluorine-19 MRI. *Magnetic Resonance in Medicine* **2014**, *72* (6), 1696–1701. https://doi.org/10.1002/mrm.25454.

(56) Tirotta, I.; Dichiarante, V.; Pigliacelli, C.; Cavallo, G.; Terraneo, G.; Bombelli, F. B.; Metrangolo, P.; Resnati, G. 19F Magnetic Resonance Imaging (MRI): From Design of Materials to Clinical Applications. *Chem. Rev.* **2015**, *115* (2), 1106–1129. https://doi.org/10.1021/cr500286d.

(57) Chalmers, K. H.; Kenwright, A. M.; Parker, D.; Blamire, A. M. 19F-Lanthanide Complexes with Increased Sensitivity for 19F-MRI: Optimization of the MR Acquisition. *Magnetic Resonance in Medicine* **2011**, *66* (4), 931–936. https://doi.org/10.1002/mrm.22881.

(58) Vinogradov, E.; Sherry, A. D.; Lenkinski, R. E. CEST: From Basic Principles to Applications, Challenges and Opportunities. *J. Magn. Reson.* **2013**, *229*, 155–172. https://doi.org/10.1016/j.jmr.2012.11.024.

(59) Chan, K. W. Y.; McMahon, M. T.; Kato, Y.; Liu, G.; Bulte, J. W. M.; Bhujwalla, Z. M.; Artemov, D.; Zijl, P. C. M. van. Natural D-Glucose as a Biodegradable MRI Contrast Agent for Detecting Cancer. *Magnetic Resonance in Medicine* **2012**, *68* (6), 1764–1773. https://doi.org/10.1002/mrm.24520.

(60) Xu, X.; Yadav, N. N.; Knutsson, L.; Hua, J.; Kalyani, R.; Hall, E.; Laterra, J.; Blakeley, J.; Strowd, R.; Pomper, M.; Barker, P.; Chan, K. W. Y.; Liu, G.; McMahon, M. T.; Stevens, R. D.; Zijl, and P. C. M. van. Dynamic Glucose-Enhanced (DGE) MRI: Translation to Human Scanning and First Results in Glioma Patients. *Tomography: A Journal for Imaging Research* **2015**, *1* (2), 105–114. https://doi.org/10.18383/j.tom.2015.00175.

(61) Aime, S.; Calabi, L.; Biondi, L.; Miranda, M. D.; Ghelli, S.; Paleari, L.; Rebaudengo, C.; Terreno, E. Iopamidol: Exploring the Potential Use of a Well-Established x-Ray Contrast Agent for MRI. *Magnetic Resonance in Medicine* **2005**, *53* (4), 830–834. https://doi.org/10.1002/mrm.20441.

(62) Anemone, A.; Consolino, L.; Longo, D. L. MRI-CEST Assessment of Tumour Perfusion Using X-Ray Iodinated Agents: Comparison with a Conventional Gd-Based Agent. *Eur Radiol* **2017**, *27* (5), 2170–2179. https://doi.org/10.1007/s00330-016-4552-7.

(63) Woods, M.; Woessner, D. E.; Sherry, A. D. Paramagnetic Lanthanide Complexes as PARACEST Agents for Medical Imaging. *Chem. Soc. Rev.* **2006**, *35* (6), 500–511. https://doi.org/10.1039/B509907M.

(64) Ratnakar, S. J.; Viswanathan, S.; Kovacs, Z.; Jindal, A. K.; Green, K. N.; Sherry, A. D. Europium(III) DOTA-Tetraamide Complexes as Redox-Active MRI Sensors. *J. Am. Chem. Soc.* **2012**, *134* (13), 5798–5800. https://doi.org/10.1021/ja211601k.

(65) Geraldes, C. F. G. C.; Laurent, S. Classification and Basic Properties of Contrast Agents for Magnetic Resonance Imaging. *Contrast Media & Molecular Imaging* **2009**, *4* (1), 1–23. https://doi.org/10.1002/cmmi.265.

(66) Sinharay, S.; Pagel, M. D. Advances in Magnetic Resonance Imaging Contrast Agents for Biomarker Detection. *Annual Review of Analytical Chemistry* **2016**, *9* (1), 95–115. https://doi.org/10.1146/annurev-anchem-071015-041514.

(67) Nelson, S. J.; Kurhanewicz, J.; Vigneron, D. B.; Larson, P. E. Z.; Harzstark, A. L.; Ferrone, M.; Criekinge, M. van; Chang, J. W.; Bok, R.; Park, I.; Reed, G.; Carvajal, L.; Small, E. J.; Munster, P.; Weinberg, V. K.; Ardenkjaer-Larsen, J. H.; Chen, A. P.; Hurd, R. E.; Odegardstuen, L.-I.; Robb, F. J.; Tropp, J.; Murray, J. A. Metabolic Imaging of Patients with Prostate Cancer Using Hyperpolarized [1-13C]Pyruvate. *Science Translational Medicine* **2013**, *5* (198), 198ra108-198ra108. https://doi.org/10.1126/scitranslmed.3006070.

(68) Chen, H.-Y.; Aggarwal, R.; Bok, R. A.; Ohliger, M. A.; Zhu, Z.; Lee, P.; Gordon, J. W.; van Criekinge, M.; Carvajal, L.; Slater, J. B.; Larson, P. E. Z.; Small, E. J.; Kurhanewicz, J.; Vigneron, D. B. Hyperpolarized 13 C-Pyruvate MRI Detects Real-Time Metabolic Flux in Prostate Cancer Metastases to Bone and Liver: A Clinical Feasibility Study. *Prostate Cancer and Prostatic Diseases* **2020**, *23* (2), 269–276. https://doi.org/10.1038/s41391-019-0180-z.

(69) Bhattacharya, P.; Chekmenev, E. Y.; Perman, W. H.; Harris, K. C.; Lin, A. P.; Norton, V. A.; Tan, C. T.; Ross, B. D.; Weitekamp, D. P. Towards Hyperpolarized 13C-Succinate Imaging of Brain Cancer. *Journal of Magnetic Resonance* **2007**, *186* (1), 150–155. https://doi.org/10.1016/j.jmr.2007.01.017.

(70) Kiryutin, A. S.; Ivanov, K. L.; Yurkovskaya, A. V.; Vieth, H.-M.; Lukzen, N. N. Manipulating Spin Hyper-Polarization by Means of Adiabatic Switching of a Spin-Locking RF-Field. *Phys. Chem. Chem. Phys.* **2013**, *15* (34), 14248–14255. https://doi.org/10.1039/C3CP52061G.

(71) Eills, J.; Blanchard, J. W.; Wu, T.; Bengs, C.; Hollenbach, J.; Budker, D.; Levitt, M. H. Polarization Transfer via Field Sweeping in Parahydrogen-Enhanced Nuclear Magnetic Resonance. *J. Chem. Phys.* **2019**, *150* (17), 174202. https://doi.org/10.1063/1.5089486.

(72) Pravdivtsev, A. N.; Yurkovskaya, A. V.; Vieth, H.-M.; Ivanov, K. L. RF-SABRE: A Way to Continuous Spin Hyperpolarization at High Magnetic Fields. *J. Phys. Chem. B* **2015**, *119* (43), 13619–13629. https://doi.org/10.1021/acs.jpcb.5b03032.

(73) Halse, M. E. Perspectives for Hyperpolarisation in Compact NMR. *TrAC Trends in Analytical Chemistry* **2016**, *83*, 76–83. https://doi.org/10.1016/j.trac.2016.05.004.

(74) Lindner, J. R. Microbubbles in Medical Imaging: Current Applications and Future Directions. *Nature Reviews Drug Discovery* **2004**, *3* (6), 527–533. https://doi.org/10.1038/nrd1417.

(75) Blomley, M. J. K.; Cooke, J. C.; Unger, E. C.; Monaghan, M. J.; Cosgrove, D. O. Microbubble Contrast Agents: A New Era in Ultrasound. *BMJ* **2001**, *322* (7296), 1222–1225. https://doi.org/10.1136/bmj.322.7296.1222.

(76) Wolbarst, A. B.; Hendee, W. R. Evolving and Experimental Technologies in Medical Imaging. *Radiology* **2006**, *238* (1), 16–39. https://doi.org/10.1148/radiol.2381041602.

(77) Gessner, R.; Dayton, P. A. Advances in Molecular Imaging with Ultrasound. *Mol Imaging* **2010**, *9* (3), 7290.2010.00022. https://doi.org/10.2310/7290.2010.00022.

(78) Kircher, M. F.; Willmann, J. K. Molecular Body Imaging: MR Imaging, CT, and US. Part I. Principles. *Radiology* **2012**, *263* (3), 633–643. https://doi.org/10.1148/radiol.12102394.

(79) Galema, T. W.; Geleijnse, M. L.; Vletter, W. B.; de Laat, L.; Michels, M.; Cate, F. J. ten. Clinical Usefulness of SonoVue Contrast Echocardiography: The Thoraxcentre Experience. *NHJL* **2007**, *15* (2), 55–60. https://doi.org/10.1007/BF03085955.

(80) Liang, H.-D.; Blomley, M. J. K. The Role of Ultrasound in Molecular Imaging. *BJR* **2003**, *76* (suppl_2), S140–S150. https://doi.org/10.1259/bjr/57063872.

(81) Weissleder, R.; Ntziachristos, V. *Weissleder, R. & Ntziachristos, V. Shedding Light onto Live Molecular Targets. Nat. Med. 9, 123-128*; 2003; Vol. 9. https://doi.org/10.1038/nm0103-123.

(82) Chung, S. H.; Feldman, M. D.; Martinez, D.; Kim, H.; Putt, M. E.; Busch, D. R.; Tchou, J.; Czerniecki, B. J.; Schnall, M. D.; Rosen, M. A.; DeMichele, A.; Yodh, A. G.; Choe, R. Macroscopic Optical Physiological Parameters Correlate with Microscopic Proliferation and Vessel Area Breast Cancer Signatures. *Breast Cancer Research* **2015**, *17* (1), 72. https://doi.org/10.1186/s13058-015-0578-z.

(83) Choe, R.; Konecky, S. D.; Corlu, A.; Lee, K.; Durduran, T.; Busch, D. R.; Pathak, S.; Czerniecki, B. J.; Tchou, J.; Fraker, D. L.; Demichele, A.; Chance, B.; Arridge, S. R.; Schweiger, M.; Culver, J. P.; Schnall, M. D.; Putt, M. E.; Rosen, M. A.; Yodh, A. G. Differentiation of Benign and Malignant Breast Tumors by In-Vivo Three-Dimensional Parallel-Plate Diffuse Optical Tomography. *J Biomed Opt* **2009**, *14* (2), 024020. https://doi.org/10.1117/1.3103325.

(84) Tu, C.; Nagao, R.; Louie, A. Y. Multimodal Magnetic-Resonance/Optical-Imaging Contrast Agent Sensitive to NADH. *Angewandte Chemie International Edition* **2009**, *48* (35), 6547–6551. https://doi.org/10.1002/anie.200900984.

(85) Atkinson, P.; Findlay, K. S.; Kielar, F.; Pal, R.; Parker, D.; Poole, R. A.; Puschmann, H.; Richardson, S. L.; Stenson, P. A.; Thompson, A. L.; Yu, J. Azaxanthones and Azathioxanthones Are Effective Sensitisers for Europium and Terbium Luminescence. *Org. Biomol. Chem.* **2006**, *4* (9), 1707–1722. https://doi.org/10.1039/B601357K.

(86) Haglund, M. M.; Hochman, D. W.; Spence, A. M.; Berger, M. S. Enhanced Optical Imaging of Rat Gliomas and Tumor Margins. *Neurosurgery* **1994**, *35* (5), 930–940; discussion 940-941. https://doi.org/10.1227/00006123-199411000-00019.

(87) Hawrysz, D. J.; Sevick-Muraca, E. M. Developments toward Diagnostic Breast Cancer Imaging Using Near-Infrared Optical Measurements and Fluorescent Contrast Agents. *Neoplasia* **2000**, *2* (5), 388–417. https://doi.org/10.1038/sj.neo.7900118.

(88) Pfister, J.; Summer, D.; Rangger, C.; Petrik, M.; von Guggenberg, E.; Minazzi, P.; Giovenzana, G. B.; Aloj, L.; Decristoforo, C. Influence of a Novel, Versatile

Bifunctional Chelator on Theranostic Properties of a Minigastrin Analogue. *EJNMMI Research* **2015**, *5* (1), 74. https://doi.org/10.1186/s13550-015-0154-7.

(89) Reivich M; Kuhl D; Wolf A; Greenberg J; Phelps M; Ido T; Casella V; Fowler J; Hoffman E; Alavi A; Som P; Sokoloff L. The [18F]Fluorodeoxyglucose Method for the Measurement of Local Cerebral Glucose Utilization in Man. *Circulation Research* **1979**, *44* (1), 127–137. https://doi.org/10.1161/01.RES.44.1.127.

(90) Miller, P. W.; Long, N. J.; Vilar, R.; Gee, A. D. Synthesis of 11C, 18F, 15O, and 13N Radiolabels for Positron Emission Tomography. *Angew. Chem. Int. Ed. Engl.* **2008**, *47* (47), 8998–9033. https://doi.org/10.1002/anie.200800222.

(91) Liu, S. The Role of Coordination Chemistry in the Development of Target-Specific Radiopharmaceuticals. *Chem. Soc. Rev.* **2004**, *33* (7), 445–461. https://doi.org/10.1039/B309961J.

(92) Levin, C. S. Primer on Molecular Imaging Technology. *Eur. J. Nucl. Med. Mol. Imaging* **2005**, *32 Suppl 2*, S325-345. https://doi.org/10.1007/s00259-005-1973-y.

(93) Clarke, B. N. PET Radiopharmaceuticals: What's New, What's Reimbursed, and What's Next? *J. Nucl. Med. Technol.* **2018**, *46* (1), 12–16. https://doi.org/10.2967/jnmt.117.205021.

(94) Becherer, A.; Szabó, M.; Karanikas, G.; Wunderbaldinger, P.; Angelberger, P.; Raderer, M.; Kurtaran, A.; Dudczak, R.; Kletter, K. Imaging of Advanced Neuroendocrine Tumors with 18F-FDOPA PET. *J Nucl Med* **2004**, *45* (7), 1161–1167.

(95) Wadas, T. J.; Wong, E. H.; Weisman, G. R.; Anderson, C. J. Coordinating Radiometals of Copper, Gallium, Indium, Yttrium, and Zirconium for PET and SPECT Imaging of Disease. *Chem. Rev.* **2010**, *110* (5), 2858–2902. https://doi.org/10.1021/cr900325h.

(96) Rösch, F. Past, Present and Future of 68Ge/68Ga Generators. *Appl Radiat Isot* **2013**, *76*, 24–30. https://doi.org/10.1016/j.apradiso.2012.10.012.

(97) Velikyan, I. 68Ga-Based Radiopharmaceuticals: Production and Application Relationship. *Molecules* **2015**, *20* (7), 12913–12943. https://doi.org/10.3390/molecules200712913.

(98) Price, T. W.; Greenman, J.; Stasiuk, G. J. Current Advances in Ligand Design for Inorganic Positron Emission Tomography Tracers 68Ga, 64Cu, 89Zr and 44Sc. *Dalton Trans.* **2016**, *45* (40), 15702–15724. https://doi.org/10.1039/C5DT04706D.

(99) Price, E. W.; Orvig, C. Matching Chelators to Radiometals for Radiopharmaceuticals. *Chem Soc Rev* **2014**, *43* (1), 260–290. https://doi.org/10.1039/c3cs60304k.

(100) Hofman, M. S.; Hicks, R. J. Gallium-68 EDTA PET/CT for Renal Imaging. *Semin Nucl Med* **2016**, *46* (5), 448–461. https://doi.org/10.1053/j.semnuclmed.2016.04.002.

(101) Stasiuk, G. J.; Long, N. J. The Ubiquitous DOTA and Its Derivatives: The Impact of 1,4,7,10-Tetraazacyclododecane-1,4,7,10-Tetraacetic Acid on Biomedical Imaging. *Chem. Commun. (Camb.)* **2013**, *49* (27), 2732–2746. https://doi.org/10.1039/c3cc38507h.

(102) Simeček, J.; Zemek, O.; Hermann, P.; Notni, J.; Wester, H.-J. Tailored Gallium(III) Chelator NOPO: Synthesis, Characterization, Bioconjugation, and Application in Preclinical Ga-68-PET Imaging. *Mol. Pharm.* **2014**, *11* (11), 3893–3903. https://doi.org/10.1021/mp400642s.

(103) Eder, M.; Wängler, B.; Knackmuss, S.; LeGall, F.; Little, M.; Haberkorn, U.; Mier, W.; Eisenhut, M. Tetrafluorophenolate of HBED-CC: A Versatile Conjugation Agent for 68Ga-Labeled Small Recombinant Antibodies. *Eur. J. Nucl. Med. Mol. Imaging* **2008**, *35* (10), 1878–1886. https://doi.org/10.1007/s00259-008-0816-z.

(104) Ma, M. T.; Cullinane, C.; Imberti, C.; Baguña Torres, J.; Terry, S. Y. A.; Roselt, P.; Hicks, R. J.; Blower, P. J. New Tris(Hydroxypyridinone) Bifunctional Chelators Containing Isothiocyanate Groups Provide a Versatile Platform for Rapid One-Step Labeling and PET Imaging with (68)Ga(3.). *Bioconjug. Chem.* **2016**, *27* (2), 309–318. https://doi.org/10.1021/acs.bioconjchem.5b00335.

(105) Zhai, C.; Summer, D.; Rangger, C.; Haas, H.; Haubner, R.; Decristoforo, C. Fusarinine C, a Novel Siderophore-Based Bifunctional Chelator for Radiolabeling with Gallium-68. *J Labelled Comp Radiopharm* **2015**, *58* (5), 209–214. https://doi.org/10.1002/jlcr.3286.

(106) Baranyai, Z.; Uggeri, F.; Maiocchi, A.; Giovenzana, G. B.; Cavallotti, C.; Takács, A.; Tóth, I.; Bányai, I.; Bényei, A.; Brucher, E.; Aime, S. Equilibrium, Kinetic and Structural Studies of AAZTA Complexes with Ga^{3+}, In^{3+} and Cu^{2+}. *European Journal of Inorganic Chemistry* **2013**, *2013* (1), 147–162. https://doi.org/10.1002/ejic.201201108.

(107) Nagy, G.; Szikra, D.; Trencsényi, G.; Fekete, A.; Garai, I.; Giani, A. M.; Negri, R.; Masciocchi, N.; Maiocchi, A.; Uggeri, F.; Tóth, I.; Aime, S.; Giovenzana, G. B.; Baranyai, Z. AAZTA: An Ideal Chelating Agent for the Development of ^{44}Sc PET Imaging Agents. *Angewandte Chemie International Edition* **2017**, *56* (8), 2118–2122. https://doi.org/10.1002/anie.201611207.

(108) Brumberg, J.; Isaias, I. U. Chapter Two - SPECT Molecular Imaging in Atypical Parkinsonism. In *International Review of Neurobiology*; Politis, M., Ed.; Imaging in Movement Disorders: Imaging in Atypical Parkinsonism and Familial Movement Disorders; Academic Press, 2018; Vol. 142, pp 37–65. https://doi.org/10.1016/bs.irn.2018.08.006.

(109) *Handbook of Radiopharmaceuticals: Radiochemistry and Applications*; Welch, M. J., Redvanly, C. S., Eds.; J. Wiley: New York, 2003.

(110) Hughes, D. K. Nuclear Medicine and Infection Detection: The Relative Effectiveness of Imaging with 111In-Oxine-, 99mTc-HMPAO-, and 99mTc-Stannous Fluoride Colloid-Labeled Leukocytes and with 67Ga-Citrate. *J Nucl Med Technol* **2003**, *31* (4), 196–201; quiz 203–204.

(111) Castiñeiras-Campos, A.; de, la C.-T. I. S.; González-Pérez, J. M.; Sicilia-Zafra, A. G.; Bugella-Altamirano, E.; Niclós-Gutiérrez, J. Synthesis, Structure and Properties of Poly > [(N-(2-Hydroxyethyl)- N'-Carboxymethyl-1,2-Ethylenediamine-N, N'-Diacetato)Copper(II) Hydrate], {[Cu(Hhedta)] · H2O }n. *Zeitschrift für Naturforschung B* **2014**, *55* (2), 171–177. https://doi.org/10.1515/znb-2000-0207.

(112) Henze, M.; Schuhmacher, J.; Hipp, P.; Kowalski, J.; Becker, D. W.; Doll, J.; Mäcke, H. R.; Hofmann, M.; Debus, J.; Haberkorn, U. PET Imaging of Somatostatin Receptors Using [68GA]DOTA-D-Phe1-Tyr3-Octreotide: First Results in Patients with Meningiomas. *J. Nucl. Med.* **2001**, *42* (7), 1053–1056.

(113) Giovenzana, G. B.; Lattuada, L.; Negri, R. Recent Advances in Bifunctional Paramagnetic Chelates for MRI. *Israel Journal of Chemistry* **2017**, *57* (9), 825–832. https://doi.org/10.1002/ijch.201700028.

(114) Maguire, W. F.; McDevitt, M. R.; Smith-Jones, P. M.; Scheinberg, D. A. Efficient 1-Step Radiolabeling of Monoclonal Antibodies to High Specific Activity with 225Ac for -Particle Radioimmunotherapy of Cancer. *Journal of Nuclear Medicine* **2014**, *55* (9), 1492–1498. https://doi.org/10.2967/jnumed.114.138347.

(115) Hofmann, M.; Maecke, H.; Börner, A.; Weckesser, E.; Schöffski, P.; Oei, M.; Schumacher, J.; Henze, M.; Heppeler, A.; Meyer, G.; Knapp, W. Biokinetics and Imaging with the Somatostatin Receptor PET Radioligand 68Ga-DOTATOC: Preliminary Data. *Eur J Nucl Med* **2001**, *28* (12), 1751–1757. https://doi.org/10.1007/s002590100639.

(116) Hennrich, U.; Kopka, K. Lutathera®: The First FDA- and EMA-Approved Radiopharmaceutical for Peptide Receptor Radionuclide Therapy. *Pharmaceuticals* **2019**, *12* (3), 114. https://doi.org/10.3390/ph12030114.

(117) Fani, M.; André, J. P.; Maecke, H. R. 68Ga-PET: A Powerful Generator-Based Alternative to Cyclotron-Based PET Radiopharmaceuticals. *Contrast Media Mol Imaging* **2008**, *3* (2), 67–77. https://doi.org/10.1002/cmmi.232.

(118) Yang, J.; Kan, Y.; Ge, B. H.; Yuan, L.; Li, C.; Zhao, W. Diagnostic Role of Gallium-68 DOTATOC and Gallium-68 DOTATATE PET in Patients with Neuroendocrine Tumors: A Meta-Analysis: *Acta Radiologica* **2014**. https://doi.org/10.1177/0284185113496679.

(119) Lenzo, N. P.; Meyrick, D.; Turner, J. H. Review of Gallium-68 PSMA PET/CT Imaging in the Management of Prostate Cancer. *Diagnostics* **2018**, *8* (1), 16. https://doi.org/10.3390/diagnostics8010016.

(120) Turner, J. H. Recent Advances in Theranostics and Challenges for the Future. *BJR* **2018**, *91* (1091), 20170893. https://doi.org/10.1259/bjr.20170893.

(121) Hofman, M. S.; Emmett, L.; Violet, J.; Zhang, A. Y.; Lawrence, N. J.; Stockler, M.; Francis, R. J.; Iravani, A.; Williams, S.; Azad, A.; Martin, A.; McJannett, M.; Davis, I. D. TheraP: A Randomized Phase 2 Trial of 177Lu-PSMA-617 Theranostic Treatment vs Cabazitaxel in Progressive Metastatic Castration-

Resistant Prostate Cancer (Clinical Trial Protocol ANZUP 1603). *BJU International* **2019**, *124* (S1), 5–13. https://doi.org/10.1111/bju.14876.

(122) Rahbar, K.; Afshar-Oromieh, A.; Jadvar, H.; Ahmadzadehfar, H. PSMA Theranostics: Current Status and Future Directions: *Molecular Imaging* **2018**. https://doi.org/10.1177/1536012118776068.

(123) Eppard, E.; de la Fuente, A.; Benešová, M.; Khawar, A.; Bundschuh, R. A.; Gärtner, F. C.; Kreppel, B.; Kopka, K.; Essler, M.; Rösch, F. Clinical Translation and First In-Human Use of [44Sc]Sc-PSMA-617 for PET Imaging of Metastasized Castrate-Resistant Prostate Cancer. *Theranostics* **2017**, *7* (18), 4359–4369. https://doi.org/10.7150/thno.20586.

(124) Chang, S. S. Overview of Prostate-Specific Membrane Antigen. *Rev Urol* **2004**, *6* (Suppl 10), S13–S18.

Chapter 2: Outline of the Thesis

As thoroughly described in the first chapter, polyaminocarboxylates and polyaminophosphonates with mesocyclic or macrocyclic structure represent the best choice for the preparation of metal complexes exploited as imaging probes. These scaffolds ensure high thermodynamic and kinetic stability of the metal complex, indispensable for the application of these CAs in human.[1] However, the preparation of these kind of chelating agents or bifunctional chelating agents is not straightforward. The complexity of the polyaza scaffold and of the side arms necessary to confer a metal complex the features listed above makes the synthetic access to these probes really difficult.[2]

For this reason, both academia and industry are continuously searching for novel chelating agents and bifunctional chelating agents with a feasible and scalable preparation and improved feature.

Therefore, during my PhD experience the work was articulated into three main work areas:

- Regioselective protection of cyclen,
- Synthesis of novel bifunctional chelating agents,
- Synthesis of new chelating agents.

The regioselective protection of cyclen is an important issue, necessary to functionalise this relevant scaffold with different side arms with the aim to prepare improved chelating agents.[3] In particular, during my PhD some efforts have been devoted to the design and realisation of a strategy for the 1,7-heterodiprotection of cyclen with orthogonal protecting groups (*i.e.* BOC, Cbz, Alloc and formyl). This protection method exploits the control of pH to sequentially implant two different and orthogonal protecting groups in the cyclen scaffold. This strategy is very useful to prepare cyclen-based ligands decorated with three different side arms with improved features. These multifunctionalised improved ligands can serve as drugs for targeted radiotherapy and as probes for many imaging techniques, *i.e.* MRI, PET, SPECT and OI.[4] **(Figure 2.1)**

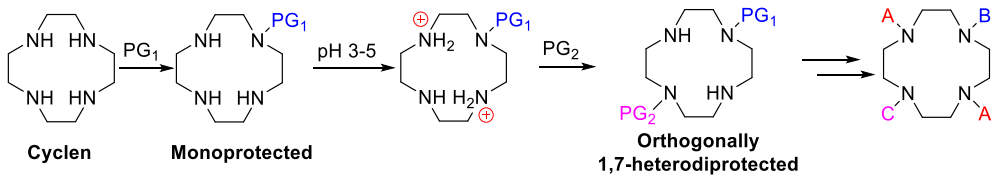

Figure 2.1. Orthogonal 1,7-heterodiprotection of cyclen.

This protection method has been exploited, during my PhD, to prepare two novel BFCAs (DO2AP(*t*Bu)$_4$ and DO3AP(*t*Bu)$_4$) bearing a phosphonic functionality. (**Figure 2.2**)

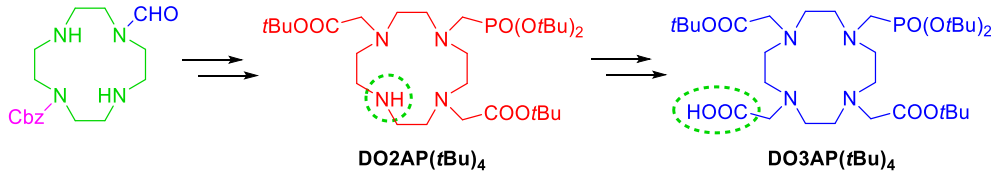

Figure 2.2. Regioselective protection of cyclen exploited for the preparation of two novel BFCAs. The reactive functional group of the BFCAs is circled in green.

These two novel BFCAs have been designed to prepare innovative and stable metal complexes conjugated with vectors such as antibody, peptides, nucleotides etc. Such compounds can be exploited to prepare drugs for targeted radiotherapy and CAs MRI, PET and SPECT.[4]

During my PhD, the research work has been focused also on the preparation of the three innovative chelating agents pictured in **Figure 2.3**.

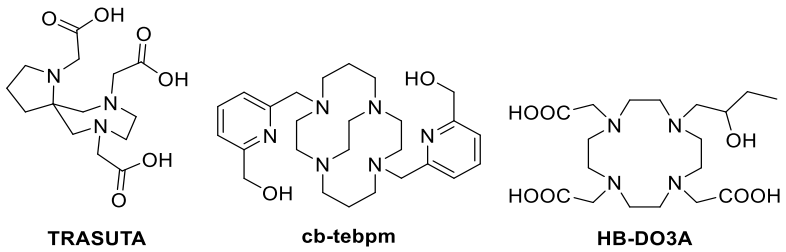

Figure 2.3. The three novel chelating agents prepared during the PhD.

TRASUTA is an innovative hexadentate mesocyclic chelating agent designed as a stiffened AAZTA-like ligand for gallium to be used as PET CA.[4,5]

Cb-tebpm, instead, has been designed to prepare stable complexes with gadolinium (or in general with lanthanides) as MRI CA.[6]

HB-DO3A is an HP-DO3A derivative designed to be a strong gadolinium chelator and a MRI CA. **HB-DO3A** has been thoroughly investigated in its safety profile. *In vitro* data have shown that, if compared to clinically approved MRI CAs, it presents low affinity to collagen, the most important biomolecule in interstitial fluids.[7] This characteristic could confer HB-DO3A the advantage of a faster and complete clearance after administration to the patient, with less release of toxic gadolinium and less side effects.[8]

References

(1) Wahsner, J.; Gale, E. M.; Rodríguez-Rodríguez, A.; Caravan, P. *Chem. Rev.* **2019**, *119* (2), 957–1057.

(2) Suchý, M.; Hudson, R. H. E. *Eur. J. Org. Chem.* **2008**, *2008* (29), 4847–4865.

(3) Skwierawska, A. M. *Tetrahedron Lett.* **2008**, *49* (44), 6308–6310.

(4) Weissleder, R. *Molecular Imaging: Principles and Practice*; PMPH-USA, 2010.

(5) Farkas, E.; Nagel, J.; Waldron, B. P.; Parker, D.; Tóth, I.; Brücher, E.; Rösch, F.; Baranyai, Z. *Chemistry - A European Journal* **2017**, *23* (43), 10358–10371.

(6) Rodríguez-Rodríguez, A.; Esteban-Gómez, D.; Tripier, R.; Tircsó, G.; Garda, Z.; Tóth, I.; de Blas, A.; Rodríguez-Blas, T.; Platas-Iglesias, C. *J. Am. Chem. Soc.* **2014**, *136* (52), 17954–17957.

(7) Smejkal, G. B.; Fitzgerald, C. *Int J Proteom Bioinform.* **2017**, *2* (1), 001–002.

(8) Guo, B. J.; Yang, Z. L.; Zhang, L. J. *Front Mol Neurosci* **2018**, *11*.

Chapter 3: First synthesis of orthogonally 1,7-diprotected cyclens

Introduction

1,4,7,10-Tetraazacyclododecane (cyclen) **1** is likely the most important macrocyclic polyamine.[1] Cyclen, apart from the coordination of metal ions in its native form, is employed as a building block for the synthesis of a wide variety of compounds such as non-viral gene vectors,[2] chemical sensors,[3] artificial nucleases[4] and bio-imaging probes.[5] In particular, cyclen is the starting material for the preparation of a family of macrocyclic ligands (e.g. DOTA[6] and derivatives thereof), whose gadolinium complexes are currently employed in diagnostic medicine as MRI contrast agents.[7] Moreover, many bifunctional chelating agents (BFCAs), frequently applied for labelling peptides or antibodies with radioactive or fluorescent metal ions, are based on the cyclen scaffold.[8]

The selective decoration of the cyclen skeleton with different substituents and functional groups is the first step in the preparation of the above cited derivatives. This is not an easy task due to the presence of four symmetrically equivalent secondary amines, thus several different synthetic strategies have been described so far to overcome the problem, most of them based on the clever use of amine protecting groups.[9] The functionalization of a single N position may be achieved by reacting the appropriate electrophile with a large excess of macrocyclic compound.[10] This strategy involves just one synthetic step and the workup is relatively simple since the excess of cyclen may be easily removed, but the high cost of cyclen has to be judiciously considered. A smaller excess of cyclen or even a 1:1 stoichiometric ratio can be used when the reactivity of the electrophilic reagent is suitably modulated as in the example of mixed *p*-nitrophenyl carbonates[11] or *N*-hydroxysuccinimidyl esters.[12] Multi-step sequences have been described to prepare mono protected cyclen, too.[13] The complementary protection of three out of four nitrogen atoms is generally simpler, as mild acylating agents react slower or sometimes not at all with the fourth nitrogen atom. This allows the preparation in high yield of triformyl-[14] and tri-BOC-cylen[15], for example. It is worthy of mention that cyclen reacts with dimethylformamide dimethyl acetal (DMFDMA)[16] or triethyl orthoformate[17] to give an isolable orthoaminal **2**, whose mild hydrolysis leads to the clean formation of the monoformyl derivative **3**. This sequence gives easily access to either a triprotected or to a monoprotected cyclen

and is currently employed for the industrial production of the clinically approved MRI contrast agent ProHance™.[18] (**Figure 3.1**)

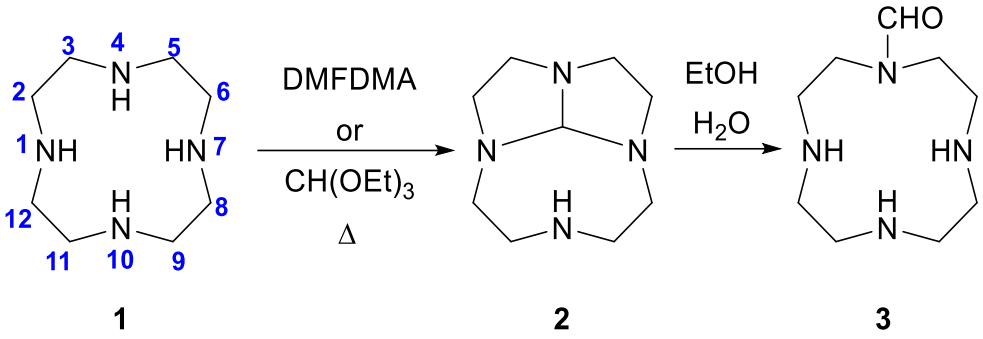

Figure 3.1. Tri/Mono-protection of cyclen

Diprotected cyclen derivatives pose the additional problem of the regioselectivity, existing either in the 1,4- or in the 1,7- isomeric forms[19] (**Figure 3.2**).

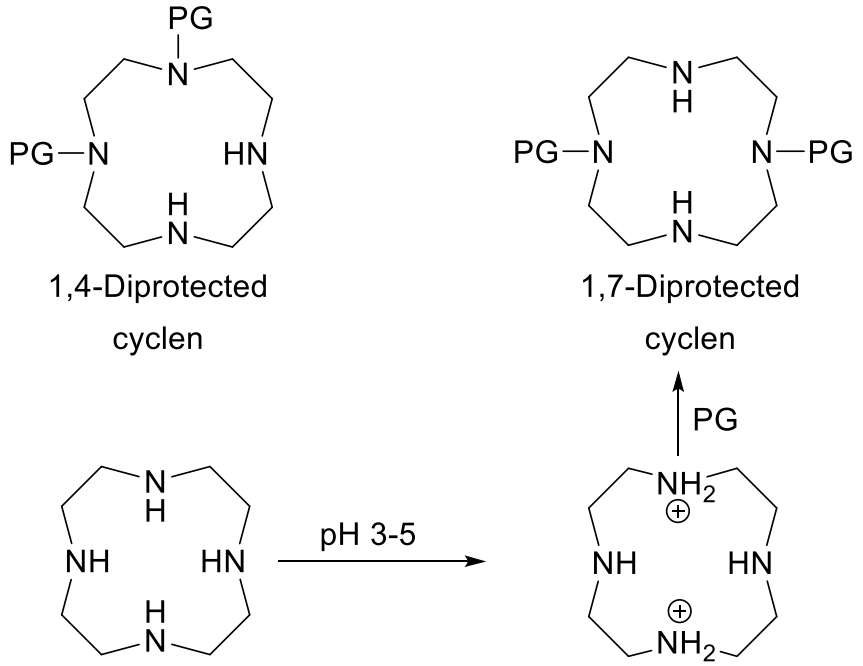

Figure 3.2. Diprotected cyclen derivatives and preparation of the 1,7-isomer (PG = protecting group).

The 1,7 di-protected pattern is easily obtained by applying the procedure reported by Kovacs and Sherry,[20] where a careful control of pH selectively leads to the protonation of the two opposite nitrogen atoms, switching off their reactivity and allowing the introduction of two identical protecting groups (**Figure 3.2**).

The easy availability of 1,7-homodiprotected derivatives of cyclen led to the use of these derivatives to prepare a range of functionalised chelating agents sharing an A_2B_2 substitution pattern (**Figure 3.3**).

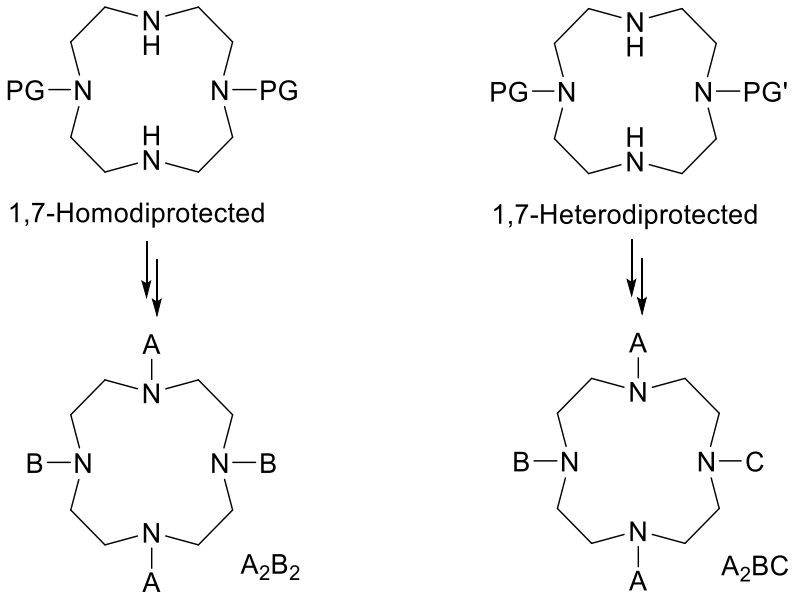

Figure 3.3. Homo- and hetero-diprotected cyclen and functionalised derivatives thereof.

The potential of cyclen for hosting more elaborate substitution patterns is anyway higher, in fact several derivatives bearing three or even four different substituents/functionalities were recently reported.[21] Indeed, part of the PhD research project, was addressed to expand this potential, focusing on the possibility to access 1,7-hetero-diprotected cyclen derivatives. The presence of two orthogonal protecting groups clearly paves the way for the systematic introduction of a third type of

substituent on the cyclen scaffold, with a specific A_2BC substitution pattern (**Figure3.3**), avoiding preparations based on statistical alkylation/acylation or on the use of large excess of expensive macrocyclic compounds.[10,22] Here an easy and efficient access to 1,7-heterodiprotected cyclen derivatives is reported.

Results and discussion

The operational simplicity of the Kovacs and Sherry procedure is especially interesting for preparative purposes as it works very efficiently on cyclen. The large pH gap between its second and third protonation steps (pK*a*s 10.51, 9.49, 1.6, 0.8)[20a] allows one to operate on the diprotonated cyclen (**Figure 3.2**). Indeed, the protonation of cyclen, at optimal value of pH 3, occurs on opposite nitrogen atoms due to electrostatic repulsion of the positive charges and this can be exploited to implant two identical protective groups with specific 1,7 regioselectivity. Moreover, this protocol is scalable to large preparations, but it is limited to protective groups resistant to the acidic condition applied.

The introduction of the two protecting groups in this procedure likely proceeds stepwise, hence the intermediate should be a monoprotected cyclen derivative, usually not isolated as the second introduction of the protecting group probably occurs quickly under the reaction conditions. This opens to the possibility of submitting a monoprotected cyclen to the pH conditions reported for the 1,7-difunctionalisation, leading to its diprotonation. In this environment, the treatment with a different acylating agent should lead to the introduction of a second distinct protecting group on the opposite nitrogen atom.

The *N*-formylcyclen **3** has been selected as the starting material in consideration of its straightforward preparation through the literature procedure[16,17] and its stability at pH 3. Moreover, the synthesis of **3**, compared to other monoprotected cyclen derivatives, is shorter and characterized by a higher yield. In addition, the formyl group can be easily removed by either acidic or basic treatment, allowing orthogonal deprotection. The overall synthetic strategy is depicted in **Figure 4**.

For the synthesis of the orthogonally 1,7-diprotected compounds, the appropriate monoprotected cyclen is dissolved in an acidified water/THF mixture (pH adjusted with conc. HCl, pH 3 for Cbz-Cl and Alloc-Cl, pH 5 for Boc_2O). A solution of the correspondent acylating agent (1 - 3 eq.) in THF is then slowly added to the vigorously stirred mixture, the pH being maintained at the correct value by constant addition of sodium bicarbonate. After complete conversion of the starting material (monitored by TLC), the reaction mixture is extracted with petroleum ether, basified with sodium carbonate and extracted with dichloromethane.

In this way, *N*-formylcyclen **3** was directly converted into the heterodiprotected cyclen derivatives 1-BOC-7-formyl (**4**), 1-Alloc-7-formyl (**7**) and 1-Cbz-7-formyl (**8**). In order to prepare other heterodiprotected cyclen derivatives and at the same time to demonstrate the orthogonality of the protection, the formamide group of **4** was selectively hydrolysed in basic conditions, leading to an alternative access to *N*-BOC-cyclen **5**.[11,23] Reiteration of the pH-controlled derivatisation with allyl chloroformate yielded the mixed 1-Alloc-7-BOC (**6**). A similar strategy was applied to compound **8**, whose formyl group was easily and selectively removed by acidic hydrolysis, realising an unprecedented preparation of *N*-Cbz-cyclen **9**.[11,12,15a,19] The latter acted as a preferential substrate for the pH-controlled insertion of BOC ($\rightarrow$ **10**) or Alloc group ($\rightarrow$ **11**), respectively, completing the array of the 6 possible 1,7-heterodiprotected cyclen derivatives arising from the combination of 4 different protecting groups.

All the pH-controlled reactions for the introduction of the second protecting groups proceeded in good yields, in the range 67%-93%, confirming the robustness of the protocol. It is noteworthy that no chromatographic separation is needed as no overreaction was observed if pH was carefully maintained in the indicated values (±0.3), while the acylating reagents and decomposition degradation products thereof were removed by extraction with petroleum ether. Furthermore, the selective removal of the formyl group from compounds **4** and **8** were successful as well (77-96% yields).

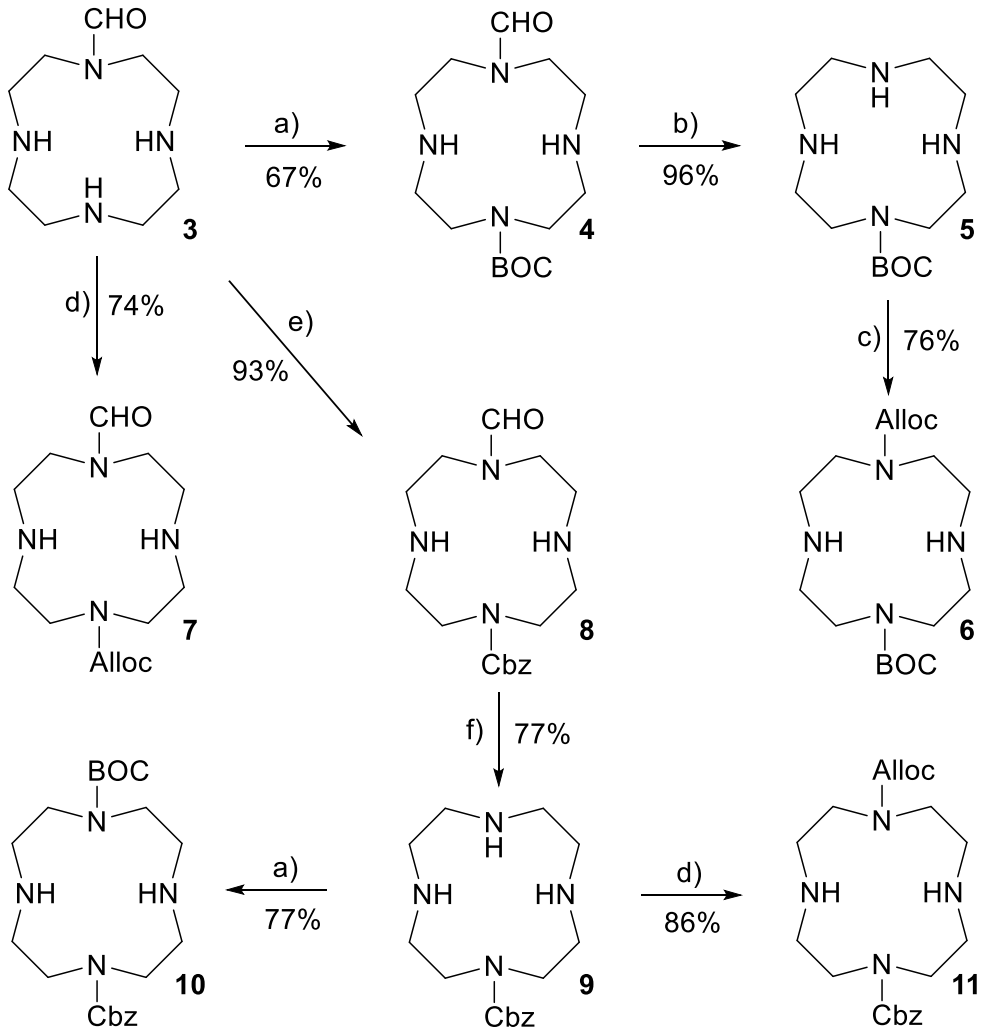

Figure 3.4. (a) Boc_2O, H_2O/THF pH 5, RT, 10h; (b) NaOH, H_2O, *i*-PrOH, 80°C, 40h; (c) Alloc-Cl, H_2O/THF pH 5, RT, 5h; (d) Alloc-Cl, H_2O/THF pH 3, RT, 10h; (e) Cbz-Cl, H_2O/THF pH 3, RT, 20h; (f) HCl, H_2O, 50°C, 20 h.

Conclusions

The preparation of six novel 1,7-heterodiprotected cyclen derivatives with all possible combinations of four distinct orthogonal protecting groups (*i.e.*: formyl, BOC, Cbz,

Alloc) is described for the first time. The easily accessed monoprotected *N*-formylcyclen **3** is the starting material for the selective, pH-controlled introduction of the second different protecting group. The efficient removal of the *N*-formyl group gives an alternative access to *N*-BOC-cyclen and *N*-Cbz-cyclen and paves the way for the preparation of the other members of this family of 1,7-heterodiprotected macrocycles. Good yields are observed in the introduction of PGs, and in the selective removal of the formyl group.

The synthetic protocol is easily applied and requires just a pH-meter to allow the preparation of these compounds; the reactions were scaled in our hands to multigram amounts of the substrates with no significant variation.

In conclusion, the protocols here reported could represent a set of new useful tools in the hands of organic chemists to be played in the sometimes tricky game of multifunctional cyclen syntheses.

Work is in progress to exploit the potential of these orthogonally protected cyclen derivatives in the synthesis of richly functionalised macrocycles and chelating agents.

Experimental section

Materials and methods

Solvents and starting materials were purchased from Sigma-Aldrich or TCI Europe and used without further purification. All aqueous solutions were prepared from ultrapure laboratory grade water (18 MΩ · cm) obtained from Millipore/MilliQ purification system. ^{1}H and ^{13}C NMR spectra were recorded at 300 MHz on a Jeol Eclipse ECP300 spectrometer. Chemical shifts are reported in ppm with the protic impurities of the deuterated solvent as the internal reference. Mass spectra were obtained with a Thermo Finningan LCQ-Deca XP-PLUS ion trap spectrometer equipped with an electrospray source. High resolution mass spectra were registered on a ThermoScientific Q-Exactive Plus spectrometer. TLC were performed with silica gel (MN Kieselgel 60F254) and visualized by UV or sprayed with Dragendorff reagent

or alkaline $KMnO_4$. *N*-Monoformylcyclen **3** was prepared following the procedure reported in literature.[16c]

Synthetic procedures and characterizations

***tert*-Butyl 7-formyl-1,4,7,10-tetraazacyclododecane-1-carboxylate (4)**. A solution of compound **3** (1.11 g, 5.54 mmol, 1 eq), in a mixture of water (4 mL) and THF (10 mL) is acidified to pH 5 with conc. HCl. A solution of di-*tert*-butyl dicarbonate (3.87 g, 1.77 mmol, 3.2 eq) in THF (6 mL) is slowly added with vigorous stirring and the pH is kept at 5.0 by continuous addition of $NaHCO_3$ during 9 h. After complete conversion of the substrate (monitored by TLC), the solution is extracted 3 times with petroleum ether. The aqueous layer is basified with Na_2CO_3 and extracted 3 times with CH_2Cl_2. The solvent is dried over Na_2SO_4 and Na_2CO_3, filtered and removed *in vacuo* to give compound **4** as a yellow oil (1.12 g, 67 %).

^{1}H NMR (300 MHz, $CDCl_3$, 333 K) δ 7.99 (s, 1H), 3.30 – 3.14 (m, 8H), 2.85 – 2.66 (m, 8H), 1.30 (s, 9H) ppm.

^{13}C NMR (75 MHz, $CDCl_3$, 333 K) δ 164.0 (CH), 156.0 (C), 79.6 (C), 50.0 (CH_2), 49.7 (CH_2), 47.5 (CH_2), 45.2 (CH_2), 28.4 (CH_3) ppm.

MS (ESI$^+$): *m*/z = 301.11 (100%, $[M+H]^+$), 201.28 (80%). Calc. for $C_{14}H_{28}N_4O_3$: 300.22.

HRMS (ESI$^+$): *m*/z = 301.22327 (100%, $[M+H]^+$). Calc. for $C_{14}H_{28}N_4O_3$: 300.21614.

***tert*-Butyl 1,4,7,10-tetraazacyclododecanecarboxylate (5)**. Compound **4** (1.67 g, 3.88 mmol) is dissolved in isopropyl alcohol (10 mL), then a 1 M solution of sodium hydroxide in water (10 mL) is added. The reaction is heated at 80°C and the conversion of the substrate is monitored by TLC (CH_2Cl_2/MeOH/NH_3 6:3.1). After 40 h, isopropyl alcohol is removed by vacuum evaporation, and the aqueous layer is extracted 3 times with CH_2Cl_2. The solvent is dried over Na_2SO_4 and Na_2CO_3, filtered and removed under vacuum to give compound **5** as a yellow oil (1.01 g, 96 %).

^{1}H NMR (300 MHz, $CDCl_3$, 333 K) δ 3.17 – 3.13 (m, 4H), 2.58 – 2.51 (m, 8H), 2.43 – 2.40 (m, 5H), 1.20 (s, 9H) ppm.

^{13}C NMR (75 MHz, $CDCl_3$, 333 K) δ 156.2 (C), 79.1 (C), 49.0 (CH_2), 48.7 (CH_2), 48.1 (CH_2), 46.5 (CH_2), 28.1 (CH_3) ppm.

MS (ESI$^+$): *m*/z (100%) = 273.23 [M+H]$^+$. Calc. for $C_{13}H_{28}N_4O_2$: 272.22.

1-Allyl 7-*tert*-butyl 1,4,7,10-tetraazacyclododecane-1,7-dicarboxylate (6). A solution of compound **5** (0.869 g, 3.19 mmol, 1 eq) in a mixture of water (10 mL) and THF (8 mL) is acidified to pH 5.0 with conc. HCl. A solution of allyl chloroformate (0.37 mL, 3.48 mmol, 1.1 eq) in THF (2 mL) is slowly added with vigorous stirring and the pH is maintained at 5.0 by continuous addition of $NaHCO_3$ during 5 h. After complete conversion of the substrate (monitored by TLC), the solution is extracted 3 times with petroleum ether. The aqueous layer is basified with Na_2CO_3 and extracted 3 times with CH_2Cl_2. The solvent is dried over Na_2SO_4 and Na_2CO_3, filtered and removed under vacuum to give compound **6** as a yellow oil (0.860 g, 76 %).
^{1}H NMR (300 MHz, $CDCl_3$, 333 K) δ 6.36 (br s, 2H), 5.89 – 5.76 (m, 1H), 5.21 – 5.11 (m, 2H), 4.52 (d, *J* = 5.1 Hz, 2H), 3.59 – 3.50 (m, 8H), 2.92 (br s, 8H), 1.37 (s, 9H) ppm.
^{13}C NMR (75 MHz, $CDCl_3$, 333 K) δ 156.0 (C), 155.4 (C), 132.4 (CH), 117.9 (CH_2), 80.7 (C), 66.3 (CH_2), 49.6 (4 CH_2), 28.3 (CH_3) ppm.
MS (ESI$^+$): *m*/z = 357.12 (79%, [M+H]$^+$), 257.27 (100%). Calc. for $C_{17}H_{32}N_4O_4$: 356.24.
HRMS (ESI$^+$): *m*/z = 357.24918 (100%, [M+H]$^+$). Calc. for $C_{17}H_{32}N_4O_4$: 356.24236.

1-Allyl 7-formyl-1,4,7,10-tetraazacyclododecane-1-carboxylate (7). A solution of compound **3** (1.02 g, 5.09 mmol, 1 eq) in a mixture of water (2 mL) and THF (4 mL) is acidified to pH 3 with conc. HCl. A solution of allyl chloroformate (1.35 mL, 12.7 mmol, 2.5 eq) in THF (4 mL) is added with vigorous stirring over 30 min. The pH is kept at 3 continuously adding $NaHCO_3$ in little portion for 10 h. After complete conversion of the substrate (monitored by TLC, CH_2Cl_2/MeOH/NH_3 6:3.1), the solution is extracted 3 times with petroleum ether, the aqueous layer is basified with Na_2CO_3 and extracted 3 times with CH_2Cl_2. The solvent is dried over Na_2SO_4 and Na_2CO_3, filtered and removed *in vacuo* to give compound **7** as a yellow oil (1.07 g, 74 %).
^{1}H NMR (300 MHz, $CDCl_3$, 333 K) δ 7.70 (s, 1H), 5.57 – 5.45 (m, 1H), 4.85 (d, *J* = 17.2 Hz, 1H), 4.76 (d, *J* = 10.4 Hz, 1H), 4.14 (s, 2H), 3.07 – 2.91 (m, 8H), 2.43 – 2.37 (m, 10H) ppm.

^{13}C NMR (75 MHz, $CDCl_3$, 333 K) δ 163.2 (CH), 155.6 (C), 132.4 (CH), 116.3 (CH_2), 64.9 (CH_2), 49.3 (CH_2), 47.8 (CH_2), 46.8 (CH_2), 44.6 (CH_2) ppm.
MS (ESI$^+$): *m*/z (100%) = 285.26 $[M+H]^+$. Calc. for $C_{13}H_{24}N_4O_3$: 284.18.
HRMS (ESI$^+$): *m*/z = 285.19193 (100%, $[M+H]^+$). Calc. for $C_{13}H_{24}N_4O_3$: 284.18484.

1-Benzyl 7-formyl-1,4,7,10-tetraazacyclododecane-1-carboxylate (8). A solution of compound **3** (1.98 g, 9.89 mmol, 1 eq) in a mixture of water (4mL) and THF (6 mL) is acidified to pH 3 with conc. HCl. A solution of benzyl chloroformate (4.2 mL, 29.7 mmol, 3 eq) in THF (10mL) is added dropwise with vigorous stirring and the pH is maintained at 3 by continuous addition of $NaHCO_3$ during for 2 h. When the pH is stable at 3 the solution is stirred at RT for 18 h. After complete conversion of the substrate (monitored by TLC, CH_2Cl_2/MeOH/NH_3 6:3.1), the mixture is extracted 3 times with petroleum ether, then the aqueous layer is basified with Na_2CO_3 and extracted 3 times with CH_2Cl_2. The solvent is dried over Na_2SO_4 and Na_2CO_3, filtered and removed under vacuum to give compound **8** as a yellow oil (3.06 g, 93 %).
^{1}H NMR (300 MHz, $CDCl_3$, 333 K) δ 7.98 (s, 1H), 7.18 (br s, 5H), 4.98 (s, 2H), 3.27 – 3.22 (m, 10H), 2.76 – 2.64 (m, 8H) ppm.
^{13}C NMR (75 MHz, $CDCl_3$, 333 K) δ 163.8 (CH), 156.4 (C), 136.5 (C), 128.2 (CH), 127.6 (CH), 127.5 (CH), 66.8 (CH_2), 49.8 (CH_2), 48.4 (CH_2), 47.3 (CH_2), 45.1 (CH_2) ppm.
MS (ESI$^+$): *m*/z = 335.25 (100%, $[M+H]^+$). Calc. for $C_{17}H_{26}N_4O_3$: 334.20. HRMS (ESI$^+$): *m*/z = 335.20752 (100%, $[M+H]^+$). Calc. for $C_{17}H_{26}N_4O_3$: 334.20049.

Benzyl 1,4,7,10-tetraazacyclododecanecarboxylate·3HCl (9·3HCl). Compound **8** (509 mg, 1.52 mmol) was dissolved in 1 M HCl and the solution was stirred at 50 °C for 20 h. The solvent was evaporated under vacuum, the residue was dissolved in boiling ethanol, filtrated, cooled to room temperature, and precipitated with diethyl ether. The product was isolated by vacuum filtration to yield compound **9**·3HCl as a white solid (486 mg, 77%).
^{1}H NMR (300 MHz, D_2O, 333 K) δ 7.28 (br s, 5H), 5.02 (s, 2H), 3.51 (br t, *J* = 4.8 Hz, 4H), 3.28 – 3.06 (m, 12H) ppm.

^{13}C NMR (75 MHz, D_2O, 333 K) δ 157.9 (C), 135.4 (C), 128.6 (CH), 128.3 (CH), 128.0 (CH), 68.3 (CH_2), 45.7 (CH_2), 44.9 (CH_2), 43.0 (CH_2), 42.6 (CH_2) ppm.
MS (ESI$^+$): *m*/z (100%) = 307.22 $[M+H]^+$. Calc. for $C_{16}H_{26}N_4O_2$: 306.21.

1-Benzyl 7-*tert*-butyl 1,4,7,10-tetraazacyclododecane-1,7-dicarboxylate (10). A solution of compound **9** (1.44 g, 3.46 mmol, 1 eq) in a mixture of water (5 mL) and THF (3 mL) is acidified to pH 5 with conc. HCl. A solution of di-*tert*-butyl dicarbonate (1.51 g, 6.91 mmol, 2 eq) in THF (2 mL) is added dropwise and the pH is kept at 5 continuously adding $NaHCO_3$ in little portion for 10h. After complete conversion of the substrate (monitored by TLC, CH_2Cl_2/MeOH/NH_3 6:3.1), the solution is extracted 3 times with petroleum ether, the aqueous layer is basified with Na_2CO_3 and extracted 3 times with CH_2Cl_2. The solvent is dried over Na_2SO_4 and Na_2CO_3, filtered and removed *in vacuo* to give compound **10** as a yellow oil (1.08 g, 77 %).
^{1}H NMR (300 MHz, $CDCl_3$, 333 K) δ 7.05 – 7.03 (m, 5H), 4.84 (s, 2H), 3.12 – 3.04 (m, 8H), 2.77 (br s, 2H), 2.53 (br s, 8H), 1.18 (s, 9H) ppm.
^{13}C NMR (75 MHz, $CDCl_3$, 333 K) δ 156.0 (C), 155.4 (C), 136.5 (C), 127.8 (CH), 127.2 (CH), 127.1 (CH), 78.7 (C), 66.3 (CH_2), 49.6 (2 CH_2), 48.3 (2 CH_2), 27.9 (CH_3) ppm.
MS (ESI$^+$): *m*/z = 429.15 (21%, $[M+Na]^+$), 407.16 (100%, $[M+H]^+$), 307.30 (23%). Calc. for $C_{21}H_{34}N_4O_4$: 406.26.
HRMS (ESI$^+$): *m*/z = 407.26487 (100%, $[M+H]^+$). Calc. for $C_{21}H_{34}N_4O_4$: 406.25801.

1-Allyl 7-benzyl 1,4,7,10-tetraazacyclododecane-1,7-dicarboxylate (11). A solution of compound **9** (1.47 g, 3.54 mmol, 1 eq), water (5 mL) and THF (3 mL) is acidified to pH 3 with HCl and stirred. Then a solution of allyl chloroformate (0.76 mL, 7.08 mmol, 2 eq) and THF (2 mL) is slowly added and the pH is maintained at 3 by continuous addition of $NaHCO_3$ for 10 h. After complete conversion of the substrate (monitored by TLC, CH_2Cl_2/MeOH/NH_3 6:3.1), the solution is extracted 3 times with petroleum ether, the aqueous layer is basified with solid Na_2CO_3 and extracted 3 times with CH_2Cl_2. The solvent is dried over Na_2SO_4 and Na_2CO_3, filtered and removed under vacuum to give compound **11** as a yellow oil (1.19 g, 86 %).

^{1}H NMR (300 MHz, $CDCl_3$, 333 K) δ 7.04 (s, 5H), 5.68 – 5.60 (m, 1H), 4.99 (d, J = 17.2 Hz, 1H), 4.91 – 4.85 (m, 3H), 4.31 (d, J = 2.2 Hz, 2H), 3.23 – 3.13 (m, 10H), 2.56 (br s, 8H) ppm.

^{13}C NMR (75 MHz, $CDCl_3$, 333 K) δ 155.9 (C), 155.7 (C), 136.3 (C), 132.6 (CH), 127.8 (CH), 127.2 (CH), 127.0 (CH), 116.4 (CH_2), 66.3 (CH_2), 65.1 (CH_2), 49.9 (2 CH_2), 48.5 (CH_2), 47.9 (CH_2) ppm.

MS (ESI^+): m/z (100%) = 391.27 $[M+H]^+$. Calc. for $C_{20}H_{30}N_4O_4$: 390.23.

HRMS (ESI^+): m/z = 391.23333 (100%, $[M+H]^+$). Calc. for $C_{20}H_{30}N_4O_4$: 390.22671.

References

(1) X. Yu and J. Zhang, *Macrocyclic Polyamines. Synthesis and Applications.* Wiley-VCH 2018.

(2) (a) Z. Huang, Y-H. Liu, Y-M. Zhang, J. Zhang, Q. Liu and X-Q. Yu, *Org. Biomol. Chem.*, 2015, **13**, 620; (b) Y-M. Zhang, D-C. Chang, J. Zhang, Y-H. Liu and X-Q Yu, *Bioorg. Med. Chem.*, 2015, **23**, 5756; (c) B-Q. Liu, W-J. Yi, J. Zhang, Q. Liu, Y-H. Liu, S-D. Fan and X-Q. Yu, *Org. Biomol. Chem.*, 2014, **12**, 3484; (d) S. Li, Y. Wang, S. Wang, J. Zhang, S-F. Wu, B-L. Wang, W. Zhu and X-Q. Yu, *Bioorg. Med. Chem.*, 2012, **20**, 1380.

(3) (a) K. Zhang, W. Dou, X. Tang, L. Yang, Z. Ju, Y. Cui and W. Liu, *Tetrahedron Lett.*, 2015, **56**, 2707; (b) H-R. Xu, K. Li, Q. Liu, T-M. Wu, M-Q. Wang, J-T. Hou, Z. Huang, Y-M. Xie and X-Q. Yu, *Analyst*, 2013, **138**, 2329; (c) M-Q. Wang, K. Li, J-T. Hou, M-Y. Wu, Z. Huang and X-Q. Yu, *J. Org. Chem.*, 2012, **77**, 8350; (d) L. M. P. Lima and R. Tripier, *Curr. Inorg. Chem.*, 2011, **1**, 36.

(4) (a) B. Gruber, E. Kataev, J. Aschenbrenner, S. Stadlbauer and B. König, *J. Am. Chem. Soc.*, 2011, **133**, 20704; (b) M-Q. Wang, J. Zhang, Y. Zhang, D-W. Zhang, Q. Liu, J-L. Liu, H-H. Lin and X-Q. Yu, *Bioorg. Med. Chem. Lett.*, 2011, **21**, 5866.

(5) (a) *Biomedical Imaging. The Chemistry of Labels, Probes and Contrast Agents.* Ed. M. Braddock, RSC Publishing, 2012; (b) R. E. Mewis and S. J. Archibald,

Coord. Chem. Rev., 2010, **254**, 1686; (c) K. Tanaka and K. Fukase, *Org. Biomol. Chem.*, 2008, **6**, 815.

(6) G. J. Stasiuk and N. J. Long, *Chem. Commun.*, 2013, **49**, 2732.

(7) (a) J. Washner, E. M. Gale, A. Rodríguez-Rodríguez and P. Caravan, *Chem. Rev.* 2019, **119**, 957; (b) G. B. Giovenzana, L. Lattuada and R. Negri, *Isr. J. Chem.*, 2017, **57**, 825; (c) *The Chemistry of Contrast Agents in Medical Magnetic Resonance Imaging*, ed. A. Merbach, L. Helm, É. Tóth, Wiley, New York, 2nd edn, 2013; (d) C. F. G. C. Geraldes and S. Laurent, *Contrast Media Mol. Imaging*, 2009, **4**, 1; (e) P. Hermann, J. Kotek, V. Kubíček and I. Lukeš, *Dalton Trans.*, 2008, 3027.

(8) (a) E. W. Price and C. Orvig, *Chem. Soc. Rev.*, 2014, **43**, 260; (b) C. F. Ramogida and C. Orvig, *Chem. Comm.*, 2013, **49**, 4720; (c) D. Sarko, M. Eisenhut, U. Haberkorn and W. Mier, *Curr. Med. Chem.* 2012, **19**, 2667; (d)L. Frullano and P. Caravan, *Curr. Org. Synth.*, 2011, **8**, 535; (e) L. Lattuada, A. Barge, G. Cravotto, G. B. Giovenzana and L. Tei, *Chem. Soc. Rev.*, 2011, **40**, 3019; (f) S. Liu and. S. Edwards, *Bioconjugate Chem.*, 2001, **12**, 7.

(9) (a) F. Denat, S. Brandès and R. Guilard, *Synlett*, 2000, 561; (b) M. Suchý and R. H. E. Hudson, *Eur. J. Org. Chem.* 2008, 4847; (c) N. Cakić, S. Gündüz, R. Rengarasu and G. Angelovski, *Tetrahedron Lett.*, 2015, **56**, 759; (d) F. Oukhatar, M. Beyler and R. Tripier, *Tetrahedron*, 2015, **71**, 3857.

(10) (a) J. Massue, S. E. Plush, C. S. Bonnet, D. A. Moore and T. Gunnlaugsson, *Tetrahedron Lett.*, 2007, **48**, 8052; (b) E. L. Que and C. J. Chang, *J. Am. Chem. Soc.*, 2006, **128**, 15942; (c) C. Li and W-T. Wong, *Tetrahedron Lett.* 2004, **45**, 6055; (d) C. Li and W-T. Wong, *Tetrahedron Lett.* 2002, **43**, 3217; (e) K-P. Eisenwiener, P. Powell and H. R. Mäcke, *Bioorg. Med. Chem. Lett.*, 2000, **10**, 2133; (f) J. J. Peterson, R. H. Pak and C. F. Meares, *Bioconjugate Chem.*, 1999, **10**, 316; (g) A. Heppeler, S. Froidevaux, H. R. Mäcke, E. Jermann, M. Béhé, P. Powell and M. Henning, *Chem. Eur. J.*, 1999, **5**, 1974; (h) P. L. Anelli, L. Calabi, P. Dapporto, M. Murru, L. Paleari, P. Paoli, F. Uggeri, S. Verona and M. Virtuani, *J. Chem. Soc. Perkin Trans. I*, 1995, 2995; (i) I. Meunier, A. K. Mishra, B. Hanquet, P. Cocolios and R. Guilard, *Can. J. Chem.*, 1995, **73**, 685.

(11) A. M. Skwierawska, *Tetrahedron Lett.*, 2008, **49**, 6308.

(12) H. Ito, T. Terai, K. Hanaoka, T. Ueno, T. Komatsu, T. Nagano and Y. Urano, *Chem. Commun.*, 2015, **51**, 8319.

(13) S. Aoki, H. Kawatani, T. Goto, E. Kimura and M. Shiro, *J. Am. Chem. Soc.*, 2001, **123**, 1123.

(14) V. Boldrini, G. B. Giovenzana, R. Pagliarin, G. Palmisano and M. Sisti, *Tetrahedron Lett.*, 2000, **41**, 6527.

(15) (a) E. Kimura, S. Aoki, T. Koike and M. Shiro, *J. Am. Chem. Soc.*, 1997, **119**, 3068; (b) S. Brandès, C. Gros, F. Denat, P. Pullumbi and R. Guilard, *Bull. Soc. Chim. Fr.*, 1996, **133**, 65.

(16) (a) D. D. Dischino, E. J. Delaney, J. E. Emswiler, G. T. Gaughan, J. S. Prasad, S. K. Srivastava and M. F. Tweedle, *Inorg. Chem.*, 1991, **30**, 1265; (b) J. Platzek, P. Blaszkiewicz, H. Gries, P. Luger, G. Michl, A. Müller-Fahrnow, B. Radüchel and D. Sülzle, *Inorg. Chem.*, 1997, **36**, 6086; (c) A-C. Ferrand, D. Imbert, A-S. Chauvin, C. D. B. Vandevyver and J-C. G. Bünzli, *Chem. Eur. J.*, 2007, **13**, 8678.

(17) G. Ripa, A. Scala, M. Murru, E. Panetta, C. F. Viscardi and M. Ausonio, WO9856776A1, 1998.

(18) (a) M. F. Tweedle, *Eur. Radiol.*, 1997, **7** (Suppl. 5), S225; (b) M. F. Tweedle and V. M. Runge, *Drugs Future*, 1992, **17**, 187.

(19) J. Yoo, D. E. Reichert and M. J. Welch, *J. Med. Chem.* 2004, **47**, 6625.

(20) (a) Z. Kovacs and A. D. Sherry, *Synthesis*, 1997, 759; (b) Z. Kovacs and A. D. Sherry, *J. Chem. Soc. Chem. Commun.* 1995, 185.

(21) (a) S. Shuvaev, M. A. Fox and D. Parker, *Angew. Chem. Int. Ed.*, 2018, **57**, 7488; (b) S. C Ghosh, S. H. Vargas, M. Rodriguez, S. Kossatz, J. Voss, K. S. Carmon, T. Reiner, A. Schonbrunn and A. Azhdarinia, *ACS Med. Chem. Lett.*, 2017, **8**, 720; (c) F. Vultos, C. Fernandes, F. Mendes, F. Marques, J. D. G. Correia, I. Santos and L. Gano, *ChemMedChem*, 2017, **12**, 1103; (d) S. Shuvaev, R. Pal and D. Parker, *Chem. Commun.*, 2017, **53**, 6724; (e) T. M. Wickramaratne and V. C. Pierre, *Bioconjugate Chem.*, 2015, **26**, 63; (f) F. Oukhatar, S. Même, W. Même, F. Szeremeta, N. K. Logothetis, G. Angelovski and É. Tóth, *ACS Chem. Neurosci.*, 2015, **6**, 219; (g) S. N. M. Chilla, S. Laurent, L. Vander Elst and R. N. Muller, *Tetrahedron*, 2014, **70**, 5450; (h) M. Polasek

and P. Caravan, *Inorg. Chem.*, 2013, **52**, 4084; (i) S. M. Vibhute, J. Engelmann, T. Verbić, M. E. Maier, N. K. Logothetis and G. Angelovski, *Org. Biomol. Chem.*, 2013, **11**, 1294; (j) P. Harvey, K. H. Chalmers, E. De Luca, A. Mishra and D. Parker, *Chem. Eur. J.*, 2012, **18**, 8748; (k) E. L. Que, E. J. New and C. J. Chang, *Chem. Sci.*, 2012, **3**, 1829.

(22) (a) J. M. M. Griffin, A. M. Skwierawska, H. C. Manning, J. N. Marx and D. J. Bornhop, *Tetrahedron Lett.*, 2001, **42**, 3823.

(23) K.-L. N. A. Finney, A. C. Harnden, N. J. Rogers, P. K. Senanayake, A. M. Blamire, D. O'Hogain and D. Parker, *Chem. Eur. J.* 2017, **23**, 7976.

Adapted from ***Org. Chem. Front.***, 2019, **6**, 1387-1390 with permission from The Royal Society of Chemistry.

For this work, I have prepared and characterised all the compounds herein presented and collaborated to the drawing up of the article.

Chapter 4: Synthesis of Two Novel Mixed Bifunctional Chelating Agents: DO2AP(*t*Bu)$_4$ and DO3AP(*t*Bu)$_4$

Introduction

Bifunctional chelating agents (BFCAs) are small molecules containing a metal chelating unit and a reactive functional group.[1] They find widespread applications in chemistry, biochemistry and medicine because they can be easily conjugated to biomolecules, such as peptides[2] or antibodies,[3] and then loaded with metals or radiometals to obtain diagnostic, therapeutic or theranostic agents, extensively employed nowadays in research, preclinical and clinical studies.[4]

Many popular and widely applied BFCAs are based on polyaminopolycarboxylic acids due to their versatility and ability to coordinate a broad variety of metal ions generating stable complexes.[5] High thermodynamic and kinetic stabilities of metal complexes are usually achieved with macrocyclic chelating agents owing to the preorganized structure of these ligands. The typical example of this class is DOTA (**Figure 4.1**), largely exploited for the preparation of metal complexes to be used *in vivo*.[6,7]

The macrocyclic derivatives DO3A tri-*t*-butyl ester **1**[8] and DOTA(*t*Bu)$_3$ **2**[9] (**Figure 4.1**), both based on the 1,4,7,10-tetrazacyclododecane ("cyclen"), are among the most used BFCAs. Both are commercially available and can be easily prepared through relatively simple procedures.[8-10] Compound **1** has been used in solid phase synthesis by derivatization of the peptide on the resin with bromoacetyl bromide (**Figure 4.1**, route a) which is then reacted with the BFCA.[11] Compound **2** can be directly conjugated to molecules of interest bearing an amino group (*e.g.*: a protected peptide) by means of a suitable coupling agent.[12] Moreover, compound **2** has been largely exploited in the solid phase synthesis of DOTA-functionalised peptides (**Figure 4.1**, route b).[13]

There is a great interest in the design and synthesis of novel BFCAs, ranging from linear DTPA to mesocyclic AAZTA[14] and to macrocyclic DOTA or HP-DO3A chelating agents.[14,15]

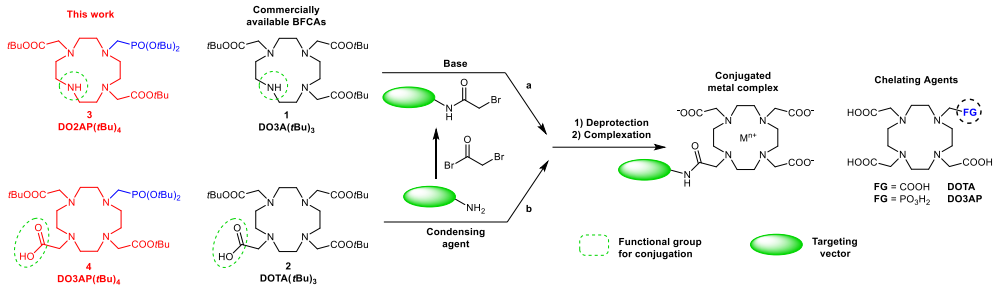

Figure 4.1. Macrocyclic BFCAs: conjugation strategies, commercially available examples and synthesised compounds.

Here the synthesis of the novel bifunctional chelating agents **3** and **4** (**Figure 4.1**) is reported, differing from **1** and **2** by the replacement of a carboxylic moiety with a phosphonic group. The phosphonic group is commonly used as a (bio)isostere of carboxylic acid in medicinal chemistry.[16] At physiological pH values the phosphonate tetrahedral deprotonated form ($-PO_3^{2-}$) offers multiple coordination modes, leading to stabilities of the metal complexes comparable to those of the carboxylic counterpart or even higher.[6] DO3AP (**Figure 4.1**) forms complexes with lanthanide (Ln^{3+}) with thermodynamic stabilities higher than those of the corresponding Ln^{3+}-DOTA chelates.[17] Moreover, the residual anionic charges left after complexation of the dianionic phosphonate group provide a beneficial effect on the solvation of the corresponding chelate, due to the establishment of an extended hydrogen bond network. This is extremely important in Gd^{3+}-complexes, currently used as MRI contrast agents and is clearly demonstrated in the comparison of Gd^{3+}-DO3AP, with the carboxylic congener Gd^{3+}-DOTA.[18] The former, in virtue of the higher hydration of the paramagnetic complex shows an improved relaxivity (*i.e.*: contrast efficiency), pointing out the importance of this specific isosteric substitution of metal-coordinating groups.

Results and discussion

N-Formyl-cyclen **5** has been selected as the starting material for the synthesis of the new monophosphonic derivatives **3** and **4**, since it can be easily prepared in two steps

from cyclen in almost quantitative yield.[19] Compound **5** was regioselectively protected at position 7 by reaction with benzylchloroformate in 1,4-dioxane/water at pH 3.[20] The regioselective protection relies on a modification of the protocol originally proposed by Kovacs and Sherry,[21] and exploits a pH-controlled procedure for the selective functionalization of polyazamacrocycles. The orthogonally heterodiprotected derivative **6** was the key intermediate for the synthesis of both BFCAs. Alkylation of the secondary amines with *t*-butyl bromoacetate in presence of *N*-ethyldiisopropyl amine (DIPEA) as the base, followed by selective removal of the formyl protective group by refluxing in ethanol in presence of hydroxylamine hydrochloride, led to the advanced synthon **7** in 88% yield. The key phosphonic moiety was introduced applying a modified Kabachnik-Fields reaction,[22] *i.e.*: treating **7** with tri-*t*-butyl phosphite and paraformaldehyde at 70°C for 36 h.[23] The resulting protected mixed phosphonic-carboxylic ester was not isolated due to observed instability. The Cbz protective group was directly and easily removed by hydrogenolysis (Pd/C in methanol), obtaining the monophosphonic DO2AP tetra-*t*-butyl ester **3** in 65% yield over two steps.

The second BFCA bears an additional side arm containing the free carboxylic acting as the remote reactive functional group. The side arm is introduced by alkylation of the secondary amine **3** with benzyl bromoacetate in acetonitrile at room temperature in the presence of K_2CO_3 as the base. Selective removal of the benzyl ester by catalytic hydrogenolysis completes the preparation of the desired bifunctional chelating agent **4** (DO3AP(*t*Bu)$_4$, **Figure 4.2**).

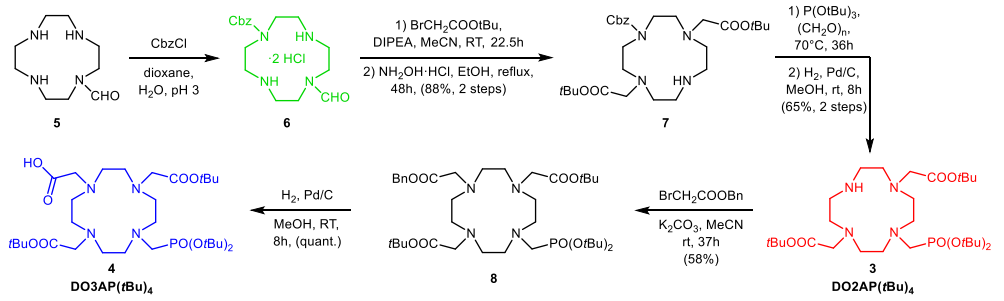

Figure 4.2. Synthesis of monophosphonic BFCAs DO2AP(tBu)$_4$ **3** and DO3AP(tBu)$_4$ **4**.

The preparation of both BFCAs was performed in gram scale, suitable for further applications.[24,25]

Conclusions

In summary, a concise entry to two macrocyclic bifunctional chelating agents, formally derived from the widely used DOTA/DO3A ligands, has been described in this work. The synthesis of the two new BFCAs starts from a readily available mono-protected cyclen and involves simple steps, requiring common and low-price reagents and exploiting a recently reported and very effective protection method.[20] Future development of this work will deal with the conjugation of the two new BFCAs to molecular vectors and evaluation of the corresponding conjugated metal complexes for diagnostic or therapeutic purposes.[24]

Experimental section

Materials and methods

Reagent-grade chemicals and solvents were obtained from commercial sources and directly used without further purification. All aqueous solutions were prepared from ultrapure laboratory grade water (18 MΩ·cm) obtained from Millipore/MilliQ purification system. 1-Formyl-1,4,7,10-tetrazacyclododecane[19a,19b] and tri-*t*-butyl phosphite[23] were synthesized as reported in the literature. TLC was performed on Merck silica gel 60 TLC plates F_{254} and visualized by using UV or spraying with 1% $KMnO_4$ in 1 M NaOH or Dragendorff reagent. Flash chromatography was carried out on Merck silica gel 60 (230-400 mesh). The ^{1}H, ^{13}C, and ^{31}P spectra were recorded on a Bruker Avance 400 instrument or on a Jeol Eclipse ECP 300 MHz. Chemical shifts are reported in ppm with the protic impurities of the deuterated solvent as the internal reference. ^{31}P spectra were recorded using phosphoric acid (85 wt. % solution in water) as an external standard. Mass spectra were recorded with a Thermo Finnigan TSQ700 triple-quadrupole instrument or with a Thermo Finnigan LCQ-Deca XP-PLUS ion trap spectrometer, both equipped with an electrospray ionization source. High

resolution mass spectra were registered on a ThermoScientific Q-Exactive Plus spectrometer. IR spectra were collected by a Bruker Alpha II instrument or by a Thermo Nicolet AVATAR 370 FT-IR.

Synthetic procedures and characterizations

7-Formyl-1,4,7,10-tetraazacyclododecane-1-carboxylic acid benzyl ester dihydrochloride (6)

1-Formyl-1,4,7,10-tetrazacyclododecane **5** (14 g, 69.9 mmol, 1.0 equiv) was dissolved in water (100 mL) and 12 N HCl was added until pH 3. 1,4-Dioxane (220 mL) was added and then a solution of benzyl chloroformate (13.8 g, 77 mmol, 1.1 equiv) in 1,4-dioxane (15 mL) was slowly added dropwise in 3.5 h while the pH of the mixture was constantly maintained at pH 3 by continuous addition of 2 N NaOH with a pHstat apparatus. When the addition was completed, the reaction mixture was stirred again for 1 h then extracted with *n*-hexane (4x100 mL) and diisopropyl ether (4x100 mL). The pH of the aqueous phase was raised to 13 by addition of 10N NaOH and extracted with $CHCl_3$ (4x100 mL). The organic phase was washed with brine (100 mL), dried (Na_2SO_4), filtered and evaporated. The oily residue was dissolved in acetone (200 mL) and 6 N HCl (26 mL) was added. The solid precipitated was filtered, washed with acetone (2x50 mL) and dried under vacuum to give compound **6** (23.6 g, 83 %) as a white solid.

M.p. > 200 °C.

Argentometric titer (0.1N $AgNO_3$): 98%**.**

IR (neat): 3449, 2931,1695, 1654, 1413, 1220, 1143, 1019, 701 cm^{-1}.

^1H NMR (400 MHz, D_2O, 298 K) δ 8.13 (s, 1H), 7.38 – 7.33 (m, 5H), 5.09 (s, 2H), 3.72 – 3.71 (m, 2H), 3.65 (br s, 2H), 3.59 – 3.56 (m, 4H), 3.37 – 3.29 (m, 8H) ppm.

^{13}C NMR (100 MHz, D_2O, 298 K) δ 169.1 (CH), 159.2 (C), 136.0 (C), 129.3 (CH), 129.2 (CH), 128.9 (CH), 69.0 (CH_2), 47.5 (2 CH_2), 47.3 (CH_2), 46.7 (CH_2), 45.7 (CH_2), 45.5 (CH_2), 44.9 (CH_2), 42.3 (CH_2) ppm.

MS (ESI^+): *m*/z = 335.25 (100%, $[M+H]^+$). Calc. for $C_{17}H_{26}N_4O_3$: 334.20.

Anal. Calcd for $C_{17}H_{28}N_4Cl_2O_3$: C, 50.13; H, 6.93; N, 13.75; Cl, 17.41. Found: C, 50.29; H, 6.87; N, 13.62; Cl, 17.24.

4-Benzyloxycarbonyl-1,4,7,10-tetrazacyclododecane-1,7-diacetic acid di-*t*-butyl ester (7)

A solution of compound **6** (14.4 g, 35.3 mmol, 1.0 equiv) and 1 N NaOH (74 mL, 74 mmol, 2.1 equiv) in water (450 mL) was stirred for 20 min then extracted with $CHCl_3$ (4x200 mL). The organic phase was separated and evaporated. The oily residue was dissolved in acetonitrile (180 mL) and *N*-ethyldiisopropylamine (15 mL) was added. A solution of *t*-butyl bromoacetate (16.8 g, 86.1 mmol, 2.4 equiv) in acetonitrile (15 mL) was slowly added in 2.5 h. The reaction mixture was stirred at room temperature for 20 h and then evaporated. The oily residue was dissolved in $CHCl_3$ (150 mL) and the solution washed with water (5x100 mL). The organic phase was dried (Na_2SO_4), filtered and evaporated. The residue was dissolved in EtOH (250 mL) and hydroxylamine hydrochloride (2.93 g, 42.2 mmol) was added. The reaction mixture was refluxed for 48 h then evaporated. The residue was dissolved in CH_2Cl_2 (250 mL), the solution washed with water (3x250 mL) then with brine (3x250 mL). The organic phase was dried (Na_2SO_4), filtered and evaporated. The oily residue was purified by flash chromatography ($CHCl_3$/MeOH = 9:1, R_f: 0.32). The glassy white solid obtained was dissolved in water (600 mL) and 1 N NaOH (90 mL) and extracted with $CHCl_3$ (3x250 mL). The organic phases were pooled, dried (Na_2SO_4) and evaporated to give compound **7** (16.6 g, 88%) as an oil.

IR (NaCl): 3304, 2978, 2933, 1724, 1702, 1497, 1393, 1115, 754 cm^{-1}.

^1H NMR (400 MHz, $CDCl_3$, 298 K) δ 7.33 – 7.28 (m, 5H), 5.10 (s, 2H), 3.46 – 3.44 (m, 4H), 3.29 (br s, 5H), 2.84 – 2.79 (m, 8H), 2.67 – 2.65 (m, 4H), 1.42 (s, 18H) ppm.

^{13}C NMR (100 MHz, $CDCl_3$, 298 K) δ 171.0 (C), 157.3 (C), 137.1 (C), 128.9 (CH), 128.4 (CH), 128.3 (CH), 81.3 (C), 67.5 (CH_2), 55.7 (CH_2), 53.0 (CH_2), 51.9 (CH_2), 48.7 (CH_2), 44.8 (CH_2), 28.6 (CH_3), ppm.

MS (ESI^+): *m*/z = 535.4 (100%, $[M+H]^+$), 479.3 (56%), 423.0 (30%). Calc. for $C_{28}H_{46}N_4O_6$: 534.3.

Anal. Calcd for $C_{28}H_{46}N_4O_6$: C, 62.90; H, 8.67; N, 10.48. Found: C, 62.47; H, 8.86; N, 10.35.

4-[[Di(*t*-butoxy)phosphoryl]methyl]-1,4,7,10-tetrazacyclododecane -1,7-diacetic acid di-*t*-butyl ester (3)

A mixture of compound **7** (13.9 g, 26 mmol, 1 equiv), tri-*t*-butyl phosphite (7.6 g, 28.6 mmol, 1.1 equiv) and paraformaldehyde (0.9 g, 30 mmol, 1.15 equiv) was stirred and heated at 70 °C. After 16 h, additional tri-*t*-butyl phosphite (1 g, 3.8 mmol, 0.15 equiv) and paraformaldehyde (0.1 g, 3.3 mmol, 0.13 equiv) were added and the mixture was heated for further 20 h. The mixture was evaporated under vacuum at 80°C to eliminate volatile by-products. The oily residue was dissolved in methanol (145 mL), 5% Pd/C (2.6 g) was added and the mixture was stirred under hydrogen atmosphere at room temperature for 8 h. The mixture was filtered through a Millipore FT 0.45 µm filter, evaporated and the residue was purified by flash chromatography (CH_2Cl_2 then CH_2Cl_2/MeOH = 9:1) to give compound **3** (10.3 g, 65% over two steps) as a brown oil.

IR (neat): 2977, 2927, 1730, 1368, 1223, 1152, 973, 917, 849, 692 cm^{-1}.

^1H NMR (300 MHz, $CDCl_3$, 333 K) δ 3.02 – 2.91 (m, 5H), 2.71 – 2.38 (m, 18H), 1.09 (s, 18H), 1.04 (s, 18H) ppm.

^{13}C NMR (75 MHz, $CDCl_3$, 333 K) δ 169.8 (C), 82.2 (C, d, J = 9.8 Hz), 80.6 (C), 57.5 (CH_2), 51.2 (CH_2), 50.9 (CH_2), 48.9 (CH_2), 46.8 (CH_2), 45.3 (CH_2, d, J = 145 Hz), 29.9 (CH_3, d, J = 3.7 Hz), 27.5 (CH_3) ppm.

^{31}P NMR (121 MHz, $CDCl_3$, 333 K): δ = 18.1 (s) ppm.

MS (ESI^+): m/z = 607.24 (100%, $[M+H]^+$), 551.20 (21%), 495.16 (35%), 439.15 (34%), 383.18 (20%). Calc. for $C_{29}H_{59}N_4O_7P$: 606.41.

HRMS (ESI^+): m/z = 607.41886 (100%, $[M+H]^+$), 629.40094 (46%, $[M+Na]^+$). Calc. for $C_{29}H_{59}N_4O_7P$: 606.41214.

7-[[Di(*t*-butoxy)phosphoryl]methyl]-1,4,7,10-tetrazacyclododecane -1,4,10-triacetic acid 1-benzyl 4,10-di-*t*-butyl ester (8)

Benzyl bromoacetate (1.4 g, 6.26 mmol, 2 equiv) was added dropwise in 1 h to a suspension of compound **3** (1.9 g, 3.13 mmol, 1 equiv), potassium carbonate (1.3 g, 9.39 mmol, 3 eq) and acetonitrile (10 mL). The mixture was stirred at room temperature for 36 h then evaporated. The residue was purified by flash chromatography (CH_2Cl_2/2-propanol = 9:1) to give compound **8** (1.38 g, 58%) as an oil.

IR (neat): 2979, 2921, 1730, 1688, 1370, 1156, 980, 800, 730, 697 cm^{-1}.

^{1}H NMR (300 MHz, CD_3OD, 313 K) δ 7.36 (s, 5H), 5.20 (s, 2H), 3.34 – 3.25 (m, 6H), 3.00 (d, J = 10.3 Hz, 2H), 2.77 – 2.39 (m, 16H), 1.54 (s, 18H), 1.48 (s, 18H) ppm.

^{13}C NMR (75 MHz, CD_3OD, 298 K) δ 175.2 (C), 174.3 (C), 137.0 (C), 129.7 (CH), 129.5 (CH), 129.4 (CH), 85.0 (C, d, J = 9.9 Hz), 83.3 (C), 67.9 (CH_2), 57.6 (8 CH_2), 56.4 (3 CH_2), 54.3 (CH_2, d, J = 151.5 Hz), 31.0 (CH_3, d, J = 3.5 Hz), 28.5 (CH_3).

^{31}P NMR (121 MHz, CD_3OD, 313 K): δ = 19.7 (s) ppm.

MS (ESI^+): m/z = 777.5 (100%, $[M+Na]^+$), 721.4 (15%). Calc. for $C_{38}H_{67}N_4O_9P$: 754.5.

7-[[Di(*t*-butoxy)phosphoryl]methyl]-1,4,7,10-tetrazacyclododecane-1,4,10-triacetic acid 4,10-di-*t*-butyl ester (4)

A mixture of compound **8** (1.38 g, 1.83 mmol), 10% Pd/C (0.28 g) and MeOH (10 mL) was stirred under hydrogen atmosphere at room temperature for 10 h. The mixture was filtered through Celite and evaporated to give compound **4** (1.20 g, 99%) as a pale-yellow oil.

IR (neat): 3381, 2975, 1725, 1650, 1367, 1151, 1070, 976, 567, 433 cm^{-1}.

^{1}H NMR (300 MHz, CD_3OD, 313 K) δ 3.79 – 2.82 (m, 24H), 1.52 – 1.48 (m, 36H) ppm.

^{13}C NMR (75 MHz, CD_3OD, 298 K) δ 170.9 (C), 169.1 (C), 82.7 (C), 79.9 (C, d, J = 8.1 Hz), 57.4 (CH_2), 54.2 (CH_2), 52.4 (CH_2, d, J = 140.6 Hz), 52.3 (CH_2), 51.8 (6 CH_2), 30.1 (CH_3, d, J = 3.8 Hz), 27.6 (CH_3) ppm.

^{31}P NMR (121 MHz, CD_3OD, 313 K): δ 5.85 (s)**.**

MS (ESI^+): m/z = 703.2 (36%, $[M+K]^+$), 687.4 (100%, $[M+Na]^+$), 630.9 (12%). Calc. for $C_{31}H_{61}N_4O_9P$: 664.4.

HRMS (ESI^+): m/z = 665.42279 (100%, $[M+H]^+$), 687.40452 (55%, $[M+Na]^+$). Calc. for $C_{31}H_{61}N_4O_9P$: 664.41762.

References

(1) For representative reviews see: (a) Sarko, D.; Eisenhut, M.; Haberkorn, U.; Mier, W. *Curr. Med. Chem.* **2012**, *19*, 2667. (b) Liu, S. *Adv. Drug Deliv. Rev.* **2008**, *60*, 1347. (c) Liu, S. *Chem. Soc. Rev.* **2004**, *33*, 445. (d) Kostelnik, T. I.; Orvig, C. *Chem. Rev.* **2019**, *119*, 902.

(2) (a) Jackson, J. A.; Hungnes, I. N.; Ma, M. T.; Rivas, C. *Bioconjugate Chem.* **2020**, *31*, 483. (b) Jamous, M.; Haberkorn, U.; Mier, W. *Molecules* **2013**, *18*, 3379. (c) Fani, M.; Maecke, H. R.; Okarvi, S. M. *Theranostics* **2012**, *2*, 481. (d) De León-Rodríguez, L. M.; Kovacs, Z. *Bioconjugate Chem.* **2008**, *19*, 391. (e) Fichna, J.; Janecka, A. *Bioconjugate Chem.* **2003**, *14*, 3.

(3) (a) Steiner, M.; Neri, D. *Clin. Cancer Res.* **2011**, *17*, 6406. (b) Boswell, C. A.; Brechbiel, M. W. *Nucl. Med. Biol.* **2007**, *34*, 757. (c) Milenic, D. E.; Brady, E. D.; Brechbiel, M. W. *Nat. Rev. Drug Discov.* **2004**, *3*, 488. (d) Larson, S. M.; Carrasquillo, J. A.; Cheung, N.-K. V.; Press, O. W. *Nat. Rev. Cancer* **2015**, *15*, 347.

(4) For representative reviews see: (a) Banerjee, S.; Pillai, M. R. A.; Knapp, F. F. *Chem. Rev.* **2015**, *115*, 2934. (b) Price, E. W.; Orvig, C. *Chem. Soc. Rev.* **2014**, *43*, 260. (c) Ramogida, C. F.; Orvig, C. *Chem. Commun.* **2013**, *49*, 4720. (d) Bartholomä, M. D. *Inorg. Chim. Acta* **2012**, *389*, 36. (e) Frullano, L.; Caravan, P. *Curr. Org. Synth.* **2011**, *8*, 535. (f) Bhattacharyya, S.; Dixit, M. *Dalton Trans.* **2011**, *40*, 6112.

(5) (a) Giovenzana, G. B.; Lattuada, L.; Negri, R. *Isr. J. Chem.* **2017**, *57*, 825. (b) Lattuada, L.; Barge, A.; Cravotto, G.; Giovenzana, G. B.; Tei, L. *Chem. Soc. Rev.* **2011**, *40*, 3019.

(6) (a) Wahsner, J.; Gale, E. M.; Rodríguez-Rodríguez, A.; Caravan, P. *Chem. Rev.* **2019**, *119*, 957. (b) Hermann, P.; Kotek, J.; Kubíček, V.; Lukeš, I. *Dalton Trans.* **2008**, 3027. (c) Stasiuk, G. J.; Long, N. J. *Chem. Commun.* **2013**, *49*, 2732.

(7) Bianchi, A.; Calabi, L.; Corana, F.; Fontana, S.; Losi, P.; Maiocchi, A.; Paleari, L.; Valtancoli, B. *Coord. Chem. Rev.* **2000**, *204*, 309.

(8) Moore, D. A. *Org. Synth.* **2008**, *85*, 10.

(9) Heppeler, A.; Froidevaux, S.; Mäcke, H. R.; Jermann, E.; Béhé, M.; Powell, P.; Hennig, M. *Chem. Eur. J.* **1999**, *5*, 1974.

(10) (a) Jagadish, B.; Brickert-Albrecht, G. L.; Nichol, G. S.; Mash, E. A.; Raghunand, N. *Tetrahedron Lett.* **2011**, *52*, 2058. (b) Li, C.; Winnard, P.; Bhujwalla, Z. M. *Tetrahedron Lett.* **2009**, *50*, 2929. (c) Oliver, M.; Jorgensen, M. R.; Miller, A. D. *Synlett* **2004**, *2004*, 453. (d) Mukai, T.; Namba, S.; Arano, Y.; Ono, M.; Fujioka,

Y.; Uehara, T.; Ogawa, K.; Konishi, J.; Saji, H. *J. Pharm. Pharmacol.* **2002**, *54*, 1073.

(11) Varshney, R.; Hazari, P. P.; Uppal, J. K.; Pal, S.; Stromberg, R.; Allard, M.; Mishra, A. K. *Cancer Biol. Ther.* **2011**, *11*, 893.

(12) (a) Marsouvanidis, P. J.; Nock, B. A.; Hajjaj, B.; Fehrentz, J.-A.; Brunel, L.; M'Kadmi, C.; van der Graaf, L.; Krenning, E. P.; Maina, T.; Martinez, J.; de Jong, M. *J. Med. Chem.* **2013**, *56*, 2374. (b) Manzoni, L.; Belvisi, L.; Arosio, D.; Bartolomeo, M. P.; Bianchi, A.; Brioschi, C.; Buonsanti, F.; Cabella, C.; Casagrande, C.; Civera, M.; De Matteo, M.; Fugazza, L.; Lattuada, L.; Maisano, F.; Miragoli, L.; Neira, C.; Pilkington-Miksa, M.; Scolastico, C. *ChemMedChem* **2012**, *7*, 1084. (c) Wardle, N. J.; Kalber, T.; Bell, J. D.; Bligh, S. W. A. *Bioorg. Med. Chem. Lett.* **2011**, *21*, 3346.

(13) (a) Azad, B. B.; Rota, V. A.; Breadner, D.; Dhanvantari, S.; Luyt, L. G. *Bioorg. Med. Chem.* **2010**, *18*, 1265. (b) Mishra, R.; Su, W.; Pohmann, R.; Pfeuffer, J.; Sauer, M. G.; Ugurbil, K.; Engelmann, *J. Bioconjugate Chem.* **2009**, *20*, 1860. (c) Sosabowski, J. K.; Mather, S. J. *Nat. Protoc.* **2006**, *1*, 972. (d) De León-Rodríguez, L. M.; Ortiz, A.; Weiner, A. L.; Zhang, S.; Kovacs, Z.; Kodadek, T.; Sherry, A. D. *J. Am. Chem. Soc.* **2002**, *124*, 3514. (e) Graham, K. A. N.; Wang, Q.; Eisenhut, M.; Haberkorn, U.; Mier, W. *Tetrahedron Lett.* **2002**, *43*, 5021.

(14) Minazzi, P.; Lattuada, L.; Menegotto, I. G.; Giovenzana, G. B. *Org. Biomol. Chem.* **2014**, *12*, 6915.

(15) (a) Giovenzana, G. B.; Guanci, C.; Dematti o, S.; Lattuada, L.; Vincenzi, V. *Tetrahedron* **2014**, *70*, 4809. (b) Barge, A.; Cappelletti, E.; Cravotto, G.; Ferrigato, A.; Lattuada, L.; Marinoni, F.; Tei, L. *Org. Biomol. Chem.* **2009**, *7*, 3810. (c) Anelli, P. L.; Lattuada, L.; Gabellini, M.; Recanati, P. *Bioconjugate Chem.* **2001**, *12*, 1081. (d) Anelli, P. L.; Fedeli, F.; Gazzotti, O.; Lattuada, L.; Lux, G.; Rebasti, F. *Bioconjugate Chem.* **1999**, *10*, 137. (e) Lattuada, L.; Gabellini, M. *Synth. Commun.* **2005**, *35*, 2409.

(16) (a) Ballatore, C.; Huryn, D. M.; Smith, A. B. *ChemMedChem* **2013**, *8*, 385. (b) Patani, G. A.; LaVoie, E. J. *Chem. Rev.* **1996**, *96*, 3147.

(17) Táborský P., Lubal P., Havel J., Kotek J., Hermann P., Lukeš I. *Collect. Czech. Chem. Commun.* **2005**, *70*, 1909.

(18) Rudovský J., Cígler P., Kotek J., Hermann P., Vojtíšek P., Lukeš I., Peters J. A., Elst L. V., Muller R. N. *Chem. Eur. J.* **2005**, *11*, 2373.

(19) (a) Ferrand, A.-C.; Imbert, D.; Chauvin, A.-S., Vandevyver, C. D. B.; Bünzli, J.-C. G. *Chem. Eur. J.* **2007**, *13*, 8678. (b) Dischino, D. D.; Delaney, E. J.; Emswiler, J. E.; Gaughan, G. T.; Prasad, J. S.; Srivastava, S. K.; Tweedle, M. F. *Inorg. Chem.* **1991**, *30*, 1265.

(20) Travagin, F.; Lattuada, L.; Giovenzana, G. B. *Org. Chem. Front.* **2019**, *6*, 1387.

(21) Kovacs, Z.; Sherry, A. D. *Synthesis* **1997**, 759.

(22) Keglevich, G.; Bálint, E.; Kangyal, R.; Bálint, M.; Milen, M. *Heteroatom Chem.* **2014**, *25*, 282.

(23) Manning, H. C.; Bai, M.; Anderson, B. M.; Lisiak, R.; Samuelson, L. E.; Bornhop, D. J. *Tetrahedron Lett.* **2005**, *46*, 4707.

(24) Lattuada, L.; Cappelletti, E.; Linder, K. E.; Nunn, A. D. *United States Patent* US20110250133A1, **2011**.

(25) Lattuada, L.; Napolitano, R.; Boi, V.; Visigalli, M.; Aime, S.; Giovenzana, G. B.; Mingo, A. F. *World Intellectual Property Organization* WO2017178301A1, **2017**.

Adapted from ***Synlett***, 2020, **31(13)**, 1291-1294 with permission from Georg Thieme Verlag.

For this work, I have prepared and characterised all the compounds herein presented and collaborated to the drawing up of the article.

Chapter 5: TRASUTA, a new hexadentate spirocyclic chelator for gallium-based contrast agents

Introduction

PET (positron emission tomography) is an essential tool in oncology since it is able to highlight the finest changes in the body at a molecular level. PET exploits radionuclides that, properly introduced in a molecular entity and administered to the patient, distribute themselves in the whole body or in specific anatomic regions. Once there, each of them emit positrons, which annihilate due to the contact with electrons of the living matter generating two collinear γ rays. These are subsequently captured by a gamma camera and a computer reconstruct the origin of the radiations generating 3D images.[1,2]

In the literature many different radiolabelled nanoparticles[3,4] and biomolecules are reported and some of them are clinically approved, such as fludeoxyglucose (^{18}F)[5], fluorodopa (^{18}F)[6], choline (^{11}C)[5] etc. (**Figure 5.1**)

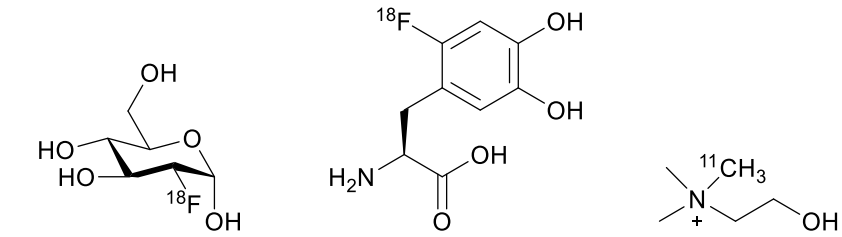

Fludeoxyglucose (^{18}F) **Fluorodopa (^{18}F)** **Choline (^{11}C)**

Figure 5.1. Fluorodopa (^{18}F), choline (^{11}C), clinically approved PET contrast agents.

These compounds are very useful since they can trace fine physio-pathological changes in the body thanks to their biobased structures.[1,2] However, the introduction of a newly synthesised radioisotope (such as ^{18}F or ^{11}C) in a non-radioactive precursor is not an easy task. In fact, this kind of labelling exploits classical organic chemistry procedures, with all their limitations, such as incomplete conversion, need for purification, long reaction times etc. Moreover, these matters are complicated by the issues deriving from the short half-life values of ^{18}F or ^{11}C, which entangle the synthetic procedures and purifications.

For this reason, in the recent years, radiometal complexes have made their appearance into the field of PET contrast agents. Radionuclides, such as ^{68}Ga, ^{64}Cu, ^{111}In, ^{89}Zr and ^{44}Sc, possess favourable half-life values for β^+ decay. [2,7]

In particular, ^{68}Ga has found the more widespread clinical application because it possesses interesting decaying features, very compatible for PET imaging purposes. ^{68}Ga, in fact, has a half-life of 68 min and decays to ^{68}Zn by β^+ emission. ^{68}Ga is produced from ^{68}Ge by a dedicated generator, recently become an inexpensive technology, affordable for hospitals. ^{68}Ge is long-lived (271 days) and it decays by electron capture to $^{68}Ga^{3+}$, which is then purified by cation-exchange chromatography.[8,9]

The synthesis of radiometal complexes requires one simple step, the complexation reactions, which usually proceeds spontaneously in solution with excellent yields. Since the short half-life values of the above mentioned radiometals, ligands with a quick complexation kinetic are preferable. However, long decomplexation kinetics and thermodynamic stability of complexes are also important to ensure that the complex does not release the metal in the body, generating side effects and loss of imaging selectivity. These characteristics are important for many applications of chelating agents and metal complexes, but sometimes are not very easy to tune.[1,2,7,8]

In fact, chelating agents may be divided into two main classes of compounds, linear and macrocyclic.

Linear chelating agents were the first CAs approved for clinical use, their preparation is straightforward and their complexes are rapidly formed, but at the same time they are thermodynamically and kinetically less stable, leading to toxic effects *in vivo*. Due to these significant disadvantages, the clinical relevance of linear CAs is fading away. On the contrary, the synthesis of macrocyclic ligands is tougher, but in exchange their complexes possess a great kinetic and thermodynamic stability, though they are slowly formed.[10]

This category of chelating agents has found widespread applications in the field of PET chelating agents, which culminated in the recent clinical approval of DOTATOC. The latter is a radiopharmaceutical developed for the functional imaging of neuroendocrine tumours. It consists of a DOTA-like bifunctional chelating agent linked

to the vector molecule octreotide, a somatostatin analogue and complexed with gallium.[11]

However, DOTA-like ligands require long reaction times, high radiometal concentrations and high temperatures (70 – 95 °C) which sometimes are not compatible with vector biomolecules.[7]

Instead, the innovative class of mesocyclic ligands, owns intermediate characteristics between the two previously listed ones. Their synthesis is relatively accessible and inexpensive, and their complexes show good kinetic and thermodynamic stability combined with a rapid kinetic of formation.[10]

AAZTA is a representative heptadentate polyaminocarboxylic mesocyclic ligand showing competitive and complementary complexing behaviour compared to both linear and macrocyclic CAs.[12,13] (**Figure 5.2**)

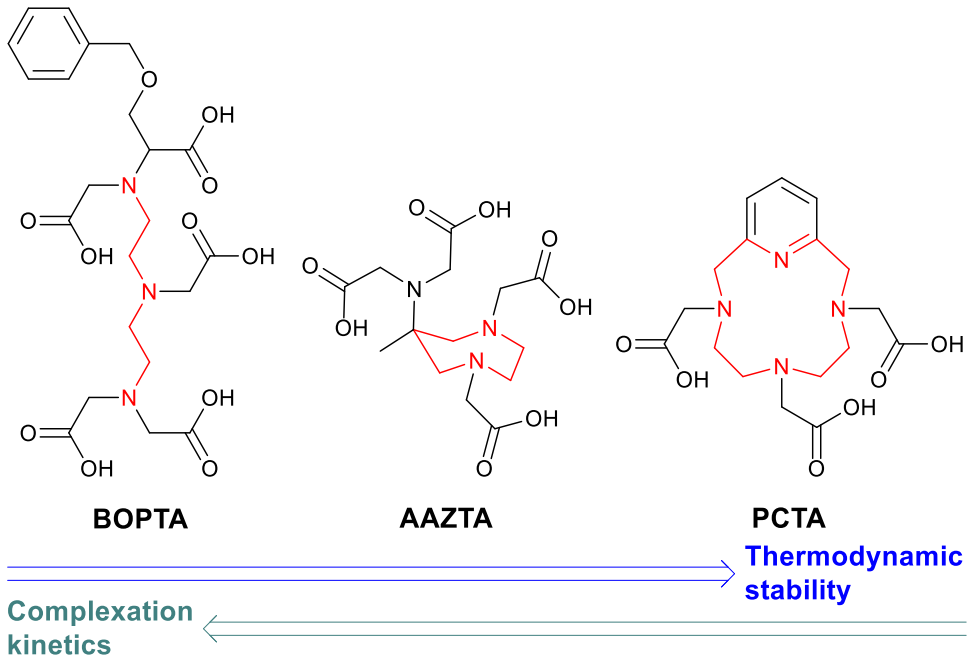

Figure 5.2. BOPTA (linear CA), AAZTA (mesocyclic CA) and PCTA (macrocyclic CA).

In fact, AAZTA form very stable complexes with post-transition metals and with block *d* and *f* elements.[7]

Because of these valuable features, a vast number of AAZTA derivatives have been synthesised and reported in literature, in the last two decades, in order to improve the metal chelates stability, efficacy and selectivity in their use as CAs.[12]

AAZTA-like bifunctional chelating agents (BFCAs) have been reported as well to conjugate imaging-related metals to diagnostic-relevant biomolecules, exploiting the advantageous structure of AAZTA.[14–16]

AAZTA and its derivatives have been also complexed with gallium to evaluate their possible use as PET contrast agents.[17–19] For example, Ga-AAZTA-MG consists in an AAZTA-like BFCA (AAZTA-C9) linked to minigastrin, a peptide which targets cholecystokinin receptors and is really useful in PET imaging of neuroendocrine tumours.[20,21]

Moreover, many AAZTA derivatives, in which the mesocyclic structure is modified are reported in the literature. Some of them exploit a very common method to modulate metal complexes characteristics, *i.e.* to rigidify the structure of the ligand. For example, fusion of the mesocycle with an additional ring reduces the degrees of freedom and the number of conformations of the resulting structure. Therefore, it is more difficult for the metal to escape from the complex.

In the literature two different successful approaches to make rigid bicyclic AAZTA derivatives are reported to date.[22]

Approach #1 (**Figure 5.3**) involves the fusion of six-membered ring with positions 2 – 3 of the 7-membered diazepane ring leading to “CyAAZTA”[23]. Approach #2 generates the alternative “PIDAZTA”, bearing the new six-membered ring implanted on atoms 1 and 2.[22]

The present work, conversely, is focused on the original preparation of an AAZTA derivative (“**TRASUTA**”) with a five-membered ring between position 6 and the exocyclic *α* amino group (**Figure 5.3**).

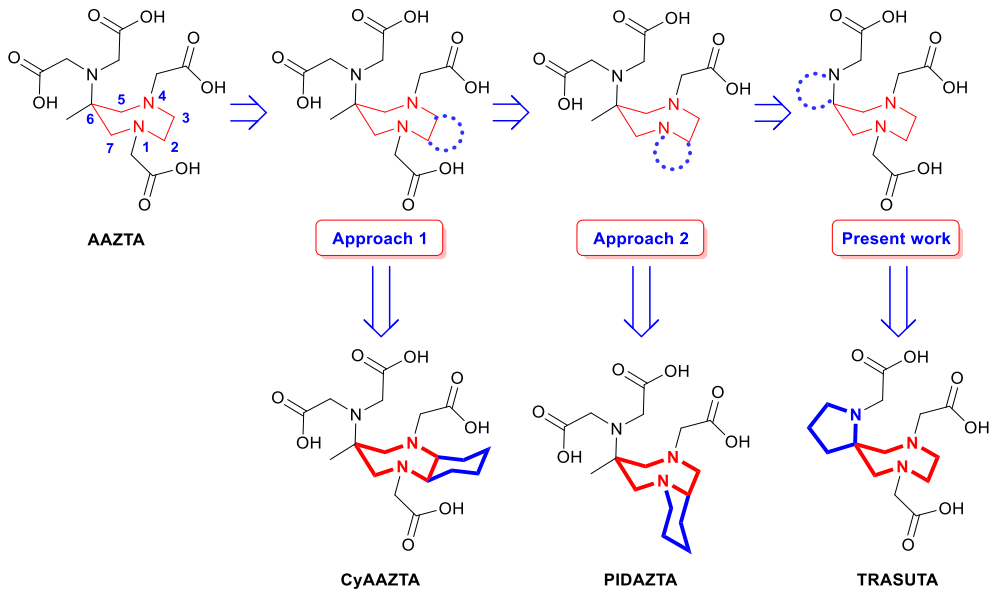

Figure 5.3. Different strategies to make AAZTA more rigid.

To evaluate if **TRASUTA** could be suitable as gallium chelating agent we have performed a complete array of potentiometric titrations to determine the stability constants of Ga-**TRASUTA** complex. These measurements are preliminary to a possible exploitation of **TRASUTA** as a novel PET contrast agent.

Results and discussion

The synthesis of **TRASUTA** (2,2',2''-(1,7,10-**tria**za**s**piro[4.6]**u**ndecane-1,7,10-triyl)**t**riacetic **a**cid) (**Figure 5.4**) implies an initial nitro-Mannich reaction between the commercial and inexpensive benzathine **1**, nitromethane and aqueous formaldehyde in refluxing ethanol to produce intermediate **2** in almost quantitative yield. Then, compound **2** is treated with potassium *tert*-butoxide in dry tetrahydrofuran at room temperature for 30 minutes with vigorous stirring. Methyl acrylate is slowly added to the mixture, then left at room temperature for 3 hours. Intermediate **3** is obtained in 95% yield over 2 steps and, in the following step, it is reduced under hydrogen atmosphere in the presence of Raney Nickel as a catalyst in methanol at room temperature for 8 days. The solvent is then exchanged with toluene and the mixture

is refluxed for another 20 hours to complete the cyclization reaction to compound **4** which crystallise from ethyl acetate in 52% yield (**Procedure 4A**). Intermediate **4** is treated with lithium aluminium hydride in refluxing THF for 24 h under nitrogen atmosphere obtaining compound **5** in almost quantitative yield. Intermediate **5** is then reduced under hydrogen atmosphere in the presence of Pd/C as a catalyst in methanol at room temperature for 28 hours quantitatively yielding compound **6**. The latter is alkylated with *tert*-butyl bromoacetate in acetonitrile using potassium carbonate as base leading to the formation of compound **7** in 31% yield (**Procedure 7A**). The final step requires the treatment of intermediate **7** with trifluoroacetic acid at room temperature for 28 h achieving the desired product **TRASUTA** in 73 % yield (**Figure 5.4**).

Analysing the synthetic strategy employed, it is evident that the third and the sixth steps are the bottlenecks of the entire synthetic process, therefore some efforts have been made to improve their yields and reaction conditions.

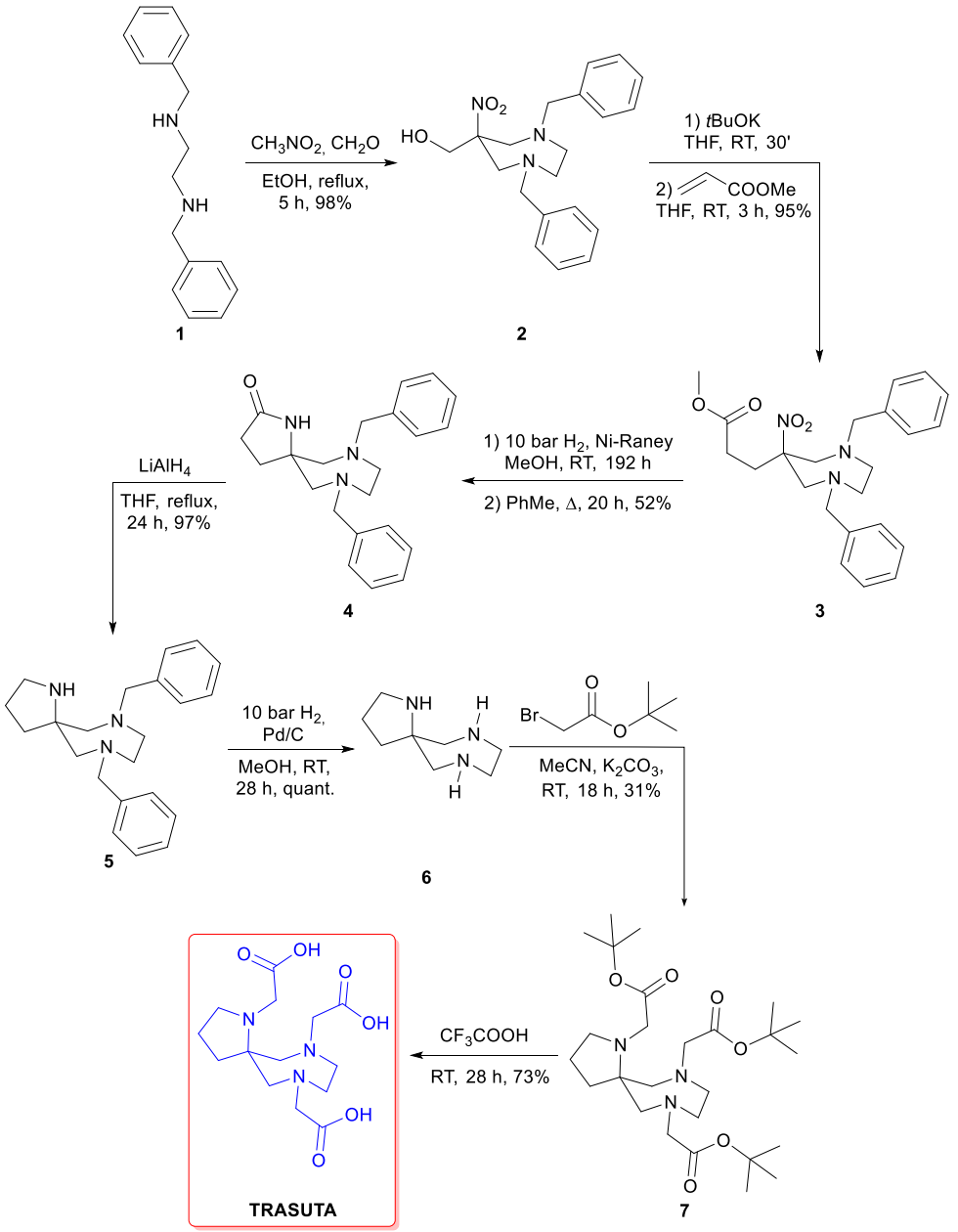

Figure 5.4. Synthesis of TRASUTA.

Precisely, in the third step, alternative reducing methodologies, such as iron (**Procedure 4B**) or zinc (**Procedure 4C**) in acetic acid, has been screened. The

dissolving-metal reduction with iron in refluxing acetic acid for 20 h performed quite well, the yield (49%) was similar to the Raney Nickel procedure (52%) but quenching and work-up were plagued by low recovery of the product (**Procedure 4B**). Zinc in refluxing acetic acid for 20 h, was the worst combination with a very low isolated yield (15%) (**Procedure 4C**).

The sixth step of TRASUTA synthesis, involving an alkylation reaction with *tert*-butyl bromoacetate, did not reach satisfying yields. Different combination of solvents, bases and temperatures were tested, with the higher results being a meagre 31% yield, nevertheless useful to accumulate enough material for our purposes (**Procedures 7A – 7C**).

The determination of pKa values of **TRASUTA** was performed by potentiometric titration at 298 K in 0.15 M NaCl and yielded the pK_{ai} values reported in **Table 5.1**.

$\log K_1^H$	9.76
$\log K_2^H$	6.15
$\log K_3^H$	4.14
$\log K_4^H$	2.53
$\Sigma \log K_i^H$	22.57

Table 5.1. pKa values of TRASUTA.

The preparation of the gallium complex (**Figure 5.5**) was straightforward, considering instantaneous the reaction of stoichiometric amounts of **TRASUTA** with the corresponding gallium salt.

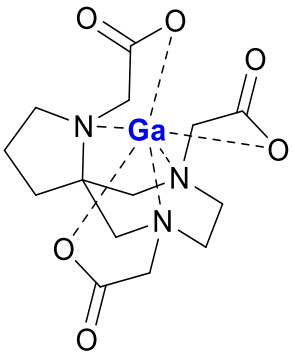

Figure 5.5. Ga^{3+}-**TRASUTA**

Stability and protonation constants of Ga(III)-complexes formed with **TRASUTA** were determined by potentiometric titration of 1:1 metal/**TRASUTA** mixtures in the pH range 2 - 12 in a 0.15 M NaCl solution at 298 K. The stability constants of **TRASUTA** are reported in **Table 5.2**.

GaL	16.53
Ga(HL)	3.11
Ga(H_2L)	2.25
Ga(L)OH	5.38
log$\beta_{Ga(L)OH}$	11.15

Table 5.2. Stability constants of Ga^{3+}-**TRASUTA**.

The species distribution of Ga^{3+}-**TRASUTA** system ([Ga^{3+}] = [**TRASUTA**] = 1.0 mM, 0.15 M NaCl, 298 K) is reported in **Figure 5.6**.

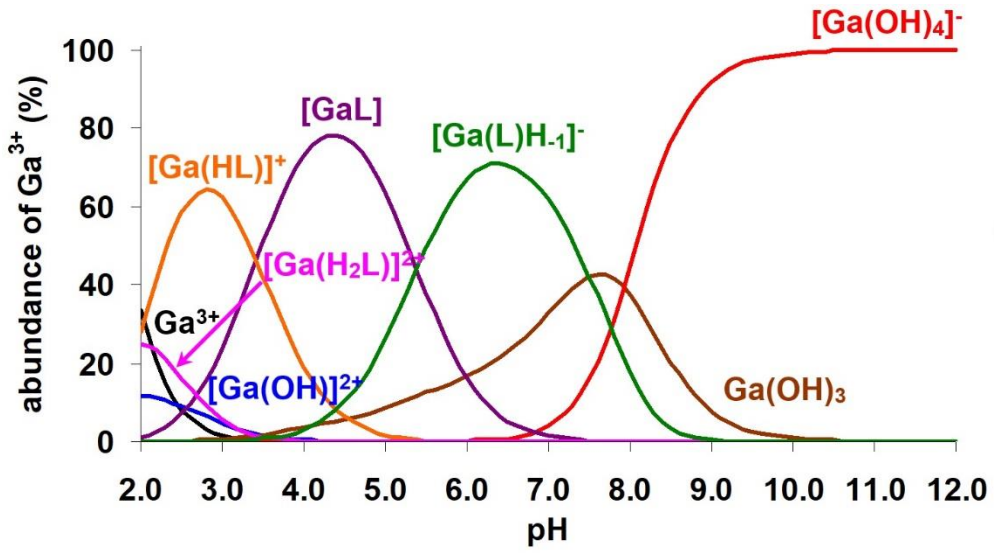

Figure 5.6. Species distribution of Ga^{3+}-**TRASUTA** system.

Conclusions

In this section an unprecedented hexadentate spirocyclic chelating agent has been presented, discussing in detail its synthesis, the characterization of its acid-base behaviour and the stability of its gallium complex. This analysis represents a preliminary assessment of **TRASUTA** as a Ga^{3+} chelator to evaluate its possible application as PET contrast agent.

Future developments will concern the optimisation of **TRASUTA** synthesis, such as reaction conditions, overall yield and purification process. Moreover, we will evaluate the complexometric behaviour of **TRASUTA** with other metal ions of diagnostic and therapeutic interest.

Experimental section

Materials and methods

Solvents and starting materials were purchased from Merck or TCI and used without further purification. All aqueous solutions were prepared from ultrapure laboratory grade water (18 MΩ · cm) obtained from Millipore/MilliQ purification system. ^{1}H and ^{13}C NMR spectra were recorded at 300 MHz on a Jeol Eclipse ECP300 spectrometer. Chemical shifts are reported in ppm with the protic impurities of the deuterated solvent as the internal reference. Mass spectra were obtained with a Thermo Finningan LCQ-Deca XP-PLUS ion trap spectrometer equipped with an electrospray source. TLC were performed with silica gel (MN Kieselgel 60F254) and visualized by UV or sprayed with Dragendorff reagent or alkaline $KMnO_4$. Column chromatography was carried out on Macherey-Nagel Silica gel 60 (0.063-0.200 mm).

Synthetic procedures

(1,4-Dibenzyl-6-nitro-1,4-diazepan-6-yl)methanol (2)

N,*N*'-dibenzylethylendiamine (freshly obtained by extraction with DCM of a NaOH aqueous solution of *N*,*N*'-dibenzylethylendiamine diacetate, 29.6 g, 82.0 mmol) and nitromethane (4.4 mL, 82.0 mmol) were dissolved in ethanol (100 mL). Formaldehyde solution (37 wt. % in water, 26.6 g, 354 mmol) was added in small portions under stirring, and the suspension was heated to reflux for 5 h. The reaction mixture was evaporated *in vacuo*, and the crude product was dissolved in basified water ($NaHCO_3$) and extracted three times with ethyl acetate. The organic phase was then dried over Na_2CO_3 and Na_2SO_4, filtered and evaporated. The waxy residue was purified on silica gel chromatography column (DCM) to give compound **2** as a brown oil (28.6 g, 98 %).
^{1}H NMR (300 MHz, $CDCl_3$, 298 K) δ 7.39 – 7.30 (m, 10H), 3.77 – 3.63 (m, 6H), 3.54 (d, J = 14.4 Hz, 2H), 3.06 (d, J = 14.3 Hz, 2H), 2.73 – 2.58 (m, 4H), 2.33 (br s, 1H) ppm.
^{13}C NMR (75 MHz, $CDCl_3$, 298 K) δ 138.8 (C), 129.0 (CH), 128.4 (CH), 127.4 (CH), 94.7 (C), 65.7 (CH_2), 63.7 (CH_2), 59.0 (CH_2), 58.6 (CH_2) ppm.

MS (ESI$^+$): *m*/z = 356.20 (100%, $[M+H]^+$). Calc. for $C_{20}H_{25}N_3O_3$: 355.19.

Methyl 3-(1,4-dibenzyl-6-nitro-1,4-diazepan-6-yl)propanoate (3)

Compound **2** (20 g, 56,3 mmol) was dissolved in anhydrous THF (148 mL), potassium *tert*-butoxide (9.47 g, 84.4 mmol) was added and the suspension was stirred at RT for 30 min. Methyl acrylate (10 mL, 113 mmol) was then added, and the mixture was stirred at room temperature for 3 hours. After that 1 mL of methanol and an aqueous solution saturated with $NaHCO_3$ were then added to the reaction. The organic layer was separated, and the aqueous phase was extracted 2 times with ethyl acetate. The organic phase was dried over Na_2SO_4 and Na_2CO_3 and evaporated to dryness. The product was purified column chromatography (Pet/EtOAc 9:1) to give compound **3** as a yellow oil (22.0 g, 95 %).

^{1}H NMR (300 MHz, $CDCl_3$, 298 K) δ 7.30 – 7.23 (m, 10H), 3.75 – 3.48 (m, 9H), 2.94 (d, J = 14.2 Hz, 2H), 2.68 – 2.54 (m, 4H), 1.97 – 1.91 (m, 2H), 1.76 – 1.70 (m, 2H) ppm.

^{13}C NMR (75 MHz, $CDCl_3$, 298 K) δ 138.6 (C), 128.6 (CH), 127.9 (CH), 126.8 (CH), 93.3 (C), 63.3 (CH_2), 60.9 (CH_2), 58.1 (CH_2), 51.0 (CH_3), 30.8 (CH_2), 27.1 (CH_2).

MS (ESI$^+$): *m*/z = 412.52 (100%, $[M+H]^+$). Calc. for $C_{23}H_{29}N_3O_4$: 411.22.

7,10-Dibenzyl-1,7,10-triazaspiro[4.6]undecan-2-one (4)

Procedure 4A. A 50 % Raney-Nickel slurry (26 g) was washed with methanol and centrifuged 3 times to completely remove water. This Raney-Nickel slurry in methanol was added to a solution of compound **3** (13.0 g, 31.6 mmol) and methanol (120 mL total). The mixture was stirred at RT under hydrogen atmosphere (10 bar) for 192 h then filtered through Celite and dried under vacuum. The residue was taken up in toluene, refluxed for 20 h and then evaporated to dryness. The product is purified by crystallization from ethyl acetate, vacuum filtration and washing with Et_2O to give compound **4** as white needles (5.76 g, 52 %).

Procedure 4B. A mixture of compound **3** (1.00 g, 2.43 mmol), iron (0.679 g, 12.2 mmol) and acetic acid (5 mL) was refluxed for 20 h. Then the mixture was quenched in water, basified with $NaHCO_3$ and treated with 5 g of EDTA disodium. The resulting suspension was filtered and extracted three times with ethyl acetate. The organic

phase was dried (Na_2SO_4, Na_2CO_3) and removed under vacuum. The product is purified by crystallization from ethyl acetate, vacuum filtration and washing with Et_2O to give compound **4** as white needles (0.419 g, 49 %).

Procedure 4C. A mixture of compound **3** (11.7 g, 28.5 mmol), zinc (9.31 g, 142 mmol) and acetic acid (70 mL) is refluxed for 20 h. Then the mixture was quenched in water, basified with $NaHCO_3$ and treated with 14 g of EDTA disodium. The resulting suspension was filtered and extracted three times with ethyl acetate. The organic phase was dried (Na_2SO_4, Na_2CO_3) and removed under vacuum. The product is purified by crystallization from ethyl acetate, vacuum filtration and washing with Et_2O to give compound **4** as white needles (1.53 g, 15 %).

^{1}H NMR (300 MHz, $CDCl_3$, 298 K) δ 7.32 – 7.26 (m, 10H), 3.71 – 3.45 (m, 4H), 2.84 – 2.57 (m, 6H), 2.21 (s, 1H), 2.04 (t, J = 7.9 Hz, 2H), 1.57 (t, J = 7.8 Hz, 2H) ppm.

^{13}C NMR (75 MHz, $CDCl_3$, 298 K) δ 176.5 (C), 129.0 (C), 128.5 (CH), 127.4 (CH), 65.3 (CH_2), 64.0 (CH_2), 62.3 (C), 58.5 (CH_2), 29.9 (CH_2), 29.2 (CH_2) ppm.

MS (ESI$^+$): *m*/z = 350.37 (100%, $[M+H]^+$). Calc. for $C_{22}H_{27}N_3O$: 349.22.

7,10-dibenzyl-1,7,10-triazaspiro[4.6]undecane (5)

Compound **4** (4.10 g, 11.7 mmol) was dissolved in dry THF (20 mL) and $LiAlH_4$ (1.34 g, 35.2 mmol) was added portionwise under nitrogen atmosphere. The reaction was stirred and refluxed under nitrogen atmosphere for 24 h. The mixture was quenched with NaOH 50% aqueous solution and then with water and the organic phase was separated. The aqueous layer was extracted three times with DCM, the organic phases were collected and dried under vacuum. The product was purified by column chromatography (EtOAc/MeOH 95:5 – 8:2) to yield compound **5** as a yellow oil (3.80 g, 97 %).

^{1}H NMR (300 MHz, $CDCl_3$, 298 K) δ 1H NMR (300 MHz, CDCl3, 298K) δ 7.33 – 7.19 (m, 10H), 6.19 (s, 1H), 3.64 (d, *J* = 13.1 Hz, 2H), 3.58 (d, *J* = 13.1 Hz, 2H), 2.81 – 2.50 (m, 8H), 1.95 – 1.91 (m, 4H), 1.51 – 1.47 (m, 2H) ppm.

^{13}C NMR (75 MHz, $CDCl_3$, 298 K) δ 139.9 (C), 129.2 (CH), 128.3 (CH), 127.1 (CH), 65.0 (CH_2), 64.8 (C), 63.7 (CH_2), 57.6 (CH_2), 44.5 (CH_2), 35.4 (CH_2), 24.0 (CH_2) ppm.

MS (ESI$^+$): *m*/z = 336.26 (100%, $[M+H]^+$). Calc. for $C_{22}H_{29}N_3$: 335.24.

1,7,10-triazaspiro[4.6]undecane (6)

Compound **5** (3.60 g, 10,7 mmol) was dissolved in methanol, Pd/C (5 %, 3.60 g) was added, and the mixture was stirred under hydrogen atmosphere (10 atm) at room temperature for 28 h. The reaction was filtered through Celite and evaporated to give compound **6** as a brown oil (1.67 g, quant.).

^{1}H NMR (300 MHz, D_2O, 298 K) δ 3.56 (t, J = 7.0 Hz, 2H), 3.47 – 3.34 (m, 6H), 2.32 – 2.11 (m, 6H) ppm.

^{13}C NMR (75 MHz, D_2O, 298 K) δ 58.2 (C), 54.7 (CH_2), 48.7 (CH_2), 45.5 (CH_2), 33.9 (CH_2), 23.2 (CH_2).

MS (ESI$^+$): m/z = 156.15 (100%, $[M+H]^+$). Calc. for $C_8H_{17}N_3$: 155.14.

tri-*tert*-Butyl 2,2',2''-(1,7,10-triazaspiro[4.6]undecane-1,7,10-triyl)triacetate (7)

Procedure 7A. Compound **6** (0.542 g, 3.49 mmol) was dissolved in acetonitrile (10 mL) and potassium carbonate (1.93 g, 14.0 mmol) was added. *tert*-Butyl bromoacetate (1.7 mL, 11.5 mmol) was added dropwise over 1 h at 0°C and then the reaction was stirred at room temperature for 18 h. The mixture was filtered, evaporated and purified by column chromatography (Pet/EtOAc 9:1 – 85:15) to give compound **7** as a yellow oil (0.531 g, 31 %).

Procedure 7B. Compound **6** (0.513 g, 3.30 mmol) was dissolved in *N*,*N*-dimethylacetamide (2 mL) and the potassium carbonate (2.74 g, 0.0198 mmol) was added. The *tert*-butyl bromoacetate (2.9 mL, 0.0198 mmol) was added dropwise over 1 h at 0°C and then the reaction was stirred at room temperature for 18 h. Then water was added to the mixture which was extracted three times with ether, dried (Na_2SO_4, Na_2CO_3), evaporated under vacuum and purified by column chromatography (Pet/EtOAc 9:1 – 85:15) to give compound **7** as a yellow oil (0.477 g, 29 %).

Procedure 7C. Compound **6** (0.500 g, 3.22 mmol) was dissolved in acetonitrile (10 mL) and potassium carbonate (1.93 g, 14.0 mmol) and sodium sulfate (1.83 g, 13.0 mmol) were added. *tert*-Butyl bromoacetate (1.7 mL, 11.5 mmol) was added dropwise over 3 h at 0 °C and then the reaction was stirred at room temperature for 18 h. The mixture was filtered, evaporated and purified by column chromatography (Pet/EtOAc 9:1 – 85:15) to give compound **7** as a yellow oil (0.485 g, 30 %).

^{1}H NMR (300 MHz, $CDCl_3$, 298 K) δ 3.37 (s, 2H), 3.04 (br s, 4H), 2.69 – 2.44 (m, 10H), 1.49 (br s, 2H), 1.35 – 1.24 (m, 29H) ppm.
^{13}C NMR (75 MHz, $CDCl_3$, 298 K) δ 171.5 (C), 170.3 (C), 80.4 (C), 79.8 (C), 65.3 (C), 63.4 (CH_2), 61.9 (CH_2), 58.8 (CH_2), 51.9 (CH_2), 51.0 (CH_2), 35.9 (CH_2), 27.9 (CH_3), 27.8 (CH_3), 21.7 (CH_2).
MS (ESI$^+$): *m*/z = 498.35 (100%, $[M+H]^+$). Calc. for $C_{26}H_{47}N_3O_6$: 497.35.

2,2',2''-(1,7,10-Triazaspiro[4.6]undecane-1,7,10-triyl)triacetic acid (8)

Compound **7** (0.262 g, 0.526 mmol) was dissolved in trifluoroacetic acid (2 mL) and left at room temperature for 28 h. The mixture was dried under vacuum and the residue was dissolved in methanol, precipitated with ether, centrifugated and the supernatant was poured away. This procedure was repeated three times. The product was purified by chromatography on XAD (eluent: H_2O) to give compound **8** as an off-white solid (0.126 g, 73 %).
^{1}H NMR (300 MHz, D_2O, 298 K) δ 4.32 (s, 2H), 3.94 (br s, 4H), 3.83 – 3.64 (m, 6H), 3.53 – 3.36 (m, 6H), 2.24 (s, 2H) ppm.
^{13}C NMR (75 MHz, D_2O, 298 K) δ 172.7 (C), 170.7 (C), 74.7 (C), 59.1 (CH_2), 59.0 (CH_2), 58.6 (CH_2), 54.3 (CH_2), 54.1 (CH_2), 33.9 (CH_2), 21.2 (CH_2) ppm.
MS (ESI$^+$): *m*/z = 330.17 (100%, $[M+H]^+$). Calc. for $C_{14}H_{23}N_3O_6$: 329.16.

References

(1) S. Vallabhajosula, *Molecular Imaging: Radiopharmaceuticals for PET and SPECT*, Springer-Verlag, Berlin Heidelberg, 2009.

(2) T. J. Wadas, E. H. Wong, G. R. Weisman and C. J. Anderson, *Chem. Rev.*, 2010, **110**, 2858–2902.

(3) S. Goel, C. G. England, F. Chen and W. Cai, *Advanced Drug Delivery Reviews*, 2017, **113**, 157–176.

(4) Z. Cheng, X. Yan, X. Sun, B. Shen and S. S. Gambhir, *Engineering*, 2016, **2**, 132–140.

(5) B. N. Clarke, *J. Nucl. Med. Technol.*, 2018, **46**, 12–16.

(6) T. Ishikawa, V. Dhawan, C. Patlak, T. Chaly and D. Fidelberg, in *Quantification of Brain Function Using PET*, eds. R. Myers, V. Cunningham, D. Bailey and T. Jones, Academic Press, San Diego, 1996, pp. 232–236.

(7) G. Nagy, D. Szikra, G. Trencsényi, A. Fekete, I. Garai, A. M. Giani, R. Negri, N. Masciocchi, A. Maiocchi, F. Uggeri, I. Tóth, S. Aime, G. B. Giovenzana and Z. Baranyai, *Angewandte Chemie International Edition*, 2017, **56**, 2118–2122.

(8) M. Fani, J. P. André and H. R. Maecke, *Contrast Media Mol Imaging*, 2008, **3**, 67–77.

(9) M. J. Welch and C. S. Redvanly, Eds., *Handbook of radiopharmaceuticals: radiochemistry and applications*, J. Wiley, New York, 2003.

(10) J. Wahsner, E. M. Gale, A. Rodríguez-Rodríguez and P. Caravan, *Chem. Rev.*, 2019, **119**, 957–1057.

(11) J. Seemann, B. Waldron, D. Parker and F. Roesch, *EJNMMI Radiopharmacy and Chemistry*, DOI:10.1186/s41181-016-0007-3.

(12) Z. Baranyai, F. Uggeri, G. B. Giovenzana, A. Bényei, E. Brücher and S. Aime, *Chemistry - A European Journal*, 2009, **15**, 1696–1705.

(13) S. Aime, L. Calabi, C. Cavallotti, E. Gianolio, G. B. Giovenzana, P. Losi, A. Maiocchi, G. Palmisano and M. Sisti, *Inorganic Chemistry*, 2004, **43**, 7588–7590.

(14) D. L. Longo, F. Arena, L. Consolino, P. Minazzi, S. Geninatti-Crich, G. B. Giovenzana and S. Aime, *Biomaterials*, 2016, **75**, 47–57.

(15) G. B. Giovenzana, L. Lattuada and R. Negri, *Israel Journal of Chemistry*, 2017, **57**, 825–832.

(16) J.-P. Sinnes, J. Nagel and F. Rösch, *EJNMMI Radiopharm. Chem*., 2019, **4**, 18. DOI:10.1186/s41181-019-0068-1.

(17) D. Parker and B. P. Waldron, *Organic & Biomolecular Chemistry*, 2013, **11**, 2827.

(18) Z. Baranyai, F. Uggeri, A. Maiocchi, G. B. Giovenzana, C. Cavallotti, A. Takács, I. Tóth, I. Bányai, A. Bényei, E. Brucher and S. Aime, *European Journal of Inorganic Chemistry*, 2013, **2013**, 147–162.

(19) L. Manzoni, L. Belvisi, D. Arosio, M. P. Bartolomeo, A. Bianchi, C. Brioschi, F. Buonsanti, C. Cabella, C. Casagrande, M. Civera, M. De Matteo, L. Fugazza, L.

Lattuada, F. Maisano, L. Miragoli, C. Neira, M. Pilkington-Miksa and C. Scolastico, *ChemMedChem*, 2012, **7**, 1084–1093.

(20) J. Pfister, D. Summer, C. Rangger, M. Petrik, E. von Guggenberg, P. Minazzi, G. B. Giovenzana, L. Aloj and C. Decristoforo, *EJNMMI Research*, 2015, **5**, 74.

(21) M. Brom, L. Joosten, P. Laverman, W. J. G. Oyen, M. Béhé, M. Gotthardt and O. C. Boerman, *Mol Imaging*, 2011, **10**, 7290.2010.00032.

(22) E. Farkas, A. Vágner, R. Negri, L. Lattuada, I. Tóth, V. Colombo, D. Esteban-Gómez, C. Platas-Iglesias, J. Notni, Z. Baranyai and G. B. Giovenzana, *Chemistry – A European Journal*, 2019, **25**, 10698–10709.

(23) G. B. Giovenzana, G. Palmisano, M. Sisti, C. Cavallotti, S. Aime, L. Calabi, R. Swenson, R. Kondareddiar, L. Lattuada and P. Morosini, US2006034773 (A1), February 16, 2006.

Chapter 6: Cb-tebpm, a new cyclam derived chelating agent

Introduction

Cyclam (1,4,8,11-tetraazacyclotetradecane) is a macrocyclic polyamine and an important starting material for the preparation of metal complexes exploited as CAs such as TETA.[1] (**Figure 6.1**)

Cyclam based chelating agent are usually believed to chelate metals forming complexes with lower thermodynamic stability and kinetic inertness if compared to the cyclen derived counterparts.[2,3] However, recently many authors reported that cross-bridged cyclam derivatives (**Figure 6.1**), bearing a 1,8-ethylene unit, form metal complexes with great kinetic inertness.[4–8]

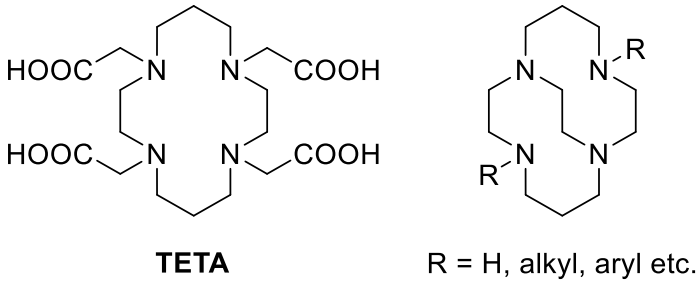

Figure 6.1. TETA and cross-bridged cyclam derivatives.

In particular, Rodríguez-Rodríguez *et al.* have reported in 2014 that a cross-bridged cyclam bearing two picolinate pendant arms (cb-tedpa) present high kinetic inertness. In fact, Ln-cb-tedpa complexes are stable even in very harsh conditions such as 2 M HCl for five months, while Ln-DOTA complexes dissociate 6.9 h under the same conditions. Even in competitions experiments, with high concentrations of endogenous metal ions and anions, Ln-cb-tedpa complexes are stable for many days. Moreover, Ln-cb-tedpa are present as a single coordination isomer both in solution and solid state due to the rigid structure of the ligand. Rodríguez-Rodríguez *et al.* report also that Ln-cb-tedpa have a q value equal to 0.25 – 0.35, which means that there is not a water molecule directly bound to the metal, but the second hydration sphere interact very efficiently with the ligand possibly due to the carboxylic moieties.[8]

Intrigued by this information we decided to prepare an analogue of cb-tedpa with two hydroxymethyl moieties (**cb-tebpm**) instead of the original carboxylic acids. (**Figure 6.2**)

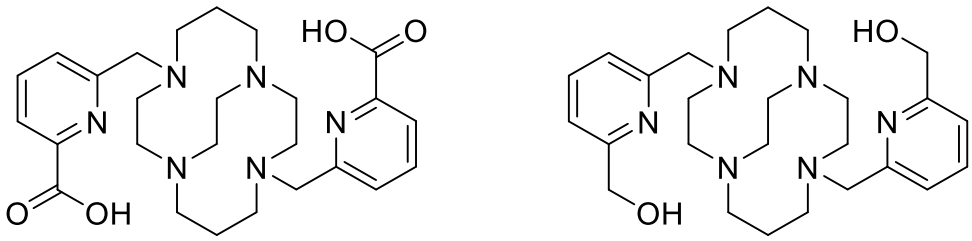

cb-tedpa **cb-tebpm**

Figure 6.2. cb-tedpa and **cb-tebpm**.

Ln-complexes of such ligand should retain the rigid structure and the kinetic inertness guaranteed by the cross-bridged cyclam and complexation properties since the very similar structure to cb-tedpa. But the two hydroxy groups should confer **cb-tebpm** additional properties, such as an extended network of hydrogen bonds and a shorter and slightly weaker Ln-O bond. These three new features can, respectively, raise the q value, increase the relaxivity and allow a partial bond to bulk water molecules.[8,9] The dichotomy between the carboxylic group and the hydroxy group as pendant arms in ligands and metal complexes thereof is also exploited in the clinically approved MRI CA gadoteridol. The latter in fact differ from DOTA just for this simple substitution (an OH instead of a COOH) but for this reason gadoteridol gains the additional features mentioned above, reaching higher transversal and longitudinal relaxivity if compared to Gd-DOTA. High relaxivity and high kinetic and thermodynamic stability are very interesting features for an MRI CA since they allow to reduce dose and the toxicity related to free gadolinium ions.[9]

Results and discussion

Compound **2B** was prepared by refluxing **1** in aqueous 48 % HBr solution for 1 h. Rapid quenching, basic extraction ad simple column chromatography afforded

compound **2B** in 40 % yield, by-product **2A** in 15 % and recovering of almost all unreacted starting material **1**. Compound **3** was then alkylated with compound **2B** in acetonitrile using potassium carbonate as base. Addition of **2B** lasted 2.5h at 0°C and the reaction finished in 20 h at room temperature. The product (**cb-tebpm**) is purified by chromatography on silica gel and obtained in 89 % yield. **[Gd(cb-tebpm)]** was prepared by reacting **cb-tebpm** with gadolinium triflate, in a *n*-butanol/DIPEA mixture, under microwave irradiation (300 W) at 150 °C and 250 psi for 18 h. Column chromatography on silica gel afforded final compound (**[Gd(cb-tebpm)]**) as a white solid in 31 % yield. (**Figure 6.3**)

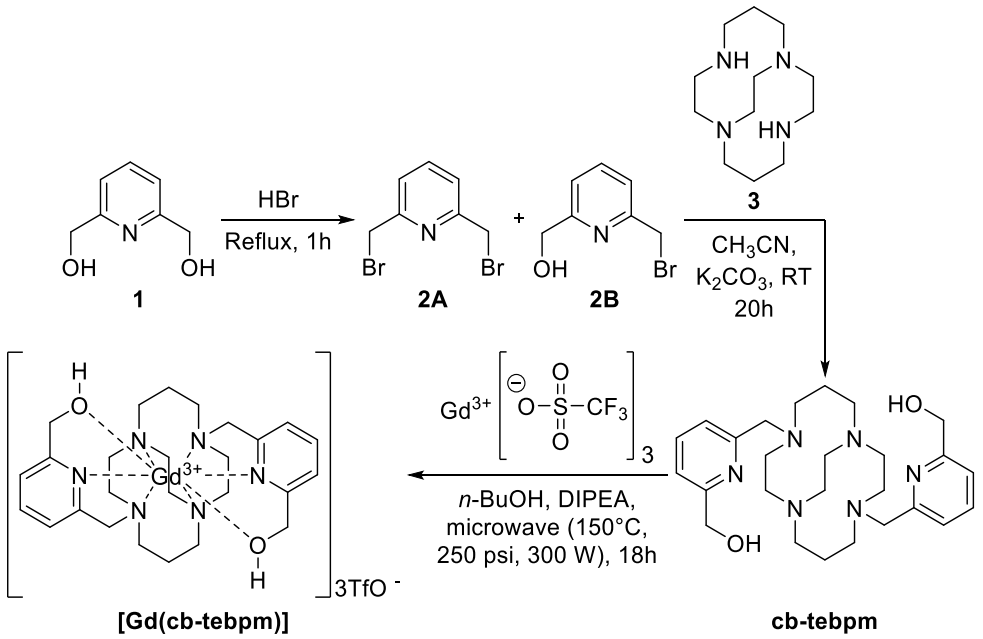

Figure 6.3. Synthesis of **cb-tebpm** and **[Gd(cb-tebpm)]**.

From preliminary complexometric data we have learned that the gadolinium complex **[Gd(cb-tebpm)]** shows a kinetic inertness comparable or even higher than [Gd(cb-tedpa)], even in strongly dissociating conditions (*i.e.* strong acidic media). However, other complexometric and relaxometric experiments must be undertaken to completely characterise this novel and interesting gadolinium complex.

Conclusions

The synthetic procedure to prepare **cb-tebpm** presents the great advantage of avoiding use of protecting groups, which is indispensable in the preparation of cb-tedpa and, unfortunately, most other chelating agents with a complex structure.[3,8,9] This aspect shortens the synthesis of **cb-tebpm** and could help in a possible future production on a larger scale.

Future development will concern the optimization of the complexation step and the substitution of chromatography techniques with other purification procedure, *i.e.* precipitations or crystallizations. Moreover, we will study the complexation properties (such as kinetic and thermodynamic stability) of **cb-tebpm** with other biomedically relevant metal ions, *i.e.* lanthanides and transition metals.

Experimental section

Materials and methods

Solvents and starting materials were purchased from Merck or TCI and used without further purification. All aqueous solutions were prepared from ultrapure laboratory grade water (18 MΩ · cm) obtained from Millipore/MilliQ purification system. ^{1}H and ^{13}C NMR spectra were recorded at 300 MHz on a Jeol Eclipse ECP300 spectrometer. Chemical shifts are reported in ppm with the protic impurities of the deuterated solvent as the internal reference. Mass spectra were obtained with a Thermo Finningan LCQ-Deca XP-PLUS ion trap spectrometer equipped with an electrospray source. TLC were performed with silica gel (MN Kieselgel 60F254) and visualized by UV or sprayed with Dragendorff reagent or alkaline $KMnO_4$. Column chromatography was carried out on Macherey-Nagel Silica gel 60 (0.063-0.200 mm).

Synthetic procedures

2,6-Bis(bromomethyl)pyridine (2A) and 2-(bromomethyl)-6-(hydroxymethyl)-pyridine (2B)

Compounds **2A** and **2B** were synthesized by refluxing a mixture of 2,6-pyridinedimethanol (**1**) (3.04 g, 21.8 mmol) and 48 % aqueous HBr (25 mL) for 1 h. The mixture was cooled to 0°C and basified by slow addition of Na_2CO_3 and water. The mixture was then extracted with methylene chloride in three portions and dried (Na_2SO_4, Na_2CO_3). The residue was purified by chromatography on silica gel (Pet/EtOAc 5:5) to yield **2A** (0.851 g, 15 %) and **2B** (1.78g, 40 %) both as white crystals.

2,6-Bis(bromomethyl)pyridine (2A)

^{1}H NMR (300 MHz, $CDCl_3$, 298 K) δ 7.69 (t, J = 7.7 Hz, 1H), 7.36 (d, J = 7.7 Hz, 2H), 4.52 (s, 4H) ppm.

^{13}C NMR (75 MHz, $CDCl_3$, 298 K) δ 156.8 (C), 138.2 (CH), 122.9 (CH), 33.6 (CH_2) ppm.

2-(Bromomethyl)-6-(hydroxymethyl)pyridine (2B)

^{1}H NMR (300 MHz, Acetone-d6, 298 K) δ 7.81 (t, J = 7.7 Hz, 1H), 7.45 (d, J = 7.2 Hz, 1H), 7.41 (d, J = 7.3 Hz, 1H), 4.68 (s, 2H), 4.62 (s, 2H) ppm.

^{13}C NMR (75 MHz, Acetone-d6, 298 K) δ 162.5 (C), 156.8 (C), 138.5 (CH), 122.5 (CH), 120.4 (CH), 65.2 (CH_2), 34.9 (CH_2) ppm.

(((1,4,8,11-Tetraazabicyclo[6.6.2]hexadecane-4,11-diyl)bis(methylene))bis(pyridine-6,2-diyl))dimethanol (cb-tebpm)

A solution of compound **2B** (0.900 g, 4.46 mmol) in acetonitrile (5 mL) was added at 0 °C in 2.5 h to a suspension of 1,4,8,11-tetraazabicyclo[6.6.2]hexadecane (**3**) (0.504 g, 2.23 mmol), CH_3CN (5 mL) and K_2CO_3 (1.54 g, 11.1 mmol) and then the mixture was stirred at RT for 20 h. The mixture was dried under vacuum and the residue was purified by chromatography on silica gel (DCM/MeOH 8:2) to afford compound **4** (0.927, 89 %) as an orange oil.

^{1}H NMR (300 MHz, CD_3OD, 298 K) δ 7.79 (t, *J* = 7.7 Hz, 2H), 7.43 (d, *J* = 7.8 Hz, 2H), 7.28 (d, *J* = 7.4 Hz, 2H), 4.69 (s, 4H), 3.86 (s, 4H), 3.16 – 2.64 (m, 20H), 1.78 – 1.71 (m, 4H) ppm.
^{13}C NMR (75 MHz, CD_3OD, 298 K) *δ* 164.8 (C), 157.9 (C), 138.8 (CH), 124.0 (CH), 120.7 (CH), 65.8 (CH_2), 59.6 (CH_2), 58.3 (CH_2), 55.9 (CH_2), 54.2 (CH_2), 53.0 (CH_2), 52.6 (CH_2), 25.3 (CH_2) ppm.
MS (ESI^+): *m*/z = 469.44 (100%, $[M+H]^+$), 235.44 (41%, $[M+2H]^{2+}$). Calc. for $C_{26}H_{40}N_6O_2$: 468.32.

Gd(III)-((6,6'-(1,4,8,11-tetraazabicyclo[6.6.2]hexadecane-4,11-diylbis-(methylene))bis(pyridine-6,2-diyl))dimethanol)triflate ([Gd(cb-tebpm)]OTf)
Gadolinium triflate (0.553 g, 0.915 mmol) and DIPEA (0.23 mL, 1.34 mmol) were added to a mixture of **cb-tebpm** (0.210, 0.448 mmol) and *n*-BuOH (2 mL) and the resulting solution was stirred under microwave radiation (300 W) at 150 °C and 250 psi for 18 h. The solvent was dried under vacuum and the product was purified by chromatography on silica gel (CH_3CN/NH_3 9:1 - 85:15 – 8:2) to yield **[Gd(cb-tebpm)]** (0.148 g, 31 %) as an off-white solid.
MS (ESI^+): *m*/z = 624.52 (100%, $[M]^+$). Calc. for $C_{26}H_{38}GdN_6O_2^+$: 624.23.

References

(1) Yu, X.; Zhang, J. *Macrocyclic Polyamines: Synthesis and Applications*; John Wiley & Sons, 2017.

(2) Wadas, T. J.; Wong, E. H.; Weisman, G. R.; Anderson, C. J. Coordinating Radiometals of Copper, Gallium, Indium, Yttrium, and Zirconium for PET and SPECT Imaging of Disease. *Chem. Rev.* **2010**, *110* (5), 2858–2902. https://doi.org/10.1021/cr900325h.

(3) Caravan, P.; Ellison, J. J.; McMurry, T. J.; Lauffer, R. B. Gadolinium(III) Chelates as MRI Contrast Agents: Structure, Dynamics, and Applications. *Chem. Rev.* **1999**, *99* (9), 2293–2352. https://doi.org/10.1021/cr980440x.

(4) Lima, L. M. P.; Halime, Z.; Marion, R.; Camus, N.; Delgado, R.; Platas-Iglesias, C.; Tripier, R. Monopicolinate Cross-Bridged Cyclam Combining Very Fast Complexation with Very High Stability and Inertness of Its Copper(II) Complex. *Inorg. Chem.* **2014**, *53* (10), 5269–5279. https://doi.org/10.1021/ic500491c.

(5) Wong, E. H.; Weisman, G. R.; Hill, D. C.; Reed, D. P.; Rogers, M. E.; Condon, J. S.; Fagan, M. A.; Calabrese, J. C.; Lam, K.-C.; Guzei, I. A.; Rheingold, A. L. Synthesis and Characterization of Cross-Bridged Cyclams and Pendant-Armed Derivatives and Structural Studies of Their Copper(II) Complexes. *J. Am. Chem. Soc.* **2000**, *122* (43), 10561–10572. https://doi.org/10.1021/ja001295j.

(6) Weisman, G. R.; Rogers, M. E.; Wong, E. H.; Jasinski, J. P.; Paight, E. S. Cross-Bridged Cyclam. Protonation and Lithium Cation (Li+) Complexation in a Diamond-Lattice Cleft. *J. Am. Chem. Soc.* **1990**, *112* (23), 8604–8605. https://doi.org/10.1021/ja00179a067.

(7) Weisman, G. R.; Wong, E. H.; Hill, D. C.; Rogers, M. E.; Reed, D. P.; Calabrese, J. C. Synthesis and Transition-Metal Complexes of New Cross-Bridged Tetraamine Ligands. *Chem. Commun.* **1996**, No. 8, 947–948. https://doi.org/10.1039/CC9960000947.

(8) Rodríguez-Rodríguez, A.; Esteban-Gómez, D.; Tripier, R.; Tircsó, G.; Garda, Z.; Tóth, I.; de Blas, A.; Rodríguez-Blas, T.; Platas-Iglesias, C. Lanthanide(III) Complexes with a Reinforced Cyclam Ligand Show Unprecedented Kinetic Inertness. *J. Am. Chem. Soc.* **2014**, *136* (52), 17954–17957. https://doi.org/10.1021/ja511331n.

(9) Wahsner, J.; Gale, E. M.; Rodríguez-Rodríguez, A.; Caravan, P. Chemistry of MRI Contrast Agents: Current Challenges and New Frontiers. *Chem. Rev.* **2019**, *119* (2), 957–1057. https://doi.org/10.1021/acs.chemrev.8b00363.

Chapter 7: Interaction of macrocyclic gadolinium-based MR contrast agents with Type I collagen. Equilibrium and kinetic studies

Introduction

Contrast Enhanced Magnetic Resonance Imaging (MRI) with gadolinium (Gd^{III})-based contrast agents (GBCAs) is fundamental for accurate diagnosis of numerous diseases and disorders. Approximately 30–40% of all MRI scans, corresponding to roughly 30 million administrations per year worldwide,[1] are performed with the intravenous (IV) administration of GBCAs. The available GBCAs are classified based on their molecular structure as either linear or macrocyclic. A major feature that distinguishes these two subclasses is kinetic inertness, which is higher for the macrocyclic GBCAs due to the closed, cage-like structure of the molecules (**Scheme 7.1**).[2–8]

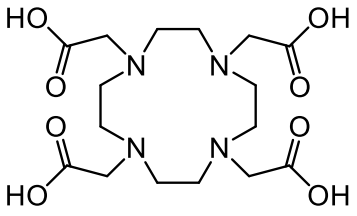

H_4**DOTA**

(NMG)Gd(**DOTA**): gadoterate meglumine (Dotarem®, Clariscan®)

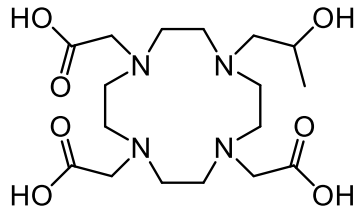

H_3**HP-DO3A**

Gd(**HP-DO3A**)+0.1% Ca(**HP-DO3A**): gadoteridol, (ProHance®)

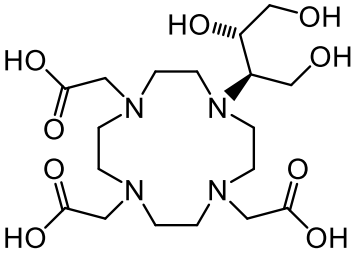

H_3**BT-DO3A**

Gd(**BT-DO3A**)+0.1% Ca(**BT-DO3A**): gadobutrol (Gadovist®)

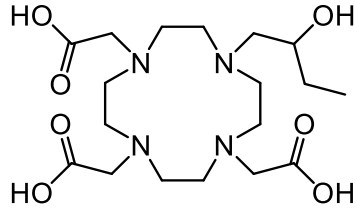

H_3**HB-DO3A**

Scheme 7.1. Structures of macrocyclic ligands. Formulas and trade names of GdL complexes used as MR contrast agents (NMG: N-methylglucamine).

The observation in 2014[9] of an increase in signal intensity on non-contrasted T_1-weighted MR images of the brain (primarily in the Dentate Nucleus and Globus

Pallidus) of patients that had undergone numerous exposures to certain linear GBCAs led to major concern worldwide about the long term safety of these GBCAs. Subsequent studies, that revealed a correlation between the degree of hyperintensity seen and the cumulative dose of linear GBCA administered, led to certain regulatory authorities (for example, the European Medicines Agency) suspending all general-purpose linear GBCAs for clinical use,[10] despite the fact that no harmful effects or clinical consequences arising from T_1-hyperintensity have been observed yet. The concern centres on the belief that dissociation of the least kinetically inert linear GBCAs leads to release of Gd^{3+} which is then retained in brain and body tissues, potentially leading to long term harmful consequences to the patient. A consequence of this concern has led to the increased use of macrocyclic GBCAs, whose dissociation half-lives under physiological conditions far exceed 1000 years.[2,8] Unfortunately, moving from linear to macrocyclic GBCAs, a limited number of persons have shown Gd retention also with macrocyclic GBCAs and fewer still have considered the notable differences amongst the macrocyclic GBCAs in terms of Gd retention. Recent studies have shown that Gd retention occurs also with macrocyclic GBCAs, even after relatively few administrations.[11,12] Murata *et al.* found markedly higher levels of Gd retention after gadobutrol administration than after gadoteridol administration, indicating that some dissociation-independent retention mechanisms play a role. Stanescu *et al.*, in a very recent study on pediatric decedents, found Gd traces after single or multiple administrations of both gadoteridol and gadoterate meglumine, with higher values for the latter. Analogously, other clinical and non-clinical studies have shown that these GBCAs can be retained for extended periods as intact Gd^{III} complex in living systems.[13–15] In support of these findings in humans, several non-clinical studies have noted marked differences amongst the macrocyclic GBCAs in terms of Gd retention, with the least retention, and most rapid elimination, consistently reported for gadoteridol.[16–20] After injection, all GBCAs distribute rapidly in the vascular system and the interstitial fluid resulting in non-specific biodistribution in the different tissues.[21] Although none of the macrocyclic GBCAs binds to plasma proteins, their interaction with components of the interstitial space has not been thoroughly investigated yet. The interstitial fluid consists of several low and high molecular weight components.[22] The concentrations of Na^+, K^+, Mg^{2+}, carbonate and

phosphate ions in the interstitial fluid and plasma are similar. However, the concentrations of the high molecular weight components (*e.g.* total protein, albumin) in the interstitial fluid are significantly lower than those in plasma. Moreover, the interstitial space cannot be regarded as a homogenous solution due to the presence of proteins and polysaccharides in solid and semi-solid phase. Interactions between the intact Gd^{III}-complexes and the solid/semi-solid components of the interstitial space may explain their long-term retention in living systems. Collagen is one of the most abundant components of the interstitial space. Approximately, 25% of the total protein mass is collagen of which 80% (*ca.* 2.65 kg in a 70 kg patient) is Type I collagen.[23–25] In the past, collagen has been considered a target for MR molecular imaging agents[26] to reveal the presence of fibrotic scars, which are typical of conditions such as myocardial infarct,[27] and liver fibrosis.[28] However, the agent developed was based on a cyclic decapeptide, purportedly selected by phage display technology to bind Type I collagen. The same peptide was also utilised to develop a PET imaging agent, after chelation of ^{68}Ga.[29,30] Using a different approach, another collagen-specific peptidomimetic was identified and labelled with ^{99m}Tc for SPECT imaging,[31] while a less specific lipophilic effect contributed to the binding of hexadecyl-4-[^{18}F] fluorobenzoate (^{18}F-HFB) to collagen matrices.[32] To the best of our knowledge, no other indications of collagen binding have been reported for commercial or research-type contrast agents. Therefore, it was important to determine the affinity of the three approved GBCAs gadoterate meglumine, gadobutrol, gadoteridol as well as Gd(HB-DO3A) to solid Type I collagen (bovine Achilles tendon) by both ultrafiltration and dialysis, with the use of cellulose membranes. Gd(HB-DO3A) is not commercially available, but it was synthesised for the study to assess the relevance, if any, of a side-chain terminal ethyl group relative to the side-chain terminal methyl group of gadoteridol. The kinetics of adsorption and desorption processes to/from collagen were also characterised. The effects of the dialysis membrane on GBCA adsorption and desorption processes were assessed in the absence of collagen.

Results and discussion

Synthesis of HB-DO3A ligand

HB-DO3A was prepared according to the synthesis reported in **Scheme 7.2**. Alkylation of DO3A(*t*Bu)$_3$[33] in refluxing 1,2-epoxybutane led to the formation of the 2-hydroxy-1-butyl derivative HB-DO3A(*t*Bu)$_3$, along with a small amount of the 1-hydroxy-2-butyl regioisomer. The latter was removed by column chromatography, allowing to isolate analytically pure HB-DO3A(*t*Bu)$_3$ in 91% yield. The chelating agent HB-DO3A was obtained in 82% yield by removal of the *t*-butyl groups with TFA/anisole, followed by crystallisation from 2-propanol. The Gd^{III}-complex was prepared by reacting HB-DO3A with an equivalent amount of $GdCl_3 \cdot 6H_2O$ in aqueous solution, kept neutral by constant addition of NaOH.

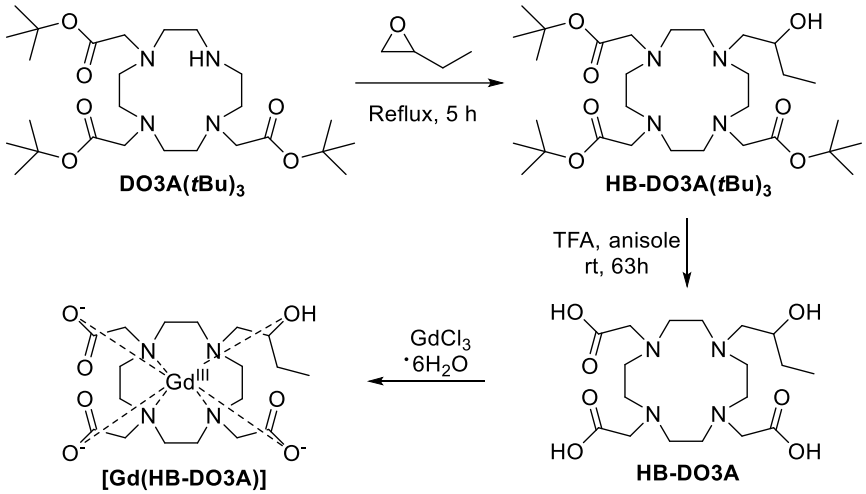

Scheme 7.2. Preparation of Gd(HB-DO3A).

Affinity of macrocyclic GBCAs to collagen

Affinity to collagen was studied by ultrafiltration of a collagen suspension after 4 h equilibration at pH = 7.4 and 37 °C in the presence of 0.5–7.0 mM GBCA. The amount of GBCAs adsorbed by collagen show saturation curves as a function of GBCA concentration (**Figure 1**).

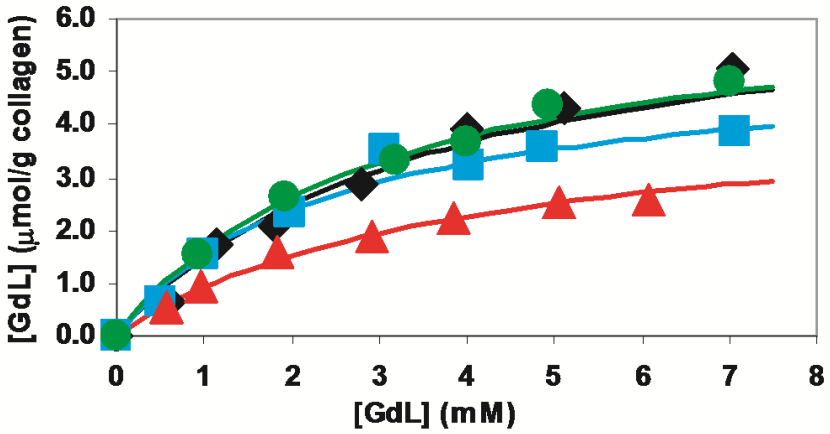

Figure 7.1. Amount of gadoterate meglumine (◆), gadobutrol (●), gadoteridol (■) and Gd(HB-DO3A) (▲) adsorbed by collagen at pH = 7.4 and 37 °C in 1.0 mM Na_2HPO_4 and 0.15 M NaCl solution. [GdL] values were obtained as the average of three parallel experiments. [GdL] values are characterized by standard deviation <3%.

These saturation curves showing the extent of the reversible monolayer adsorption of the GBCAs on the surface of solid materials and can be described by the Langmuir isoterm:[34]

$$\frac{q}{Q} = \frac{b \times [GdL]}{1 + b \times [GdL]} \qquad (7.1)$$

where *q*, *Q*, *b* and [GdL] are the amounts of adsorbed GBCA, the respective maximum amount, the affinity constant and the equilibrium concentration of GBCA in the buffer solution, respectively. The affinity constant (*b*) and maximum amount of adsorbed GBCA (*Q*) were obtained by fitting the data in **Figure 7.1** to **Equation 7.1** and are shown in **Table 7.1**.

	gadoterate meglumine	gadobutrol	gadoteridol	Gd(HB-DO3A)
log*b*	2.54 ± 0.05	2.52 ± 0.04	2.55 ± 0.05	2.41±0.06
***Q* ×10^6**	7.1 ± 0.8	6.7 ± 0.9	5.1 ± 0.8	4.4 ± 0.5
log*P*^{a}	-2.87 [b]	-2.2 [b]/-2.0[c]	-1.91[d]/-1.98[b]	-1.71[d]

Table 7.1. The affinity constant (*b*) and maximum amount (*Q*, mol Gd^{III}/g dry collagen) of adsorbed GBCAs on collagen obtained by ultrafiltration (pH = 7.4 and 37 °C in 1.0 mM Na_2HPO_4 and 0.15 M NaCl solution). [a] log*P* values were determined in butanol:water, [b] Ref. 35, [c] Ref. 36, [d] In this work: $[GdL]_{tot}$ = 10 mM, [HEPES] = 25 mM, pH = 7.4.

To compare lipophilicity, log *P* values of the GBCAs (partition coefficients in butanol:water), are indicated in **Table 7.1**. While the affinity of the different GBCAs to collagen is comparable, the maximum loading capacity of collagen with gadoteridol and Gd(HB-DO3A) is somewhat lower (*ca.* 26% and 36%, respectively) than with gadoterate meglumine and gadobutrol, possibly reflecting their different physico-chemical properties at physiological pH Gadoterate has a net negative charge, while the hydroxyl groups of gadobutrol, gadoteridol and Gd(HB-DO3A) are characterized by different protonation constants. In pH-potentiometric titrations of 0.002 M solutions of Gd(BT-DO3A), Gd(HP-DO3A) and Gd(HB-DO3A) complexes with 0.2 M NaOH solution, base consumption was observed at pH slightly above 7.0, due to the dissociation of H^+ ion from the alcoholic –OH groups of the pendant arm (**Equation 7.2**).

$GdLH_{-1} + H^+ \rightleftharpoons GdL$ $\qquad K^{H}_{GdLH_{-1}} = \dfrac{[GdL]}{[GdLH_{-1}][H^+]}$ *(7.2)*

The protonation constants of gadobutrol, gadoteridol and Gd HB-DO3A) obtained by pH-potentiometry at 25 °C and 37 °C in 0.15 M NaCl solution are shown in **Table 7.2**.

T (°C)	Gd(BT-DO3A)	Gd(HP-DO3A)	Gd(HB-DO3A)
25	8.99 ± 0.04, 9.48[a]	11.36[a], 11.31[b]	10.92 ± 0.01
37	8.73 ± 0.03	11.39 ± 0.04	10.88 ± 0.02

Table 7.2. Protonation constants ($\log K^{H}_{GdLH-1}$) Gd(BT-DO3A), Gd(HP-DO3A) and Gd(HB-DO3A) complexes (0.15 M NaCl). [a] Ref. 8 (0.1 M NaCl, 25°C); [b] Ref. 37 (0.15 M NaCl, 25°C).

The log K_{GdLH-1} values (**Table 7.2**) that characterize the protonation of the coordinated $-O^-$ groups of gadobutrol, gadoteridol and Gd(HB-DO3A) are slightly influenced by temperature. Moreover, whereas the protonation constants of gadoteridol and Gd(HB-DO3A) are very similar, the log K_{GdLH-1} value of gadobutrol is significantly lower, which might be explained by the electron withdrawing and electrostatic repulsion effects of the neighbouring non-coordinated –OH groups in the butrol pendant. Additionally, the alkoxide $-O^-$ group might form the local H bond with the neighbouring –OH groups which can stabilize the conjugate base of gadobutrol. Based on these values, their species distribution was calculated under physiological conditions (**Figures 7.6 – 7.8**). While gadoteridol and [Gd(HB-DO3A)] are fully neutral, the species distribution of gadobutrol shows the presence of ~5.7% of an anionic form ($[GdLH_{-1}]^-$) with a negative charge under physiological conditions. Type I collagen has positive charges under physiological conditions due to lysine and hydroxyproline rich domains (pI = 9.3).[38,39] Consequently, electrostatic interactions between collagen and both gadoterate and partially ionized gadobutrol might explain their higher *Q* values compared to gadoteridol and Gd(HB-DO3A) at physiological pH. The presence of the methyl and ethyl groups in the gadoteridol and Gd (HB-DO3A) sidechains may be responsible for their lower *Q* values, with the more hydrophobic ethyl group less in harmony with the heavily hydrated collagen molecule.

Rates of the adsorption and desorption processes

It is known that retention of GBCAs in living systems is strongly influenced by their pharmacokinetic properties. The faster they are eliminated from blood, the lower the opportunity to distribute into other deeper compartments. However, also their rates of adsorption and desorption on collagen, as a major representative of interstitial tissue components, might play a role. These kinetic parameters have been determined by dynamic dialysis. The amounts of GBCAs adsorbed onto collagen as a function of time were used to calculate the rate of adsorption and desorption (**Figure 7.2** and **Figure 7.3**).

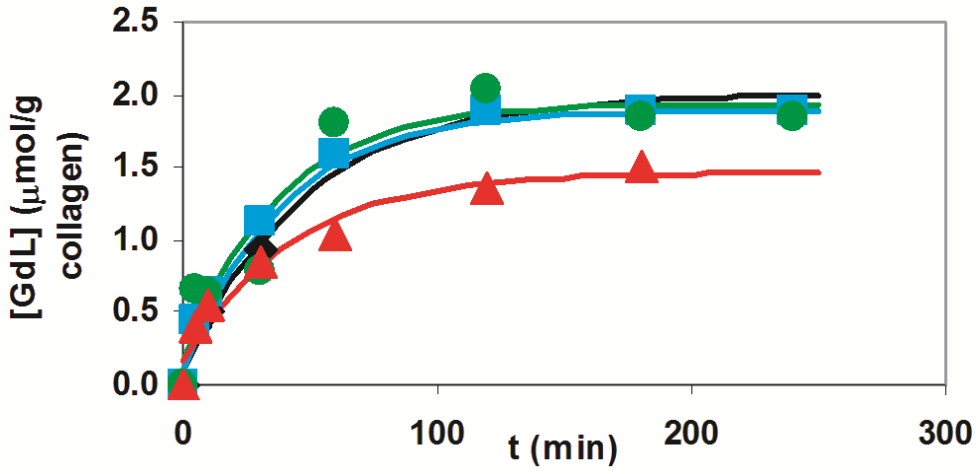

Figure 7.2. Amount of gadoterate meglumine (◆), gadobutrol (●), gadoteridol (■) and Gd(HB-DO3A) (▲) adsorbed by collagen (~150 mg dry collagen) as a function of time ([GBCA] = 1.0 mM, pH = 7.4, 37 °C, 1.0 mM Na_2HPO_4, 0.15 M NaCl).

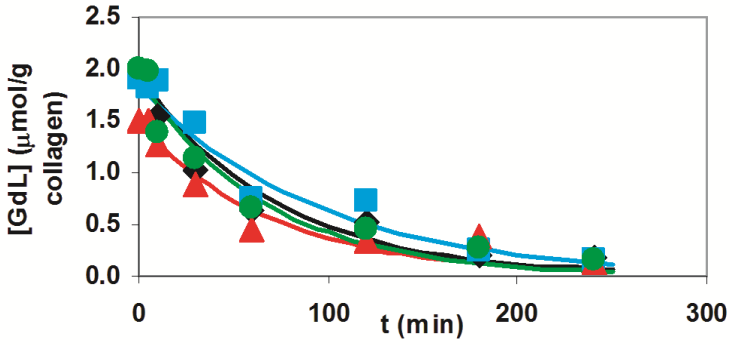

Figure 7.3. Amount of gadoterate meglumine (◆), gadobutrol (●), gadoteridol (■) and Gd(HB-DO3A) (▲) desorbed from collagen (~150 mg dry collagen) as a function of time ([GBCA] = 1.0 mM, pH = 7.4, 37 °C, 1.0 mM Na_2HPO_4, 0.15 M NaCl).

The rate constants characterizing the adsorption (k^{ad}) and desorption (k^{de}) of GBCAs on collagen were calculated by fitting the kinetic data in **Figure 7.2** and **Figure 7.3** to **Equation 7.6**. By considering the volume of collagen suspension in the membrane, we calculated also the rate constants (k^{in} and k^{out}) characterizing the in- and out-diffusion of the GBCAs through the dialysis membrane in the absence of collagen, using eqn (7.7). k^{ad}, k^{de}, k^{in} and k^{out} are shown in **Table 7.3**.

	gadoterate meglumine	**gadobutrol**	**gadoteridol**	**Gd(HB-DO3A)**
k^{ad}/(mol g^{-1})$^{-1}$ min^{-1}	0.020 ± 0.004	0.026 ± 0.008	0.025 ± 0.003	0.018 ± 0.007
k^{de}/(mol g^{-1})$^{-1}$ min^{-1}	0.014 ± 0.002	0.013 ± 0.003	0.012 ± 0.003	0.009 ± 0.002
k^{in}/min^{-1}	0.021 (1.20 mL)	0.024 (1.20 mL)	0.015 (1.30 mL)	0.014 (1.40 mL)
k^{out}/min^{-1}	0.017 (1.60 mL)	0.017 (1.70 mL)	0.017 (1.70 mL)	0.011 (1.63 mL)

Table 7.3. The rate constants characterizing the adsorption (k^{ad}) and desorption (k^{de}) of GBCAs on collagen and the diffusion of the GBCAs (k^{in} and k^{out}) through the dialysis membrane (pH = 7.4 and 37 °C in 1.0 mM Na_2HPO_4 and 0.15 M NaCl solution).

The rate constants characterizing the adsorption and desorption of gadoterate meglumine, gadobutrol and gadoteridol on collagen (k^{ad}, k^{de}) are very similar and essentially identical to those for free diffusion through the dialysis membrane (k^{in}, k^{out}) in the absence of collagen. Based on these data, it can be assumed that the diffusion of the GBCAs through the dialysis membrane is the rate determining step before the fast adsorption, or after the fast desorption, of GBCAs to/from collagen. The k^{ad} and k^{de} rate constants of Gd(HB-DO3A) are somewhat lower than those of other GBCAs, which might be explained by the hydrophobic character of the 2-hydroxybutyl sidechain which results in slightly slower in- and out-diffusion processes of Gd(HB-DO3A) through the membrane.

The extent of the *in vivo* retention of macrocyclic GBCAs on collagen

The extent of the retention of GBCAs can be estimated based on the interaction between GBCAs and collagen (**Table 7.1**) and the known pharmacokinetic data of GBCAs, reported previously.[21,40] After IV administration, the GBCAs distribute very rapidly in the vascular system and diffuse into the interstitial space of the body, which occurs simultaneously with the elimination of the GBCAs from the blood *via* kidneys. By considering the collagen adsorbent as a third compartment in the interstitium, the concentration of GBCAs in blood, interstitial space and collagen can be described by an open three compartment model (**Figure 7.4**). The rate constant characterizing the distribution ($k_{int} = k_{-int} = \ln 2/t_{1/2}\ \alpha$) was set equal to $9.6 \times 10^{-4}\ s^{-1}$, the value measured for gadopentetate dimeglumine ($Gd(DTPA)^{2-}$) previously[40] since corresponding data for macrocyclic GBCAs have not yet been published.

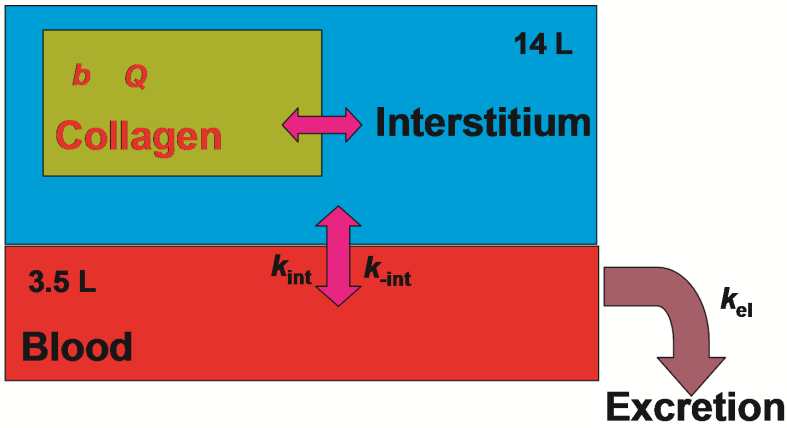

Figure 7.4. The distribution, adsorption/desorption and the elimination of GBCAs in open three-compartment model.

The elimination rate (k_{el} = ln 2/$t_{1/2}$ β) was set equal to 1.2 × 10^{-4} s^{-1} for gadoterate meglumine, gadoteridol and Gd(HB-DO3A) and equal to 1.28 × 10^{-4} s^{-1} for gadobutrol.[21] Based on the model presented in **Figure 7.4**, the interaction with collagen can be described as a homogenous linear system of first-order differential equations, each subjected to an initial condition as described elsewhere.[3] The concentrations of the GBCAs during their distribution in the collagen, vascular and interstitial spaces and the elimination from the vascular space were calculated and the data obtained are shown in **Figure 7.12**. The GBCA amount adsorbed by collagen as a function of time is shown in **Figure 7.5**.

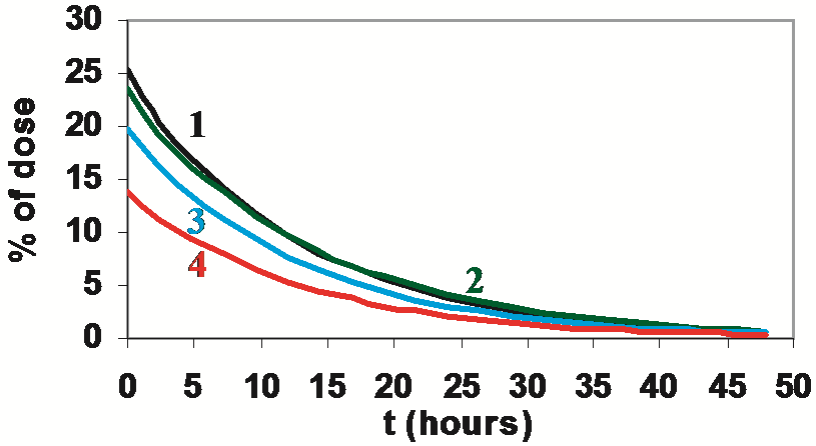

Figure 7.5. Simulation of the amounts of gadoterate meglumine (**1**), gadobutrol (**2**), gadoteridol (**3**) and Gd(HB-DO3A) (**4**) adsorbed by collagen. The distribution volume was 0.25 L per kg body weight, the weight of total collagen was 2.65 kg, the volume of the plasma was taken 3.5 L and the dose of CA was 0.1 mmol per kg body weight for a 70 kg patient.

These data are in agreement with clinical evidence that approximately 98% of the GBCA is eliminated from the body of patients with normal kidney function in about 48 h.[21] After the same length of time, the amount of the GBCAs adsorbed by collagen was found to be 0.6, 0.5, 0.4 and 0.3% of the dose for gadoterate meglumine, gadobutrol, gadoteridol and Gd (HB-DO3A), respectively. These findings suggest that the maximum loading capacity (*Q* values) influences the amount of GBCAs that can be adsorbed by collagen in vivo. It is conceivable that the whole or fractional charge has a relevant role for the adsorption of gadoterate meglumine and gadobutrol, the latter being further assisted by the possibility of establishing hydrogen bonds with collagen fibrils, through the free pair of hydroxy groups, as already hypothesized to explain the higher retention of gadobutrol in rats.[19,20] Conversely, for gadoteridol and Gd(HB-DO3A) the presence of the hydrophobic methyl and ethyl groups, respectively, may act synergistically with their neutrality to decrease adsorption, preventing both electrostatic and hydrogen-bonding interactions with the hydrated collagen fibers.[41]

Experimental

General information

Solvents and starting materials were purchased from SigmaAldrich or TCI Europe and used without further purification. All aqueous solutions were prepared from ultrapure laboratory grade water (18 MΩ · cm) obtained from Millipore/MilliQ purification system. ^{1}H and ^{13}C NMR spectra were recorded at 300 MHz on a Jeol Eclipse ECP300 spectrometer. Chemical shifts are reported in ppm with the protic impurities of the deuterated solvent as the internal reference. Mass spectra were obtained with a Thermo Finningan LCQ-Deca XP-PLUS ion trap spectrometer equipped with an electrospray source. TLC were performed with silica gel (MN Kieselgel 60F254) and visualized by UV or sprayed with Dragendorff reagent or alkaline $KMnO_4$.

Synthesis of HB-DO3A and Gd(HB-DO3A)

1,4,7-Tris(t-butoxycarbonylmethyl)-10-(2-hydroxybutyl)-1,4,7,10-tetraazacyclo-dodecane (HB-DO3A-tBu): DO3A(tBu)$_3$ (1.73 g, 3.36 mmol)[33] was suspended in 5 mL of 1,2-epoxybutane and refluxed for 5 h. The clear solution was evaporated under vacuum and the residue purified by column chromatography (EtOAc/MeOH 8:2 – 7:3) to remove a small amount of the 1-hydroxy-2-butyl regioisomer, giving compound HB-DO3A(tBu)$_3$ as a light brown oil (1.80 g, 91 %).

^{1}H NMR (300 MHz, $CDCl_3$, 298 K) δ 3.75 – 2.65 (m, 26H), 1.44 – 1.33 (m, 29H), 0.87 (t, J = 7.2 Hz, 3H) ppm.

^{13}C NMR (75 MHz, $CDCl_3$, 298 K) δ 170.5 (3 C), 81.2 (3 C), 67.6 (CH), 65.7 (CH_2), 59.7 (CH_2), 56.6 (CH_2), 56.4 (CH_2), 53.4 (CH_2), 52.9 (CH_2), 51.4 (CH_2), 50.2 (CH_2), 28.2 ($3CH_3$), 9.8 (CH_3) ppm.

MS (ESI^+): m/z = 587.4 (100%, $[M+H]^+$). Calc. for $C_{30}H_{58}N_4O_7$: 586.8.

1,4,7-Tris(carboxymethyl)-10-(2-hydroxybutyl)-1,4,7,10-tetraazacyclododecane (HB-DO3A): HB-DO3A(tBu)$_3$ (1.80 g, 3.07 mmol), 2 mL of anisole and 10 mL of TFA were mixed and stirred at RT for 63 h. The mixture was evaporated under vacuum and the residue was dissolved in methanol, precipitated with ether, centrifugated and the

supernatant removed by decantation. This procedure was repeated three times. The product was crystallised from isopropyl alcohol to give compound HB-DO3A as a white crystalline solid (1.05 g, 82%).

^{1}H NMR (300 MHz, D_2O, 298 K) δ 3.95 – 2.95 (m, 25H), 1.47 (m, 2H), 0.88 (t, *J* = 7.3 Hz, 3H) ppm.

^{13}C NMR (75 MHz, D_2O) δ 174.3 (2C), 170.2 (C), 67.5 (CH), 59.3 (CH_2), 56.8 (CH_2), 53.9 (2 CH_2), 51.7 (8 CH_2), 28.2 (CH_2), 9.1 (CH_3) ppm. MS (ESI$^+$): *m*/z = 419.3 (100%, $[M+H]^+$). Calc. for $C_{18}H_{34}N_4O_7$: 418.5.

Gd(HB-DO3A): **Gd**(HB-DO3A) was prepared by dissolving $GdCl_3 \cdot 6\ H_2O$ (1.85 g, 5.0 mmol) in 10 mL aqueous solution of H_3HB-DO3A (2.10 g 5.0 mmol). The solution was stirred at room temperature for 16 h. The pH of the solution was kept constant by addition of solid NaOH (pH = 7.0). The formation of Gd^{III}-complexes was confirmed by mass spectrometry.

MS (ESI+): m/z = 596.2 (100%, $[M+Na]^+$). Calc. for $C_{18}H_{35}N_4O_7Gd$: 575.7.

Acid-base properties of Gd(BT-DO3A), Gd(HP-DO3A) and Gd(HB-DO3A) complexes

Materials: The chemicals used for the experiments were of the highest analytical grade. The concentration of the aqueous solution HB-DO3A ligand was determined by pH-potentiometric titrations in the presence and absence of 40-fold excess of Ca^{2+}. The titrations were performed with standardized 0.2 M NaOH. For the experiments commercially available gadobutrol (Gadovist®, Gd(BT-DO3A); Bayer Schering Pharma AG) and gadoteridol (ProHance®, Gd(HP-DO3A); Bracco Imaging S.p.a) contrast agents were used. The concentration of the Gd(HB-DO3A) stock solution was determined as it was described in Ref. 42.

Equilibrium studies: The equilibrium studies were performed similarly as it was described in Ref. 3. The protonation constants of Gd(BT-DO3A), Gd(HP-DO3A) and Gd(HB-DO3A) were determined by pH-potentiometry in 0.15 M NaCl, at 25°C and

37°C ([GdL] = 0.002 M). For the calibration of pH-meter at 25°C and 37°C, 0.05 M KH-phthalate (pH = 4.005 and 4.028 at 25 °C and 37 °C) and 0.01 M borax (pH = 9.177 and 9.081 at 25 °C and 37 °C) buffers were used.[43] To calculate the H^+ concentration from the measured pH values, the method proposed by *Irving et al.* was used.[44] The ionization constant of water at 25°C and 37°C in 0.15 M NaCl was found to be 13.81 and 13.40, which agrees with the published value (pK_w=13.85 and 13.38 at 25°C and 37°C).[37,45] The protonation constants of Gd(BT-DO3A), Gd(HP-DO3A) and Gd(HB-DO3A) complexes were calculated by the PSEQUAD program.[46] The species distribution calculations were performed with the use of the MEDUSA program.[47]

Ultrafiltration

The interactions between Type I Collagen from bovine Achilles tendon (*Sigma Aldrich*) and the macrocyclic Gd^{III} complexes (gadoterate meglumine, gadobutrol, gadoteridol and Gd(HB-DO3A)) were studied at pH = 7.4 and 37 °C in 1.0 mM Na_2HPO_4 and 0.15 M NaCl solution. Commercially available gadoterate meglumine (Dotarem®, Gd(DOTA); *Guerbet*) was used, in addition to other already described compounds. In these experiments, 4×8×150 mg dry collagen was suspended in 2 mL buffer solution (pH = 7.4, 1.0 mM Na_2HPO_4, 0.15 M NaCl) spiked with 0, 0.5, 1.0, 2.0, 3,0, 4.0, 5.0 and 7.0 mM macrocyclic Gd^{III} complexes. Before preparing the suspension, the pH of the buffer was adjusted to 7.4 by addition of concentrated HCl or NaOH solution. The suspensions were stirred for 4 h at 37°C in a closed vial. Then, the samples were filtered in Amicon® Ultra-4 10K centrifugal filter devices at 37°C and 3000 rpm for 30 s, to obtain about 30 μL solution with low molecular weight (< 10 kD) components. Our preliminary experiments confirmed that the separation of 30 μL solution from the suspensions by the use of a short filtration time (30 s) does not influence the chemical equilibria reached between type I collagen and the macrocyclic Gd^{III}-complexes. Micellar Electrokinetic Capillary Chromatography (MEKC, see below) was used to determine the amount of the macrocyclic Gd^{III}-complexes in the buffer solution and in the samples obtained by ultrafiltration, allowing to obtain the amount of the Gd^{III} complex adsorbed by collagen.

Capillary electrophoresis

Micellar Electrokinetic Capillary Chromatography (MEKC) was successfully used for the separation and determination of the macrocyclic GBCAs in serum and urine samples.[48] A *Hewlett-Packard HP*^{3D} capillary electrophoresis system was used and separations were performed using bare fused-silica capillaries of 56 cm x 50 μm i.d. (*Agilent*). Before use, the capillaries were washed with 1.0 M NaOH (15 min), 0.1 M NaOH (30 min) and with the buffer electrolyte (30 min). All buffers had been filtered through a 0.45 μm syringe filter and stored in refrigerator at +4°C. Samples were injected hydrodynamically at the anodic end of the capillary (50 mbar, 20 s). The capillary was preconditioned with the buffer electrolyte (25 mM Na_2HPO_4, 70 mM sodium dodecyl sulphate-SDS, pH = 9.1) for 3 min. The separation was performed at 12°C with the application of 20 kV voltage. After analysis, postconditioning with 0.1 M NaOH (3 min) and buffer (3 min) was applied to remove all possibly adsorbed materials from the capillary. In all measurements, 5 mM DMSO as internal standard was applied in order to correct the migration time of components on the electropherogram. Detection was carried out by on-column DAD measurement at 200 nm. The electropherograms were recorded and processed by a *ChemStation* (*Agilent* - B.04.02 version). Some characteristic electropherograms for the determination of the macrocyclic Gd^{III}-complexes are shown in **Figure 7.9**. The individual linear regression equations (response-concentration) for each macrocyclic Gd^{III}-complex were based on seven concentrations. The peak areas were linear (R^2>0.998) in the concentration range specified in **Table 7.5**, in each case with a precision better than 3%. The molar integral and LOD values obtained at 200 nm are summarized in **Table 7.5**.

Dialysis

The interactions between Type I Collagen from bovine Achilles tendon (*Sigma Aldrich*) and the macrocyclic Gd^{III} complexes (gadoterate meglumine, gadobutrol, gadoteridol and Gd(HB-DO3A)) were studied by dialysis with the use of cellulose membrane (12 kD, *Sigma Aldrich*) at pH = 7.4 and 37 °C in 1.0 mM Na_2HPO_4 and 0.15 M NaCl solution. For these experiments, 5 g dry collagen was suspended in 46 g buffer

solution as indicated by *Sigma Aldrich* (50 mM TRIS buffer, 0.36 mM $CaCl_2$, pH 7.4). Removal of glycerol included as a humectant of the cellulose membrane was accomplished by washing the membrane for 3 – 4 h at pH = 7.4 and 37 °C in 1.0 mM Na_2HPO_4 and 0.15 M NaCl solution. In the dialysis experiments 6.5×2.3 cm membranes with the collagen suspension (~150 mg dry collagen) were dialysed in 500 mL buffer solution in the presence and absence of macrocyclic Gd^{III} complexes. Before the dialysis, the membranes with the collagen suspension were equilibrated for 4 h at pH = 7.4 and 37 °C in 1.0 mM Na_2HPO_4 and 0.15 M NaCl solution.

The adsorption rate of macrocyclic Gd^{III} complexes was studied by the dialysis of 7 membranes with about 150 mg collagen suspension at pH = 7.4 and 37 °C in 1.0 mM Na_2HPO_4 and 0.15 M NaCl solution in the presence of 1.0 mM gadoterate meglumine, gadobutrol, gadoteridol and Gd(HB-DO3A). Membranes with the collagen suspension were removed from the buffer solution 5, 10, 30, 60, 120, 180 and 240 min after the start of the dialysis.

In order to determine the effect of membrane on the adsorption rate of macrocyclic Gd^{III} complexes, the dialysis of 5×3 membranes containing 1, 2 and 3 mL buffer (1.0 mM Na_2HPO_4 and 0.15 M NaCl solution, pH = 7.4) was performed at pH = 7.4 and 37 °C in 1.0 mM Na_2HPO_4 and 0.15 M NaCl solution in the presence of 1.0 mM gadoterate meglumine, gadobutrol, gadoteridol and Gd(HB-DO3A). Membranes with the buffer were removed from the solution 5, 10, 30, 60 and 120 min after the start of the dialysis.

The desorption rate of macrocyclic Gd^{III} complexes was studied by dialysis of 7 membranes with about 150 mg collagen suspension at pH = 7.4 and 37°C in 1.0 mM Na_2HPO_4 and 0.15 M NaCl solution after the equilibration for 4 h at pH = 7.4 and 37°C in 1.0 mM Na_2HPO_4 and 0.15 M NaCl solution in the presence of 1.0 mM gadoterate meglumine, gadobutrol, gadoteridol and Gd(HB-DO3A). Membranes with the collagen suspension were removed from the buffer solution 5, 10, 30, 60, 120, 180 and 240 min after the start of the dialysis.

In order to calculate the volume of the dialysed collagen suspension, the density of the collagen suspension was determined by pycnometry ($\rho_{collagen}$=1.0218 g/mL, 25°C).

After the dialysis experiment, the collagen suspension was removed from the membrane and filtered on a Büchner funnel with filter paper in order to remove the buffer solution (filtration time did not affect the amount of Gd^{III} complex adsorbed by collagen). Collagen samples were then dried at 105°C overnight. The Gd^{3+} content of collagen samples and buffer solutions was determined by ICP-OES after atmospheric remineralisation carried out 4 times by addition of 30% H_2O_2 and 65% HNO_3 solutions.

ICP-OES measurements

Inductively Coupled Plasma-Optical Emission Spectrometry analysis of gadolinium content was performed on an OPTIMA 2100 DV Perkin Elmer spectrophotometer. Instrumental parameters of ICP-OES are shown in **Table 7.4**.

Nebulizer gas flow	0.6 L/min
Argon auxiliary gas flow	0.2 L/min
Argon plasma gas flow	15 L/min
Air pressure (shear gas)	7 bar
Nitrogen pressure	5 bar
Argon pressure	7.5 bar
RF power	1400 W
Pump flow rate	1.5 mL/min

Table 7.4. Instrumental parameters setting for the measurements.

Quantification was carried out focusing on 376.839 nm wavelength of gadolinium in axial view, using rhodium 1 mg/L (wavelength 343.489 nm) as internal standard. Samples resulting from dialysis experiments were properly diluted in 2% HNO_3 and then analyzed by ICP-OES.

Calibration blanks, calibration standards, and control standard solutions for the analytical sequence were prepared in 2% HNO_3 by dilution of a gadolinium oxide (Gd_2O_3) standard solution (1000 mg/L in 2% HNO_3, Certipur, *Merck*). Linearity of the analytical method was explored considering eight solutions at different gadolinium

concentration in the range of 10 - 1000 µg/L. The correlation between signal intensities and concentration was found to be linear with a coefficient of determination R^2 > 0.999. The limit of quantification was set to the first point of the calibration curve (10 µg/L) and verified considering the signal-to-noise ratio (S/N > 60).

Conclusions

These studies reveal that macrocyclic GBCAs interact differently with collagen. Gadoterate meglumine may form an electrostatic interaction with collagen, whereas weak electrostatic interactions and concurrent hydrogen-bonds may be formed between gadobutrol and collagen. The weaker interactions of collagen with gadoteridol and Gd(HB-DO3A) may be explained by the presence of hydrophobic methyl and ethyl groups and the more basic -OH groups (the formation of $GdLH_{-1}$ species occurs at more elevated pH). Although these data are based on a simplified *in vitro* model, subtle differences in molecular structure seem to cause measurable differences in the interaction of macrocyclic GBCAs with type I collagen, which may explain in part the mechanisms that govern the ultimate retention of gadolinium in living systems. Indeed, the reported results are compatible with experimental data collected in rats, which reveal lower levels of retained gadolinium in soft tissues for gadoteridol, compared to gadoterate meglumine and gadobutrol.

Supplementary Information

Acid-base properties of Gd(BT-DO3A), Gd(HP-DO3A) and Gd(HB-DO3A) complexes at 37°C in 0.15 M NaCl solution.

The distributions of GdL and $GdLH_{-1}$ species formed by Gd(BT-DO3A), Gd(HP-DO3A) and Gd(BT-DO3A) as a function of pH are shown **Figures 7.6 – 7.8**.

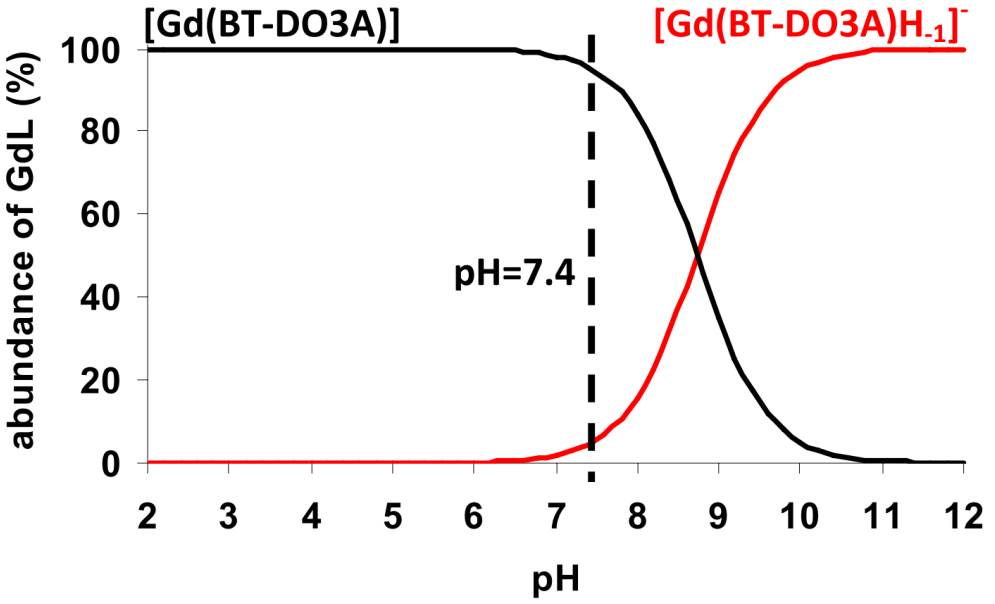

Figure 7.6. Distribution of [Gd(BT-DO3A] – $[Gd(BT\text{-}DO3A)H_{-1}]$ species as a function of pH ([Gd(BT-DO3A)] = 0.001 M, 37 °C, 0.15 M NaCl).

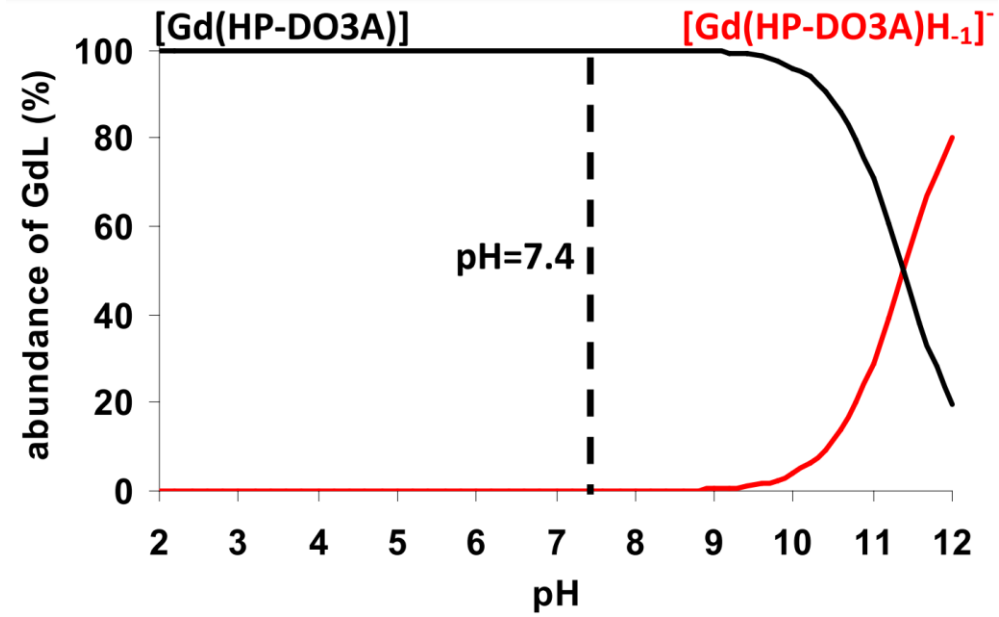

Figure 7.7. Distribution of [Gd(HP-DO3A] – [Gd(HP-DO3A)H_{-1}] species as a function of pH ([Gd(HP-DO3A)] = 0.001 M, 37 °C, 0.15 M NaCl).

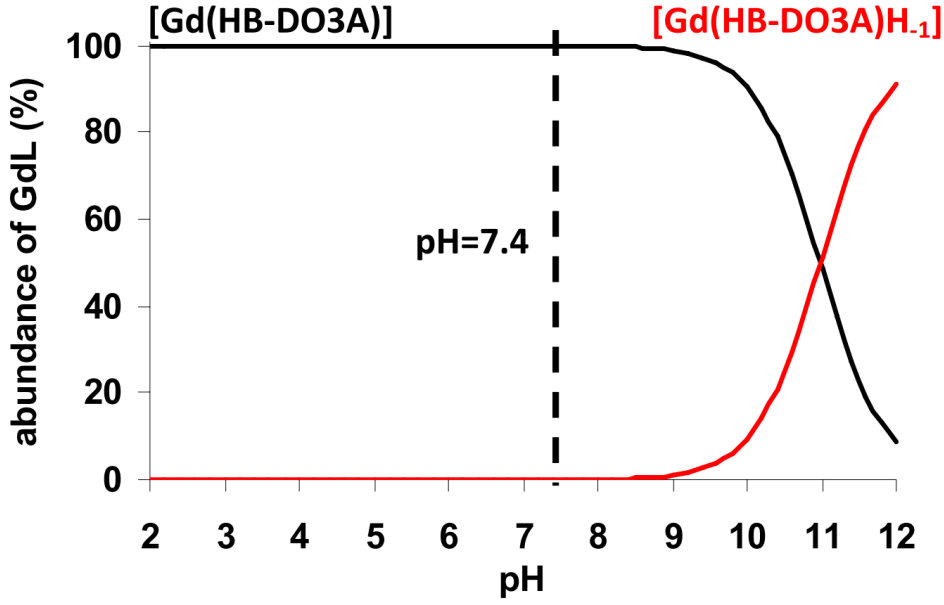

Figure 7.8. Distribution of [Gd(HB-DO3A] – [Gd(HB-DO3A)H_{-1}] species as a function of pH ([Gd(HB-DO3A)]=0.001 M, 37°C, 0.15 M NaCl).

The data presented in **Table 7.5** demonstrate that the deprotonation of the alcoholic -OH group proceeds at much lower pH values for Gd(BT-DO3A) than for Gd(HP-DO3A) or Gd(HB-DO3A). Based on the species distribution, the deprotonation of the alcoholic –OH group of Gd(BT-DO3A) complex takes place via the formation of Gd(BT-DO3A)H_{-1} species (5.7 %) at physiological conditions (pH = 7.4, 37 °C, 0.15 M NaCl). Conversely, the acidity of the –OH proton of the Gd(HP-DO3A) and Gd(HB-DO3A) complexes is significantly lower and results in the formation of Gd(HP-DO3A)H_{-1} and Gd(HB-DO3A)H_{-1} species only at pH > 9 in both cases, therefore outside the physiological range conditions.

Capillary electrophoresis

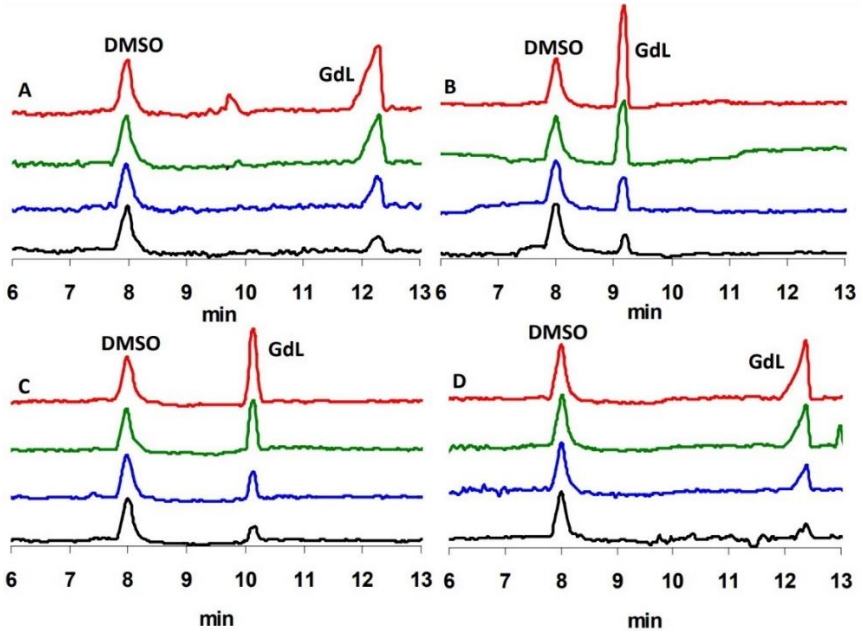

Figure 7.9. MEKC electropherograms of gadoterate meglumine (**A**), gadobutrol (**B**), gadoteridol (**C**) and Gd(HB-DO3A) (**D**) (Samples: [GdL] = **1.0**, **2.0**, **3.0** and **4.0** mM, pH = 7.4, 1.0 mM Na_2HPO_4 0.15 M NaCl, 5.0 mM DMSO, Conditions: 20 kV, 50 mbar for 20 s, λ = 200 nm; 25 Na_2HPO_4, 70 mM sodium dodecyl sulphate-SDS, pH=9.1, 12°C).

	molar integral (mAu/M)	LOD[a] (μM)	Linear range (M)
gadoterate meglumine	$(9.9\pm0.3)\times10^4$	6.7	5.0×10^{-4} – 7.0×10^{-3}
gadobutrol	$(7.5\pm0.1)\times10^4$	5.8	
gadoteridol	$(6.2\pm0.1)\times10^4$	7.0	
Gd(HB-DO3A)	$(8.3\pm0.1)\times10^4$	6.2	

Table 7.5. Analytical performance data of MEKC determination of gadoterate meglumine, gadobutrol, gadoteridol and Gd(HB-DO3A). [a] LOD = 3σ/μmolar integral.

Diffusion of the macrocyclic Gd^{III}-complexes in the absence of collagen

In order to determine the effect of the membrane on the adsorption and desorption of macrocyclic Gd^{III} complexes on/from collagen, dialysis of 5 membranes with 1, 2 and 3 mL solutions (wash in: 1.0 mM Na_2HPO_4, 0.15 M NaCl, pH = 7.4; wash out: 1.0 mM Gd^{III}-complex, 1.0 mM Na_2HPO_4, 0.15 M NaCl, pH = 7.4) was performed in 500 mL buffer (pH = 7.4 and 37°C in 1.0 mM Na_2HPO_4 and 0.15 M NaCl) in the presence (wash in) and absence (wash out) of 1.0 mM gadoterate meglumine, gadobutrol, gadoteridol or Gd(HB-DO3A). Rates of the wash-in and wash-out processes (**Equation 7.3**) were obtained by the ICP-OES determination of the macrocyclic Gd^{III} complexes in the solutions within the membranes:

$$GdL_{buffer} \rightleftharpoons GdL_{membrane} \qquad \textit{(7.3)}$$

where GdL_{buffer} and $GdL_{membrane}$ are the macrocyclic Gd^{III} complexes in the buffer and in the membrane, respectively. The amounts of the Gd^{III} complexes in the membranes are shown in **Figure 7.10** (wash in) and **Figure 7.11** (wash out).

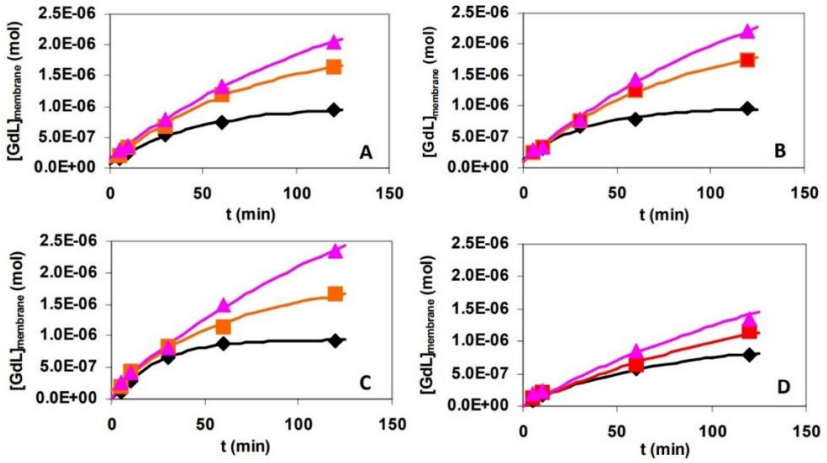

Figure 7.10. Amounts of Gd^{III} complexes in the membrane as a function of time (wash in). (gadoterate meglumine (**A**), gadobutrol (**B**), gadoteridol (**C**) and Gd(HB-DO3A) (**D**), 1 mL (◆), 2 mL (■) and 3 mL (▲), buffer: [GdL] = 1.0 mM, pH = 7.4, 37 °C, 1.0 mM. Na_2HPO_4, 0.15 M NaCl) Symbols and solid lines represent the experimental and the calculated [GdL] values, respectively.

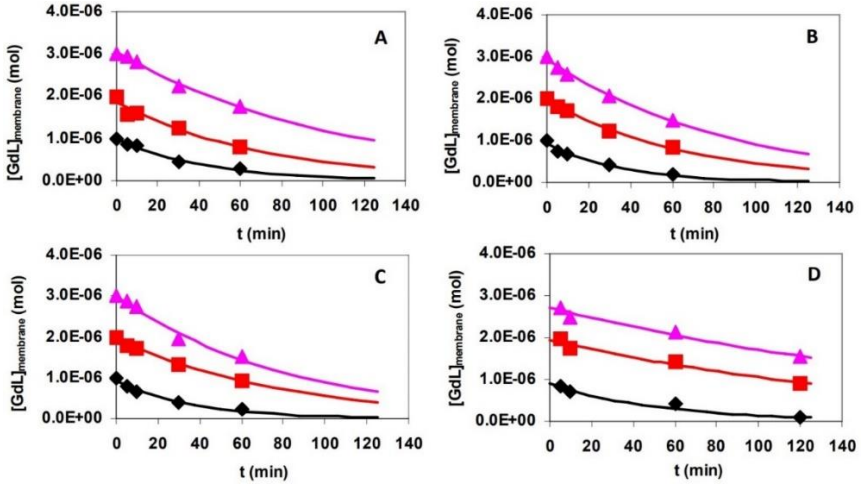

Figure 7.11. Amounts of Gd^{III} complexes in the membrane as a function of time (wash out). (gadoterate meglumine (**A**), gadobutrol (**B**), gadoteridol (**C**) and Gd(HB-DO3A) (**D**), 1 mL (◆), 2 mL (■) and 3 mL (▲), buffer: pH = 7.4, 37°C, 1.0 mM Na_2HPO_4, 0.15 M NaCl). Symbols and solid lines represent the experimental and the calculated [GdL] values, respectively.

In the presence (wash-in) and absence (wash-out) of GdL excess in the buffer solution (500 mL), the wash-in and the wash-out can be treated as a pseudo-first-order process and the rate can be expressed with the **Equation 7.4** and **Equation 7.5**, where k_{obs} is a pseudo-first-order rate constant and $[GdL]_t$ is the total concentration of the macrocyclic Gd^{III} complex in the buffer (wash-in) and in the membrane (wash-out).

$$\frac{d[GdL]_t}{dt} = k_{obs}[GdL]_t \qquad \textit{(7.4)}$$

$$-\frac{d[GdL]_t}{dt} = k_{obs}[GdL]_t \qquad \textit{(7.5)}$$

The rate constants (k_{obs}) characterizing the wash-in and wash-out of Gd^{III} complexes were calculated by fitting the kinetic data in **Figure 7.10** and **Figure 7.11** to **Equation 7.6**.

$$[GdL] = ([GdL]_0 - [GdL]_\infty)e^{(-k_{obs}t)} + [GdL]_\infty \qquad \textit{(7.6)}$$

where $[GdL]_0$, $[GdL]_\infty$ and [GdL] are the concentrations of GdL complex at the start, the end and at the time *t* of the reaction. The k_{obs} rate constants are shown in **Table 7.6**, with standard deviations.

Wash-IN	Dotarem	Gadovist	ProHance	Gd(HB-DO3A)
k_{obs}/min^{-1} (1 mL)	0.022 ± 0.001	0.026 ± 0.003	0.030 ± 0.004	0.016 ± 0.001
k_{obs} /min^{-1} (2 mL)	0.014 ± 0.001	0.016 ± 0.001	0.018 ± 0.002	0.009 ± 0.0003
k_{obs} /min^{-1} (3 mL)	0.009 ± 0.002	0.010 ± 0.001	0.010 ± 0.001	0.007 ± 0.0003
k^{in} (min^{-1}cm)	(8.6 ± 0.8)×10^{-4}	(1.0 ± 0.1)×10^{-3}	(1.1 ± 0.1)×10^{-3}	(6.4 ± 0.4)×10^{-4}
Wash-OUT	**Dotarem**	**Gadovist**	**ProHance**	**Gd(HB-DO3A)**
k_{obs}/min^{-1} (1 mL)	0.024 ± 0.002	0.027 ± 0.004	0.026 ± 0.004	0.018 ± 0.001
k_{obs}/min^{-1} (2 mL)	0.014 ± 0.001	0.014 ± 0.001	0.014 ± 0.003	0.010 ± 0.001
k_{obs}/min^{-1} (3 mL)	0.009 ± 0.001	0.011 ± 0.001	0.011 ± 0.001	0.006 ± 0.0004
k^{out} (min^{-1}cm)	(9.0 ± 0.5)×10^{-4}	(1.0 ± 0.1)×10^{-3}	(1.0 ± 0.1)×10^{-3}	(6.0 ± 0.3)×10^{-4}

Table 7.6. Rate constant characterizing the wash-in and wash-out of macrocyclic Gd^{III}-complexes (buffer: $[GdL]_t$=1.0 mM (wash in), 0.0 mM (wash out), pH=7.4, 37°C, 1.0 mM Na_2HPO_4, 0.15 M NaCl).

The k_{obs} rate constants characterizing the wash-in and wash-out process of gadoterate meglumine, gadobutrol and gadoteridol in the presence of 1.0 mM Gd^{III} complexes in the buffer (wash-in) and in the membrane (wash-out) are essentially identical and decrease with the increase of the volume in the membrane. However, the k_{obs} values of Gd(HB-DO3A) are somewhat lower than those of other complexes, which might be explained by the more hydrophobic character of the 2-hydroxy-butyl sidechain that results in the slower wash-in and wash-out processes of Gd(HB-DO3A) through the membrane. The rate of dialysis is directly proportional to the concentration

of molecules and to the ratio of membrane surface area to membrane volume (specific surface of the membrane).[34] Since the wash-in and wash-out experiments were performed in the presence of 1.0 mM Gd^{III} complex in the buffer (wash-in) and in the membrane (wash-out), the k_{obs} can be expressed by the following equation:

$$k_{obs} = k^{in/out} \times \frac{area}{volume} \qquad \textbf{(7.7)}$$

where $k^{in/out}$ is the rate constant characterizing the diffusion of the Gd^{III} complexes in the presence of 1.0 mM Gd^{III} complex in the buffer (wash-in) and in the membrane (wash-out). Considering the surface area of the membrane ($2\times6.5\times2.3=29.9$ cm^2) and the volume of the buffer (1, 2 and 3 mL) in the membrane, k^{in} and k^{out} rate constants characterizing the permeability of the membrane for the Gd^{III} complexes were calculated in the presence of 1.0 mM Gd^{III} complex in the buffer (wash-in) or in the membrane (wash-out) (Table S4). k^{in} and k^{out} rate constants characterizing the diffusion of the gadoterate meglumine, gadobutrol and gadoteridol in the presence of 1.0 mM Gd^{III} complex in the buffer (wash-in) and in the membrane (wash-out) are essentially identical, which reveals that the cellulose membrane (12 kD, *Sigma Aldrich*) has practically no influence on the rate of the adsorption and desorption of gadoterate meglumine, gadobutrol and gadoteridol on collagen.

The distribution, adsorption/desorption and elimination of the GBCAs in an open three-compartment model.

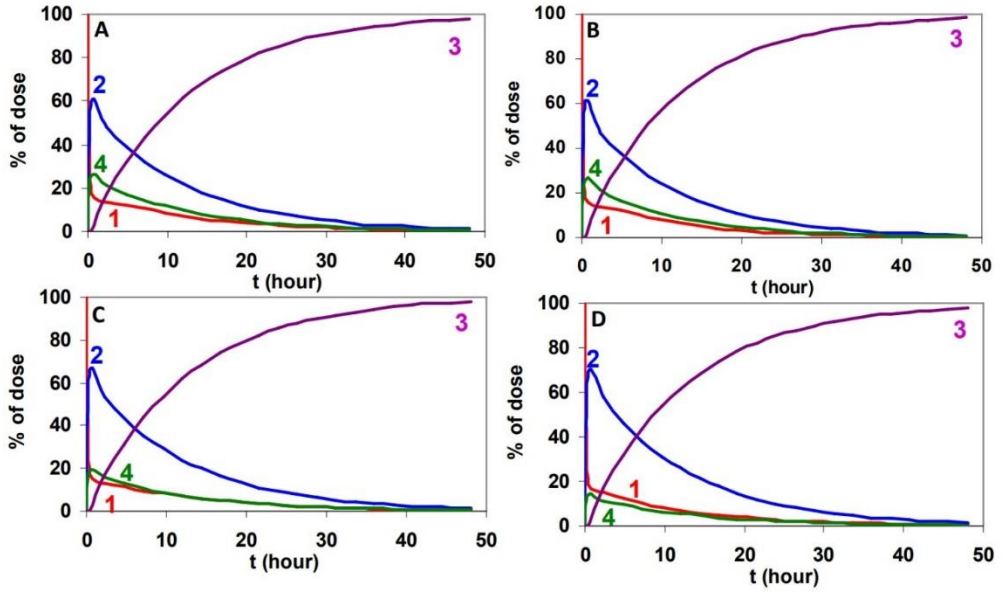

Figure 7.12. The distribution, adsorption and elimination of gadoterate meglumine (**A**), gadovist (**B**), gadoteridol (**C**) and Gd(HB-DO3A) (**D**) Amounts of GdL in the plasma (**1**), in the interstitium (**2**), the eliminated GdL (**3**) and the adsorbed GdL by collagen (**4**). The distribution volume was 0.25 L/kg body weight, the weight of total collagen was 2.65 kg, the volume of the plasma was taken 3.5 L and the dose of CA was 0.1 mmol/kg body weight for a 70 kg patient.

T (hours)	gadoterate meglumine	gadobutrol	gadoteridol	Gd(HB-DO3A)
24	85.251	82.898	85.266	85.283
48	97.832	97.084	97.834	97.837
168	100.000	99.999	100.000	100.000
720	100.000	100.000	100.000	100.000

Table 7.7. The amount of retained Gd(III)-complexes (% of dose) for the whole body.

References

(1) J. Lohrke, T. Frenzel, J. Endrikat, F. C. Alves, T. M. Grist, M. Law, J. M. Lee, T. Leiner, K. C. Li, K. Nikolaou, M. R. Prince, H. H. Schild, J. C. Weinreb, K. Yoshikawa and H. Pietsch, *Adv. Ther.*, 2016, **33**, 1-28.

(2) Z. Baranyai, Z. Palinkas, F. Uggeri, A. Maiocchi, S. Aime and E. Brucher, *Chem. Eur. J.*, 2012, **18**, 16426-16435.

(3) Z. Baranyai, E. Brucher, F. Uggeri, A. Maiocchi, I. Toth, M. Andrasi, A. Gaspar, L. Zekany and S. Aime, *Chem. Eur. J.*, 2015, **21**, 4789-4799.

(4) L. Sarka, L. Burai, R. Kiraly, L. Zekany and E. Brucher, *J. Inorg. Biochem.*, 2002, **91**, 320-326.

(5) L. Sarka, L. Burai and E. Brucher, *Chem. Eur. J.*, 2000, **6**, 719-724.

(6) Z. Baranyai, Z. Palinkas, F. Uggeri and E. Brucher, *Eur. J. Inorg. Chem.*, 2010, 1948-1956.

(7) L. Burai, E. Brücher, R. Király, P. Solymosi and T. Vig, *Acta Pharm. Hung.*, 2000, **70**, 89-96.

(8) É. Tóth, R. Király, J. Platzek, B. Radüchel and E. Brücher, *Inorg. Chim. Acta*, 1996, **249**, 191-199.

(9) T. Kanda, K. Ishii, H. Kawaguchi, K. Kitajima and D. Takenaka, *Radiology*, 2014, **270**, 834-841.

(10) E. M. Agency, 2017, vol. 2017.

(11) N. Murata, K. Murata, L. F. Gonzalez-Cuyar and K. R. Maravilla, *Magn. Reson. Imaging*, 2016, **34**, 1359-1365.

(12) A. L. Stanescu, D. W. Shaw, N. Murata, K. Murata, J. C. Rutledge, E. Maloney and K. R. Maravilla, *Pediatr. Radiol.*, 2020, **50**, 388-396.

(13) E. Gianolio, P. Bardini, F. Arena, R. Stefania, E. Di Gregorio, R. Iani and S. Aime, *Radiology*, 2017, **285**, 839-849.

(14) M. Birka, K. S. Wentker, E. Lusmoller, B. Arheilger, C. A. Wehe, M. Sperling, R. Stadler and U. Karst, *Anal. Chem.*, 2015, **87**, 3321-3328.

(15) T. Frenzel, C. Apte, G. Jost, L. Schockel, J. Lohrke and H. Pietsch, *Invest. Radiol.*, 2017, **52**, 396-404.

(16) R. J. McDonald, J. S. McDonald, D. Dai, D. Schroeder, M. E. Jentoft, D. L. Murray, R. Kadirvel, L. J. Eckel and D. F. Kallmes, *Radiology*, 2017, **285**, 536-545.

(17) S. Bussi, A. Coppo, C. Botteron, V. Fraimbault, A. Fanizzi, E. De Laurentiis, S. Colombo Serra, M. A. Kirchin, F. Tedoldi and F. Maisano, *J. Magn. Reson. Imag.*, 2018, **47**, 746-752.

(18) G. Jost, T. Frenzel, J. Boyken, J. Lohrke, V. Nischwitz and H. Pietsch, *Radiology*, 2019, **290**, 340-348.

(19) S. Bussi, F. Maisano, F. Tedoldi and M. A. Kirchin, *Pediatr. Radiol.*, 2019, **49**, 1110-1111.

(20) S. Bussi, A. Coppo, R. Celeste, A. Fanizzi, A. Fringuello Mingo, A. Ferraris, C. Botteron, M. A. Kirchin, F. Tedoldi and F. Maisano, *Insights Imag.*, 2020, **11**, 11.

(21) M. F. Bellin and A. J. Van Der Molen, *Eur. J. Radiol.*, 2008, **66**, 160-167.

(22) N. Fogh-Andersen, B. M. Altura, B. T. Altura and O. Siggaard-Andersen, *Clin. Chem.*, 1995, **41**, 1522-1525.

(23) K. Henriksen and M. A. Karsdal, ed. M. A. Karsdal, Academic Press, 2019.

(24) G. B. Smejkal and C. Fitzgerald, *Int. J. Proteomics & Bioinformatics*, 2017, 001-002.

(25) R. E. Neuman and M. A. Logan, *J. Biol. Chem.*, 1950, **186**, 549-556.

(26) P. Caravan, B. Das, S. Dumas, F. H. Epstein, P. A. Helm, V. Jacques, S. Koerner, A. Kolodziej, L. Shen, W.-C. Sun and Z. Zhang, *Angew. Chem. Int. Ed. Eng.*, 2007, **46**, 8171-8173.

(27) P. A. Helm, P. Caravan, B. A. French, V. Jacques, L. Shen, Y. Xu, R. J. Beyers, R. J. Roy, C. M. Kramer and F. H. Epstein, *Radiology*, 2008, **247**, 788-796.

(28) B. C. Fuchs, H. Wang, Y. Yang, L. Wei, M. Polasek, D. T. Schuhle, G. Y. Lauwers, A. Parkar, A. J. Sinskey, K. K. Tanabe and P. Caravan, *J. Hepatol.*, 2013, **59**, 992-998.

(29) P. Désogère, L. F. Tapias, L. P. Hariri, N. J. Rotile, T. A. Rietz, C. K. Probst, F. Blasi, H. Day, M. Mino-Kenudson, P. Weinreb, S. M. Violette, B. C. Fuchs, A. M. Tager, M. Lanuti and P. Caravan, *Sci. Trans. Med.*, 2017, **9**, eaaf4696.

(30) P. Désogère, L. F. Tapias, T. A. Rietz, N. Rotile, F. Blasi, H. Day, J. Elliott, B. C. Fuchs, M. Lanuti and P. Caravan, *J. Nuc. Med.*, 2017, **58**, 1991-1996.

(31) J. Muzard, L. Sarda-Mantel, S. Loyau, A. Meulemans, L. Louedec, C. Bantsimba-Malanda, F. Hervatin, J. Marchal-Somme, J. B. Michel, D. Le Guludec, P. Billiald and M. Jandrot-Perrus, *PLoS One*, 2009, **4**, e5585.

(32) A. Ahmadi, S. L. Thorn, E. I. Alarcon, M. Kordos, D. T. Padavan, T. Hadizad, G. O. Cron, R. S. Beanlands, J. N. DaSilva, M. Ruel, R. A. deKemp and E. J. Suuronen, *Biomaterials*, 2015, **49**, 18-26.

(33) D. Moore and L. Patterson, *Org. Synth.*, 2008, **85**, 10.

(34) P. W. Atkins, *Physical Chemistry*, fourth edition edn., Oxford University Press, Walton Street, Oxford OX2 6DP, Oxford, 1990.

(35) P. Wedeking, K. Kumar and M. F. Tweedle, *Magn. Reson. Imaging*, 1992, **10**, 641-648.

(36) H. Vogler, J. Platzek, G. Schuhmann-Giampieri, T. Frenzel, H. J. Weinmann, B. Raduchel and W. R. Press, *Eur. J. Radiol.*, 1995, **21**, 1-10.

(37) S. Aime, S. Baroni, D. Delli Castelli, E. Brucher, I. Fabian, S. C. Serra, A. Fringuello Mingo, R. Napolitano, L. Lattuada, F. Tedoldi and Z. Baranyai, *Inorg. Chem.*, 2018, **57**, 5567-5574.

(38) F. Jiang, H. Horber, J. Howard and D. J. Muller, *J. Struct. Biol.*, 2004, **148**, 268-278.

(39) R. S. Bhatnagar, C. A. Gough, J. J. Qian and M. B. Shati'uck, *Proc. Indian Acad. Sci. (Chem. Sci.)*, 1999, **111**, 301-317.

(40) H. J. Weinmann, M. Laniado and W. Mutzel, *Physiol. Chem. Phys. Med. NMR*, 1984, **16**, 167-172.

(41) J. Gross and D. Kirk, *J. Biol. Chem.*, 1958, **233**, 355-360.

(42) L. Helm, J. R. Morrow, C. J. Bond, F. Carniato, M. Botta, M. Braun, Z. Baranyai, R. Pujales-Paradela, M. Regueiro-Figueroa, D. Esteban-Gómez, C. Platas-Iglesias and T. J. Scholl, in *Contrast Agents for MRI: Experimental Methods*, The Royal Society of Chemistry, 2018, pp. 121-242.

(43) *Pure & Appl. Chem.*, 1978, **50**, 1485-1517.

(44) H. M. Irving, M. G. Miles and L. D. Pettit, *Anal. Chim. Acta*, 1967, **38**, 475-488.

(45) G. Berthon, P. M. May and D. R. Williams, *J. Chem. Soc., Dalton Trans.*, 1978, 1433-1438.

(46) L. Zékány and I. Nagypál, in *Computational Methods for the Determination of Formation Constants*, ed. D. J. Leget, Plenum Press, New York, 1985, 291 - 353.
(47) I. Puigdomenech, *MEDUSA*, (2010) Royal Institute of Technology, Stockholm.
(48) M. Andrási, A. Gáspár, O. Kovács, Z. Baranyai, Á. Klekner and E. Brücher, *Electrophoresis*, 2011, **32**, 2223-2228.

Adapted from ***Dalton Trans.***, 2020, **49**, 14863-14870 with permission from The Royal Society of Chemistry.

For this work, I have prepared and characterised HB-DO3A(*t*Bu)$_3$ and HB-DO3A and collaborated to the drawing up of the article.

Chapter 8: General discussion

As thoroughly explained in the previous pages, during my PhD the utmost attention was paid to the improved synthesis of chelating agents with the aim of preparing novel contrast agents primarily for MRI, PET and SPECT.

This interest derives from an open research issue, since chemical industries producing CAs have a continuous need for new synthetic strategies and more complex compounds possessing refined profiles of safety, efficacy and cost.

Currently, polyazamacrocyclic polycarboxylate and phosphonates complexes, represent the best combination of performances and *in vivo* stability when used as imaging contrast agents and drugs for targeted radiotherapy.[1] Nevertheless, the synthesis of functionalised polyazamacrocycles is not straightforward and requires simple and efficient regioselective protection methods.[2]

Therefore, as stated in **Chapter 2**, my PhD has been focused on three main objectives:

- Regioselective protection of cyclen,
- Synthesis of novel bifunctional chelating agents,
- Synthesis of new chelating agents.

The first project was developed designing a strategy for the orthogonal 1,7 diprotection of cyclen. The latter is an important starting material since it represents the basic skeleton of several complexes used as CAs (mainly for MRI, PET, SPECT and OI). The functionalization of this macrocycle often requires complex strategies of protection and deprotection. The presence of four symmetrically arranged nitrogen atoms makes possible a series of protected derivatives, summarized in **Figure 8.1**.[3]

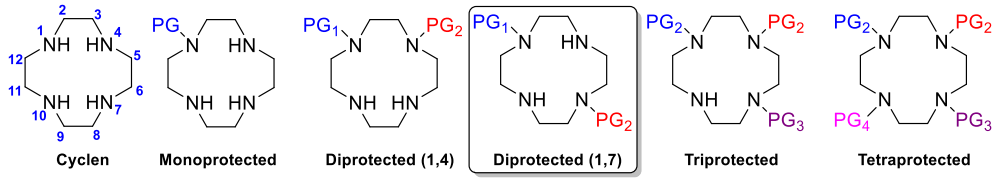

Figure 8.1. Cyclen, protected derivatives (PG = Protective Group).

A novel strategy for the preparation of orthogonally 1,7-heterodiprotected cyclen-based compounds was developed during my PhD, by using a simple route,

inexpensive reagents, and mild conditions. Our method is inspired by a protocol developed by A. D. Sherry *et al.*,[4] and based on the control of pH to modulate the reactivity of the equivalent amine groups. The original method is based on the peculiar behaviour of polyazamacrocycles, *i.e.* the fact that the protonation of amino groups is sequential, and the first two protonation steps occur on opposite nitrogen atoms due to electrostatic repulsion of the incoming positive charges. This property allows to operate on the diprotonated cyclen and can be exploited to implant protective groups with an high 1,7 regioselectivity. This property allows the functionalisation of cyclen with two different side arms (A_2B_2 arrangement). The protocol developed during my PhD, instead, allows the functionalisation of cyclen with three different side arms (A_2BC arrangement), widening the chemical space of multifunctionalised cyclens and improving its chelating properties. (**Figure 8.2**)

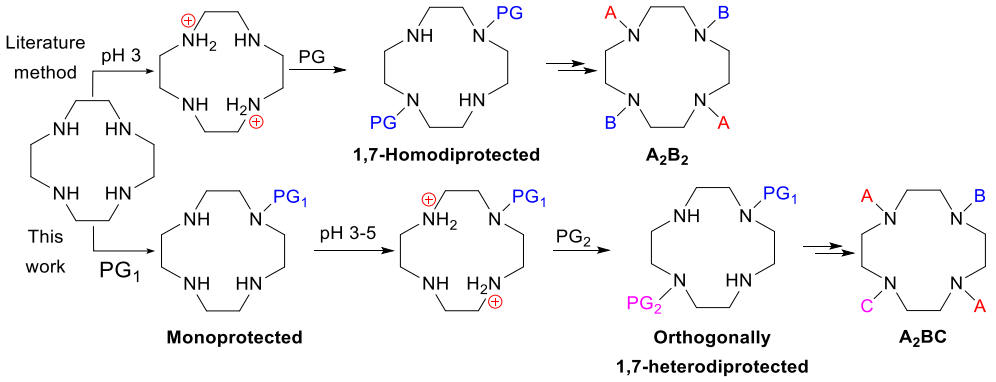

Figure 8.2. Strategies for the 1,7-protection of cyclen.

Our protocol starts from a monoprotected cyclen, the *N*-formylderivative, easily available in large amount following a published procedure.[5] Products and isolated yields are reported in **Figure 8.3**.

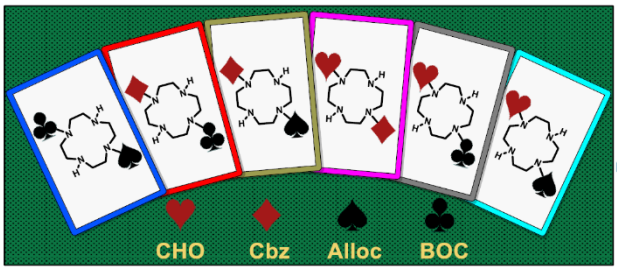

PG_2 \ PG_1	Cbz	Alloc	CHO
Boc	**7** 77%	**9** 76%	**4** 67%
Cbz		**8** 86%	**3** 93%
Alloc			**2** 74%

Figure 8.3. Scheme of the products and corresponding isolated yields.

The advantages of this method are:

1. The protecting groups are easily removed under mild conditions and are orthogonal to each other (they can be selectively and independently cleaved leaving the other group intact),
2. This protocol gives an efficient and alternative entry to Cbz and BOC monoprotected cyclens,
3. This method does not require chromatographic separation or high dilution techniques,
4. The final compounds are easily obtained with good yields (**Figure 8.3**).

Future developments of this topic will be devoted to the realization of 1,4-diprotected derivatives of cyclen.

The second topic of my PhD was focused on the design and synthesis of two novel BFCAs (**DO2AP(*t*Bu)$_4$** and **DO3AP(*t*Bu)$_4$**) as derivatives of DO3AP. (**Figure 8.4**)
The phosphonic group is commonly used as a (bio)isostere of carboxylic acid in medicinal chemistry.[6] At physiological pH values the phosphonate deprotonated form (-PO_3^{2-}) offers multiple coordination modes, leading to stabilities of the metal complexes comparable to those of the carboxylic counterpart or even higher.[1,7,8] (**Figure 8.4**)
This feature is very important for the application of a BFCA as drug for targeted radiotherapy or imaging probes. Moreover, the anions left after complexation on the phosphonate group provide an extended and beneficial hydrogen bond network. This property gives paramagnetic complexes an improved relaxivity (*i.e.*: contrast efficiency), very important in the preparation of MRI CAs.

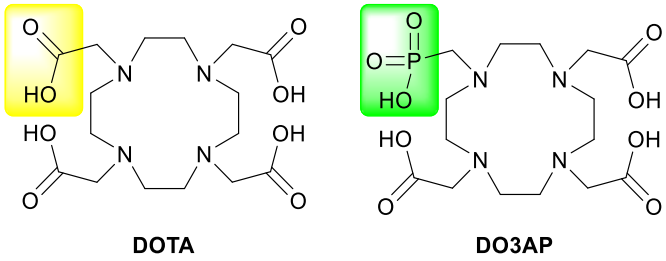

Figure 8.4. DOTA and DO3AP.

For these reasons, during my PhD I have prepared two new bifunctional chelating agents, derivatives of DO3AP, *i.e.*: **DO2AP(*t*Bu)$_4$** and **DO3AP(*t*Bu)$_4$** (**Figure 8.5**), prepared by a straightforward and economic synthetic access.

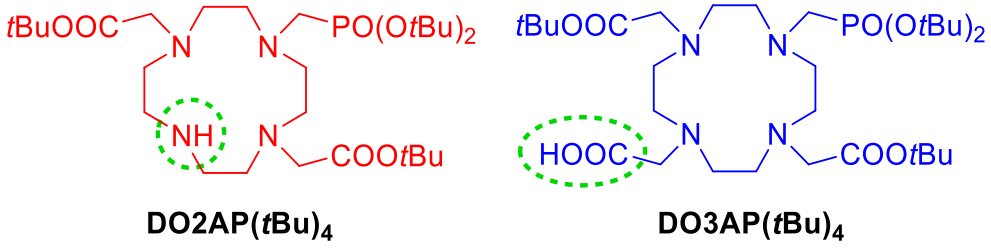

Figure 8.5. **DO2AP(*t*Bu)$_4$** and **DO3AP(*t*Bu)$_4$**.

The synthesis of these BFCA derivatives takes advantage of the orthogonally 1,7-heterodiprotected cyclen derivatives showed in the previous section, precisely of 1-Cbz-7-formyl derivative of cyclen.

The secondary amino group of **DO2AP(*t*Bu)$_4$** is the reactive functional group of this novel BFCA and can be used to link the coordinating cage to suitable vectors by simple alkyation of the nitrogen atom.

In **DO3AP(*t*Bu)$_4$**, instead, the free carboxylic group is the key functionality that can be activated and coupled to vector-molecules.

Future developments will concern the conjugation of the BFCAs presented here to vectors of diagnostic interest.

Regarding the third issue of my PhD, the research was focused on the design and preparation of three innovative chelating agents (**TRASUTA**, **cb-tebpm** and **HB-DO3A**) and metal complexes thereof.

TRASUTA consists of a new hexadentate mesocyclic chelating agent for gallium as a derivative of AAZTA for application as a PET CA.

In particular, **TRASUTA** consist in a rigidified derivative of AAZTA, bearing, on its mesocyclic structure a newly introduced five-membered cycle. (**Figure 8.6**)

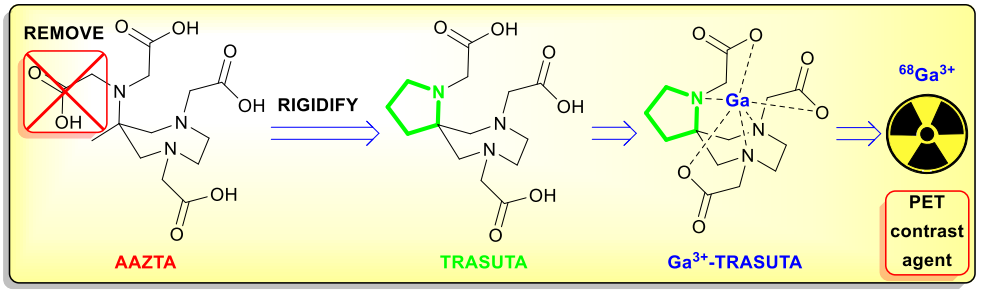

Figure 8.6. **TRASUTA** consist in a rigidified hexadentate analogue of AAZTA rigidified by the introduction of a new five-membered cycle (highlighted in green).

TRASUTA has been synthesised in seven steps using, as starting materials, commercial and cheap products. The stability constant of Ga^{3+}-**TRASUTA** have been measured by potentiometric titration and the corresponding data are reported in **Chapter 5**.

Future developments of this project will concern the improvement of the synthesis of **TRASUTA**, with a special focus on the reaction conditions and their influence on the overall yield.

Cb-tebpm is another novel chelating agent prepared during this PhD and designed as a ultrastabilised chelator for gadolinium, to be exploited as MRI CA. (**Figure 8.7**)

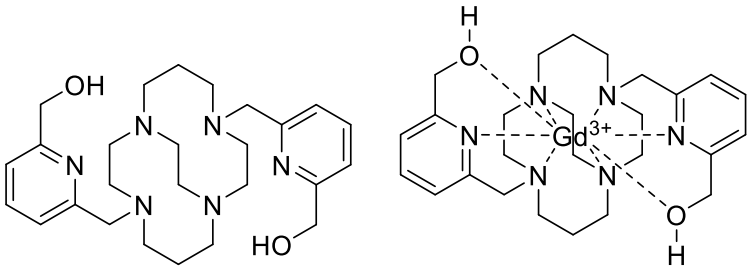

cb-tebpm **[Gd(cb-tebpm)]**

Figure 8.7. **Cb-tebpm** and **[Gd(cb-tebpm)]**.

In the recent literature has been reported that cross-bridged cyclams (such as **cb-tebpm**) form metal complexes with great kinetic inertness, very important for their application as MRI CAs.[9]

Cb-tebpm has been prepared by a two-step synthesis (three steps for its gadolinium complex).

Preliminary complexometric experiments revealed that **[Gd(cb-tebpm)]** shows a kinetic inertness comparable or even higher than other cyclam derivativatives previously reported in the literature even in strongly dissociating conditions (*i.e.* strong acidic media).

This synthetic access presents the great advantage of avoiding the use of protecting groups, shortening the preparation of **cb-tebpm**.

Future development of this project will concern the optimization of the reaction condition, yields and purification procedure with the perspective of a possible future scale up of the synthesis of **cb-tebpm**.

Moreover, we will study of the complexation properties of **cb-tebpm** with other lanthanides and transition metals.

HB-DO3A has been the last innovative chelating agent designed and prepared during my PhD. Its gadolinium complex has been studied from a complexometric, pharmacokinetic and toxicological point of view. These experiments were devoted to the comparison of three clinically approved MRI CAs (gadoterate meglumine,

gadoteridol and gadobutrol) and Gd(**HB-DO3A**) in their interaction with type I collagen. (**Figure 8.8**) The latter is one of the most important components of interstitial fluids[10] and the interaction of the previously mentioned gadolinium complexes with collagen has never been thoroughly studied.

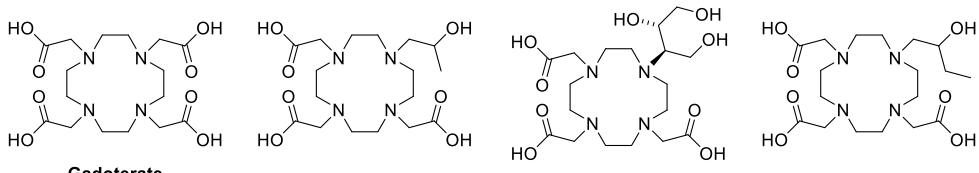

Figure 8.8. Structures of macrocyclic ligands gadoterate meglumine, gadoteridol gadobutrol and Gd(**HB-DO3A**).

HB-DO3A was prepared in two easy synthetic steps and purification procedures in high isolated yield (75 % over two steps) on a multigram scale.

Ex vivo experiments have demonstrated that owing to their different chemical structure, gadoterate meglumine, gadoteridol, gadobutrol and Gd(**HB-DO3A**) present different affinity to collagen and therefore different pharmacokinetic profiles.

In fact, the net negative charge of gadoterate and the partial negative charge and the OH groups of gadobutrol allow stronger ionic and hydrogen bonds to the positively charged and highly hydrated collagen molecules. Neutral gadoteridol and Gd(**HB-DO3A**) interact less efficiently with collagen, and affinity decreases as lipophilicity (and therefore the length of the side chain bearing the OH) increases.

The lower affinity to collagen can be reflected in a lower accumulation in the body after administration, in a faster and complete clearance and therefore fewer side effects related to the deposit of free gadolinium in the organism.

The insight provided by this work could represent an actual step forward for the treatment of patients which need repeated contrast enhanced MRI scans to follow the course of a pathology or of a treatment.

In fact, these patients and those with chronic conditions, such as renal failure, are particularly sensitive to the administration of gadolinium-based CAs which are sometimes indispensable for them.

These patients tend to accumulate more than others free gadolinium ions, which can lead to toxic effect in an already compromised organism.[11]

Therefore, in particular for these patients a careful evaluation of the gadolinium-based MRI CA to be administered is necessary to prevent aggravation of pre-existing diseases.

Future developments of this work will concern the validation of the thesis presented herein with other *in vitro*, *ex vivo* and *in vivo* models.

References

(1) Wahsner, J.; Gale, E. M.; Rodríguez-Rodríguez, A.; Caravan, P. Chemistry of MRI Contrast Agents: Current Challenges and New Frontiers. *Chem. Rev.* **2019**, *119* (2), 957–1057. https://doi.org/10.1021/acs.chemrev.8b00363.

(2) Suchý, M.; Hudson, R. H. E. Synthetic Strategies Toward N-Functionalized Cyclens. *Eur. J. Org. Chem.* **2008**, *2008* (29), 4847–4865. https://doi.org/10.1002/ejoc.200800636.

(3) Skwierawska, A. M. Selective Monoprotection of 1,4,7,10-Tetraazacyclododecane via Direct Reaction with 4-Nitrophenyl Active Esters. *Tetrahedron Letters* **2008**, *49* (44), 6308–6310. https://doi.org/10.1016/j.tetlet.2008.08.059.

(4) Kovacs, Z.; Sherry, A. D. A General Synthesis of 1,7-Disubstituted 1,4,7,10-Tetraazacyclododecanes. *J. Chem. Soc., Chem. Commun.* **1995**, *0* (2), 185–186. https://doi.org/10.1039/C39950000185.

(5) Ripa, G.; Scala, A.; Murru, M.; Panetta, E.; Viscardi, C. F.; Ausonio, M. A Process for the Preparation of 1,4,7,10-Tetraazacyclododecane-1,4,7-Triacetic Acid and the Derivatives Thereof. WO1998056776A1, December 17, 1998.

(6) Ballatore, C.; Huryn, D. M.; Smith, A. B. Carboxylic Acid (Bio)Isosteres in Drug Design. *ChemMedChem* **2013**, *8* (3), 385–395. https://doi.org/10.1002/cmdc.201200585.

(7) Hermann, P.; Kotek, J.; Kubíček, V.; Lukeš, I. Gadolinium(III) Complexes as MRI Contrast Agents: Ligand Design and Properties of the Complexes. *Dalton Trans.* **2008**, No. 23, 3027–3047. https://doi.org/10.1039/B719704G.

(8) Stasiuk, G. J.; Long, N. J. The Ubiquitous DOTA and Its Derivatives: The Impact of 1,4,7,10-Tetraazacyclododecane-1,4,7,10-Tetraacetic Acid on Biomedical Imaging. *Chem. Commun.* **2013**, *49* (27), 2732. https://doi.org/10.1039/c3cc38507h.

(9) Rodríguez-Rodríguez, A.; Esteban-Gómez, D.; Tripier, R.; Tircsó, G.; Garda, Z.; Tóth, I.; de Blas, A.; Rodríguez-Blas, T.; Platas-Iglesias, C. Lanthanide(III) Complexes with a Reinforced Cyclam Ligand Show Unprecedented Kinetic Inertness. *J. Am. Chem. Soc.* **2014**, *136* (52), 17954–17957. https://doi.org/10.1021/ja511331n.

(10) Smejkal, G. B.; Fitzgerald, C. Revised Estimate of Total Collagen in the Human Body. *Int J Proteom Bioinform.* **2017**, *2* (1), 001–002.

(11) Guo, B. J.; Yang, Z. L.; Zhang, L. J. Gadolinium Deposition in Brain: Current Scientific Evidence and Future Perspectives. *Front Mol Neurosci* **2018**, *11*. https://doi.org/10.3389/fnmol.2018.00335.

List of Publications

1. Travagin, F.; Lattuada, L.; Giovenzana, G. B. First Synthesis of Orthogonally 1,7-Diprotected Cyclens. *Org. Chem. Front.* **2019**, *6* (9), 1387–1390.

2. Travagin, F.; Biondi, L.; Lattuada, L.; Giovenzana, G. B. Synthesis of Two Novel Mixed Bifunctional Chelating Agents: DO2AP(*t*Bu)$_4$ and DO3AP(*t*Bu)$_4$. *Synlett* **2020**, *31* (13), 1291–1294.

3. Guidolin, N.; Travagin, F.; Giovenzana, G. B.; Vágner, A.; Lotti, S.; Chianale, F.; Brücher, E.; Maisano, F.; Kirchin, M. A.; Tedoldi, F.; Giorgini, A.; Colombo Serra, S.; Baranyai, Z. Interaction of macrocyclic gadolinium-based MR contrast agents with Type I collagen. Equilibrium and kinetic studies. *Dalton Trans.* **2020**, *49*, 14863–14870.

4. Aime, S.; Travagin, F.; Terreno, E.; Giovenzana, G. B. Chemistry of Molecular Imaging: An Overview. In *Molecular Imaging: Principles and Practice*; Elsevier, **2021**, *accepted for publication*.

Ringraziamenti

Non est ad astra mollis e terris via.

In questa breve (a differenza del resto della tesi) chiosa in lingua italica vorrei rivolgere alcuni accorati ringraziamenti.
Desidero ringraziare Bracco Imaging S.P.A. per aver finanziato la mia borsa di dottorato e per avermi permesso di vivere quello che prima era solamente il sogno di un bambino di un minuscolo paesino piemontese.
In particolare, desidero ringraziare il Dott. Luciano Lattuada, depositario della conoscenza omnia sulla chimica dei macrocicli e degli agenti di contrasto e sempre pronto con una soluzione o con una parola di conforto nei momenti difficili.
Ringrazio anche il Dott. Zsolt Baranyai per il suo importantissimo contributo a questa tesi e per i suoi inestimabili insegnamenti.
Un ringraziamento va anche all'azienda CAGE Chemicals per il suo prezioso supporto alla mia esperienza di dottorato. Tra sue fila ho conosciuto maestri di chimica e di vita, diventati poi anche fratelli maggiori e preziosi amici.
Desidero ringraziare anche tutti gli altri dottorandi (Mauro e Michele) e tesisti (Stefano, Arianna, Letizia, Eraldo, Julio, Alessandro, Elisa, Vitaliano, Matteo, Laura, Mario, Alex e Rachele) con cui ho condiviso questi tre anni straordinari. In loro ho trovato non solo dei validi colleghi, ma anche dei grandi amici. Da loro ho imparato molto, e spero di aver insegnato loro anche qualcosa.
Ringrazio anche i miei amici Davide, Francesco, Marta, Silvia, Ivan, Paolo e Luca per essere sempre stati presenti per me. Con loro ho condiviso i momenti migliori di cui abbia memoria.
Ringrazio anche mia mamma Maria Gabriella, mia sorella Francesca e i miei nonni Luigia e Severino per l'affetto e il sostegno che mi hanno sempre dimostrato.
Infine, vorrei rivolgere un ringraziamento speciale a mio nonno, lui mi ha insegnato la curiosità verso il mondo e lo stupore nella ricerca del nuovo. Anche grazie a lui oggi faccio un lavoro che amo e perciò a lui dedico questa tesi.